The Planning of Visually Guided Arm Movements: Feedback Perturbation and Obstacle Avoidance Studies

by

Philip N. Sabes

Submitted to the Department of Brain and Cognitive Sciences
in partial fulfillment of the requirements for the degree of

Doctor of Philosophy

at the

MASSACHUSETTS INSTITUTE OF TECHNOLOGY

September 1996

Author .....
Department of Brain and Cognitive Sciences
September 5, 1996

Certified by .....
Michael I. Jordan
Associate Professor
Thesis Supervisor

Accepted by .....
Gerald E. Schneider
Professor
Chairman, Department Graduate Committee

The Planning of Visually Guided Arm Movements: Feedback Perturbation and Obstacle Avoidance Studies

by

Philip N. Sabes

Submitted to the Department of Brain and Cognitive Sciences
on September 5, 1996, in partial fulfillment of the
requirements for the degree of
Doctor of Philosophy

Abstract

With little conscious effort, the Central Nervous System (CNS) is capable of coordinating visual information from the distal environment with the complex commands required to organize action. One account of this remarkable ability is that CNS hierarchically organizes movement control, with an effector independent planner superordinate to the variable details of movement execution. This thesis is concerned with the extent to which arm movements are preplanned in extrinsic, Cartesian space. Two fundamental questions are addressed: what aspects of movement are centrally planned, and by what criteria is the plan chosen?

The first part of this thesis presents two sets of visual feedback perturbation experiments supporting the notion of Cartesian planning of movement trajectories. A novel prism adaptation technique is employed to investigate the relationship between the static visuomotor map and path planning. Reorganization of the mapping from extrinsic space to intrinsic coordinates is found to result in a corresponding adaptation in movement path. The planning of movement velocity is addressed by perturbing the visual feedback velocity without altering the path. While the production of rhythmic arm movements are insensitive to such perturbations, discrete pointing movements are susceptible to perturbations in the feedback velocity. When the feedback is artificially skewed, subjects adapt their behavior by skewing movement velocity in the opposite direction.

The second part of the thesis focuses on the planning of obstacle avoidance movements. The obstacle rotation paradigm is introduced, and a series of experiments in two and three dimensions show that such movements are not consistent with strictly Cartesian planning of end-point trajectories: the movement path varies in a systematic manner as the orientation of the movement changes. Two stability models are presented to account for these observations, one based on the arm's kinematics and one on its inertial properties. Finally, evidence is presented ruling out both perceptual and execution level explanations of the observed path variation. Together, these results show that the structure of the actuator is taken into account to optimize the movement path. In the final chapter, a modified hierarchical model is discussed which accounts for the results of both parts of the thesis.

Thesis Supervisor: Michael I. Jordan
Title: Associate Professor

Acknowledgments

I thank my advisor, Michael Jordan, for his support throughout my graduate career. In particular, I am grateful for the opportunity to have been a member of the excellent group of researchers he has brought together over the past years. The vibrancy of this group combined with Michael's insatiable thirst for new and more difficult material created an ideal environment for a researcher-in-training.

Daniel Wolpert brought motor psychophysics to our lab, and I am deeply grateful to him for his enthusiasm and his guidance. Emilio Bizzi and Neville Hogan also served as members of my thesis committee, and I thank them for their participation in this process and for the challenging, helpful discussions we had about this work over the course of the past few years. I also thank Dick Held for his useful advice on Chapter 2.

Zoubin Ghahramani and John Houde have been good friends and good colleagues – in the lab, at the Muddy, or snoring away in conference hotel rooms, their company made has made the past five years more productive and more fun. I also thank the other members of Jordan Lab, including Marina Meila, Tommi Jaakkola, David Cohn, Satinder Singh and Lawrence Saul. Our three-hour lab meetings were usually enjoyable, which gives an idea of just how extraordinary a group this was. Emanual Todorov and I spent many hours together in the lab this year, and I thank him for engaging discussions and masterly technical advice.

I thank Jan Ellertsen for showing me the way through MIT and remaining sympathetic and friendly when it got crowded near the exit. I also thank Ellie Bonsaint for her administrative support over the past five years.

The formative years of my graduate career were centered around the E10 lounge. That was where we went to talk about science or cinema, meta-theories or Mary Chung's. The lounge was the real core course, and I am grateful to all my colleague-instructors. In particular, I thank Jacob Feldman for showing me the proper lounge skepticism in my first days at MIT, Kevin Broihier for letting me sleep (most of the time), Kelly Jaakkola for taking me to get ice-cream, Cristina Sorrentino for pushing me out the door, Jenny Ganger for putting us all to shame, and Fei Xu for providing some humor and normalcy in the last busy weeks. I am especially grateful to John Houde, Adee Matan and Yaoda Xu who have been my family in my home-away-from-home over the long months of this summer.

My friends deserve the most credit for putting up with me through everything. For complaining, celebrating, relaxing, and just living, Adee Matan, Lisa Horvitz, and Heidi Wald have all been great company and a source of strength and joy. Joshua Gordon has been a friend, a comrade-on-wheels, my best e-correspondent, and an intellectual influence for years – he helped save me from physics, and I helped damn him to neurophysiology.

Finally, I want to thank my parents and Karen, Jeff, and Polly. Although Chicago sometimes seems far away, they are always with me, providing love and support and reminding me of who I am and why. And Adam deserves special mention for giving me additional incentive to finish this thesis.

Contents

Appendices

List of Figures

List of Tables

Chapter 1

Introduction

The essence of motor skill is the ability to interact with the world around us in a flexible, robust manner. Particularly remarkable is the ease with which the Central Nervous System (CNS) is able to process the primarily visual information it receives from the distal environment into motor commands appropriate to the situation. This unconscious ability to maneuver ourselves in the world around us is even more astonishing when we consider the complexity of a typical motor task. Movements of the upper body can involve the coordination of a dozen or more degrees of mechanical freedom, a number which grows rapidly as we look further up the control structure: there are approximately 40 muscles which control the 7 degrees of freedom of the arm, not including the hand (Yamaguchi et al., 1990), and so on. Furthermore, there are often stringent demands on the precision of the movement, in terms of position (handwriting, eating), timing (swinging a baseball bat, typing), and force (hammering, playing the piano). Finally, these specifications must be met in the face of a changing and often unpredictable environment.

The execution of visually guided arm movements is the particular concern of this thesis. We will investigate the strategies employed by the CNS for transforming visual information into action and for overcoming the problem of excess degrees of freedom. There are two fundamental questions which this thesis hopes to address: what does the CNS plan when it plans arm movements, and by what criteria does it choose the plan? We will begin in the section by defining what is meant by a movement plan.

1.1 The Planning of Human Movement

In Bernstein's seminal 1967 book, "The Co-ordination and Regulation of Movement", he argues clearly for a central representation of movement based not on the details of the effector's action, but on the desired movement in an effector independent space. He was led to this conclusion by a variety of evidence, such as the fact that humans are capable of repeating the same movement with relative accuracy independent of the exact details of the movement implementation. We routinely perform the same motor tasks in different postures, with either arm, at different orientations with respect to gravity, and in the face of small perturbations. Bernstein recognized the degree of complexity involved in controlling the many degrees of freedom used in a particular movement, and argued that a central, effector independent, representation of the movement must exist. Taking his example of tracing a circle in space with the hand, the dynamics of the movement are quite complex, and the muscle commands required to perform it can change radically as the location of the hand in the workspace shifts. Nevertheless, it is a simple matter to continue drawing roughly the same circle after the arm is repositioned.

In this context, Bernstein introduced what he called the *Principle of Equal Simplicity*: classes of equally "simple" actions, as measured by movement error, reaction time, etc., tell us about the structure of the underlying control system. In the example above, it is equally simple to describe a circle independent of the details of the joint torques or motorneuron activity required. Therefore, Bernstein would argue, the movement is the result of a central command which represents not the details of the motor neuron firing patterns, but the circle itself.

Decades after this argument was first published, modern research on the kinematics of human arm movements began to reveal that movement trajectories[1] tend to exhibit invariance such as roughly straight paths and symmetric, bell-shaped velocity profiles (Morasso, 1981; Soechting and Lacquaniti, 1981; Abend et al., 1982). It was also noted that the joint trajectories of arm movements displayed regularities such as linear dependencies between the joint velocities (Soechting and Lacquaniti, 1981; Soechting and Terzuolo, 1986). Furthermore, these invariances were maintained over a wide variety of conditions, such as

[1] "Trajectory" will be used throughout the thesis to refer to both the temporal and spatial components of a movement. "Path" refers only to the spatial information. Knowing the trajectory is equivalent to knowing the path and the tangential velocity profile along that path.

varying movement speeds, changes in orientation with respect to gravity, and the addition of loads to the arm (Soechting and Lacquaniti, 1981; Atkeson and Hollerbach, 1985). Following Bernstein, these researchers argued that such regularities were evidence for the explicit central representation of the invariant property, superordinate to the variable dynamic details of movement implementation. In other words, these quantities are *planned* by the CNS. This line of argumentation has become one of the primary theoretical tools in the study of movement control.

Although many of the live issues in motor control research can be boiled down to what variables are preplanned and in what representation, there is widespread agreement that central mechanisms of control exist and that these processes are primarily concerned with an abstract level of movement planning. In the rest of this thesis, when we refer to planning or the planner, we mean it in exactly this sense – that which is prespecified by the CNS; that which is represented, in some form or other, in the central neural commands.

1.2 Pitfalls of the Invariance Argument

In his discussion of the principle of equal simplicity, Bernstein applied it to Helmholtz's then current theory of auditory perception (Bernstein, 1967). Helmholtz had claimed that the inner ear is composed of resonators of various frequencies, and that acoustic signal drives these resonators, at which point auditory perception can proceed in the same manner as tactile perception. Bernstein argued that it is relatively difficult for humans to perceive pure tones compared to, say, phonemes, and that conversely analyzing speech with a series of resonators would be a formidable task. "The lines of equal simplicity are distributed in an essentially different way for the function of auditory perception and for a resonant harp.... It is this circumstance which is critically dangerous for Helmholtz's hypothesis...." However, the intervening years have shown that Helmholtz was largely right.

Bernstein was led to his erroneous conclusion by overlooking the levels of processing involved in auditory perception. His conclusions regarding the computational structure of perception may be correct for high level cortical processing, but not for the workings of the inner ear.

In the case of action, the problem is inverted. Say for example that one makes the observation that some quantity Φ, such as path shape or the relative phases of the joint

angles, is preserved over a class of natural movements $\mathcal{X}$:

$$\Phi(x) = 0, \forall x \in \mathcal{X}. \tag{1.1}$$

It is tempting to conclude to that the CNS uses the constraint $\Phi(x) = 0$ explicitly as a means of dealing with the redundancy of the manipulator. However, there are two serious pitfalls to the argument. First, one can invert Bernstein's error and attribute to the CNS what is in fact a emergent property of the dynamics of the plant and low-level control structure. Secondly, one can draw conclusions about $\Phi(x)$ based on an insufficiently comprehensive $\mathcal{X}$. Two examples will illustrate the problem.

There have been numerous studies on the velocity of movements along curvilinear paths (Viviani and Terzuolo, 1982; Lacquaniti et al., 1983; Viviani and Cenzato, 1985; Viviani and Flash, 1995). These results will be discussed in detail in Chapter 3, but for now it is important just to note that the data strongly suggest that the velocity of arm movements is determined by the path of the movement. Lacquiniti et al. (1983) state, "As a working hypothesis, we can then postulate the existence of control processes that actually translate an essentially static description of the form of the movement into dynamic commands compatible with the execution of that form." But at what level does this occur? Lacquiniti and colleagues presumably wanted the reader to understand that these processes were part of the high level control of movement. However, recent computational studies have suggested that the observed regularities of velocity profiles could be completely emergent from the low level neuromuscular properties of the arm (Gribble and Ostry, 1996).

The issue of the planning of velocity movements is far from resolved, but the point made by Gribble and Ostry is well taken – observed invariances in movement do not necessarily tell is about the movement plan. In Part I of this thesis we show that one way past this theoretical crisis is by designing more directed experiments. In particular, Chapter 3 will address the issue of velocity planning.

As a second example, Soechting and Lacquaniti (1981) measured the kinematics of arm movements in a sagittal plane through the shoulder. In accordance with previous studies they found that both the path and velocity profile were roughly constant and independent of movement speed. However they also discovered an invariant linear relationship between the angular velocities of the elbow and shoulder joints during the deceleratory phase of

the movement. They focused on this relationship, proposing that movements are planned in intrinsic (joint level) space, remarking, "given the invariance [in joint space], the fact that trajectories described in extrinsic coordinates are approximately rectilinear may be coincidental."

However, Hollerbach and Atkeson (1986) noted that given the non-linear kinematics of a two joint arm, it is surprising to find a coincidence of straight lines in both extrinsic and intrinsic coordinates (the latter being the implication of linearly related joint velocities). They performed an analytic and computational analysis of the kinematics and showed that straight lines in Cartesian space approach straight lines in joint space near the outer boundaries of the workspace. Furthermore, they display that this fact can account for the findings of Soechting and Lacquaniti, showing for example that had the movements been made in the other direction, the ratio of joint angle velocities would have been constant in the acceleratory phase instead.

While the issue of intrinsic versus extrinsic planning is still very much an open question, this example highlights both difficulties of the argument by invariance. First, the class of movements recorded in the study was clearly overly restrictive. But this same criticism can arguably made against the field as a whole, since with only a few exceptions researchers investigating pointing and reaching movements have considered point-to-point movements in a plane. This issue is addressed directly in Part II of the thesis.

Secondly, Soechting and Lacquaniti relied too heavily on the appearance of invariance. Even if a large class of movements exhibits some regularity, it may be due not to central planning, but to the kinematics or dynamics of the actuator.

1.3 The Hierarchical Model of Planning and Control

The previous two sections made frequent use of the terms "high level" and "low level", and so it is time to be more specific about the notion of levels of control. Many authors have presented the idea that the control of movement is hierarchically organized(Bernstein, 1967; Saltzman, 1979; Hollerbach, 1982), and as Hogan and Winters (1990) point out, the notion of hierarchical control is an implicit assumption in most of the current research in motor control. Since the idea is central to the approach taken in this thesis, I will discuss our interpretation of hierarchical control and how various current models fit into the hierarchical

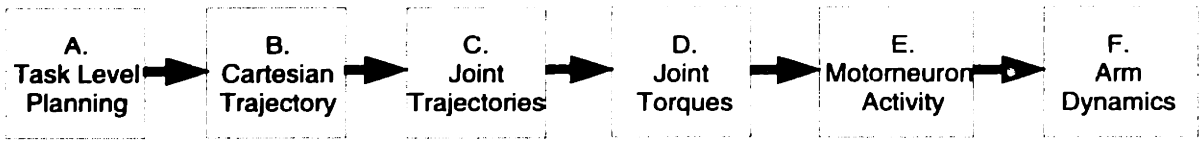

Figure 1-1: A hierarchy for motor control.

framework. The goal is to provide an understanding of what is meant by the first question of the thesis: "What does the CNS plan when it plans arm movements?"

We will begin with the assumption that there exists in the CNS a task level planner which specifies the externally imposed constraints on the movement, usually driven by a visual stimulus. This specification will be assumed to be as minimal as possible – e.g. for a simple point to point movement, it would consist of the start and end points in visual or extrinsic coordinates. In the case of an obstacle avoidance movement, it would also include the location of the obstacle.

The process of visuomotor control can most easily be thought of as a series of underconstrained computations. The task level planner sends a description of the movement to the end-point[2] planner, which is responsible for choosing a trajectory for the finger tip through the environment (i.e. the extrinsic, or Cartesian space). Here, such considerations as other objects in the environment need to be taken into account. At the next level down, the kinematics of the arm must be inverted to compute a trajectory through joint space which will attain the desired end-point trajectory. In general, the overall task is irrelevant to the joint level planner, but certain information about the environment would be required to avoid, for example, knocking into objects with the elbow. Up to this point, the dynamics of the arm and its neuromuscular controller have been completely ignored. The next level inverts the arm's dynamics to find a set of joint torques for each instant that will yield the desired joint trajectory. These joint torques will have to be accomplished with some set of neural commands, which the next level of the hierarchy must compute. Finally, the dynamics of the arm and its neural feedback loop will shape the command signal into the actual arm movement.

There are two important points to be made about this framework. First, the computational problem is ill-posed or underconstrained at every step. Given the task level

[2]Throughout the thesis the term "end-point" will refer to the end of the manipulator, not the target of the movement (which is sometimes called the end point).

description, there are an infinite variety of acceptable paths, and so on down the hierarchy. This is due to the excess of degrees of freedom in the system. In the next section, we will discuss a method for dealing with this redundancy. Secondly, there is a modularity to the model which is appealing: each level must solve only a small part of the overall problem, without worrying about the details of the levels above or below. The joint trajectory planner does not need to know about the arm's musculature or the relationship between the motorneuron activity and the resulting torques. Each level of the hierarchy is subordinate to its predecessor (e.g. the joint trajectory must be chosen to attain the end-point trajectory), but otherwise independent of the rest of the computational machinery of control.

This strictly hierarchical model is by no means definitive. We have presented it here to serve as a reference point, as many of the active debates in the field of motor control can be couched in terms of which of these independencies and uni-directional flows of information hold (Kawato, 1994).

For example, the claim that joint trajectory planning is subordinate to the Cartesian end-point plan is controversial. This notion is supported by observational studies (Morasso, 1981; Soechting and Lacquaniti, 1981; Abend et al., 1982), dynamic perturbation experiments (Flash and Gurevich, 1991; Shadmehr and Mussa-Ivaldi, 1994; Lackner and DiZio, 1994), visual perturbation experiments (Wolpert et al., 1995; Flanagan and Rao, 1995), and computational models(Hogan, 1984; Flash and Hogan, 1985; Jordan et al., 1994). On the other hand, many researchers have argued that trajectory planning originates with the joint level description, i.e. that module B and C in Figure 1-1 should be combined, or that B should be discarded altogether. This point of view is also supported by observational studies (Soechting and Lacquaniti, 1981; Soechting and Terzuolo, 1986; Kaminsky and Gentile, 1986), analysis of movement error (Soechting and Flanders, 1989a; Flanders and Soechting, 1990) and computational models (Cruse, 1986; Flanagan and Ostry, 1991).

Others have argued that trajectory planning is linked to the dynamics of the arm, and so modules B through D (in Figure 1-1) must be combined. Uno, et al. (1989) propose an optimal control model based on a dynamic cost function and present a variety of experimental evidence supporting the model, including observations of natural movements and adaptation to elastic loads (see Kawato, 1994, for a review).

So far, the process has been to combine the higher levels of planning, increasing the level of detail with which the primary levels of processing are involved. One can also aggregate

modules from the bottom up, easing the hypothesized computational complexity of executing the planner's command. As an example, the original Equilibrium Point Hypothesis (Bizzi et al., 1976) suggests that movement can be controlled merely by changing the equilibrium point of the actuator's musculature; the spring-like neuromuscular dynamics will take care of the rest. This model of control obviates the need for modules B, C and D in Figure 1-1; only the mapping from end-point locations to motorneuron commands need be known. While physiological evidence soon ruled out this simple model (Bizzi et al., 1984), the idea of using the viscoelastic properties of the arm to simplify movement control is still influential (Feldman, 1986; Bizzi et al., 1992). Current models posit that instead of only specifying the final position of the limb, there is a Cartesian planner which specifies either a series of equilibrium points over time or an entire "virtual trajectory" (Flash, 1987).

These examples were meant to illustrate what we mean by the structure of the control process: what is planned and using what information. The discussion also suggests a general approach for addressing this kind of question experimentally, an approach we will use throughout the thesis. Begin by assuming independence or uni-directional flow of information between two variables of movement (e.g. the mapping from vision to target location and the shape of the trajectory, or the path of a movement and its velocity profile), and determine a means of perturbing one of those variables, either through direct experimental manipulation or by choosing a suitable class of natural movements. Finally, measure the effect of the perturbation on the second variable.

Knowing that the CNS plans a particular aspect of movement does not tell us how it chooses the plan, how it deals with the system's redundancies. An approach to solving this problem is discussed in the next section.

1.4 The Optimal Control Hypothesis

Each module in the hierarchy of Figure 1-1 must deal with an ill-posed, or underconstrained, problem. Formally, the solution of such problems requires the application of a regularizer (Poggio and Girosi, 1990), that is an extra criterion, such as smoothness, which is used to choose between the infinite solutions to the original problem. Control theorists call this method *optimal control*, and use it overcome the redundancy of the controlled system (Kirk, 1970).

This concept has had a profound influence on the study of motor control, most clearly in the direct application of the optimal control methods to the modeling of movement planning. Hogan (1984) first introduced the idea of using a mathematically explicit cost function to solve the underconstrained problem of trajectory planning. He posited that the CNS would try to achieve maximally smooth rotations of a single joint by minimizing the integral of the squared rate of change of joint acceleration, or jerk. The minimum jerk model was soon generalized to multijoint arm movements (Flash and Hogan, 1985). Shortly thereafter, a number of other researchers proposed different criteria, such as minimum energy (Nelson, 1983), minimum effort (Hasan, 1986), and minimum change in joint torques (Uno et al., 1989). As a whole, these models account remarkably well for the observed trajectories of human movements.

Other researches have inverted the problem, starting with experimental data, and using non-linear statistical methods to fit a cost-function to the data (Cruse, 1986; Brüwer and Cruse, 1990). The goal of this work was to identify which variables the cost function needed to use in order to successfully model human movement. These studies were limited in that they focused mainly on the static positioning of the arm (the inverse kinematics problem) and only considered cost functions which depend on the joint angles. However, the approach is suggestive. One could fit a variety of functions based on different movement variables and see which accounted best for the observed data. In this sense, the Optimal Control Hypothesis can be viewed as a "soft" version of the Invariance Principle.

This last comment leads to an important point: the most interesting distinction between the various optimal control models is not their exact functional form, but what kinds of information the criteria employ. Minimum jerk is a model of planning in cartesian space; minimum torque change is a model in which planning and dynamics are inseparable. It is this aspect of the optimal control hypothesis which we wish to emphasize. In Part II of this thesis, for example, we will introduce two candidate models for the planning of obstacle avoidance movements. While these models do not make explicit use of the variational optimization methods which are the hallmark of the optimal control models above (c.f. Kirk, 1970), we consider them to be in the same spirit. They make predictions about what quantities the CNS is trying to regulate (optimize) when planning movement.

1.5 Implicit and Explicit Planning

Of special concern in this thesis is the extent to which the planning of goal directed movements is visually based, or in other words the nature of the Cartesian planner. In the hierarchical model of Section 1.3, the planner selects a complete trajectory in visual space, and that plan is converted to intrinsic coordinates via an inverse kinematic mapping. This is an example of explicit visual planning, that is planning *in Cartesian space.*

The previous section on Optimal Control suggests a slightly different interpretation of what is meant by the visual planning of movement: the planner employs a cost function based on the Cartesian end-point trajectory. We call this version implicit visual planning, or visual *based* planning.

The distinction between the two interpretations lie in what is actually represented in the central command. In explicit visual planning, the Cartesian end-point trajectory is computed on-line in the CNS. Implicit visual planning does not require that the Cartesian trajectory ever be explicitly represented in the neural signal, only that the movement command reflect a set of visually defined criteria. Clearly these two interpretations are not mutually exclusive. Any control system which utilizes explicit visual planning is likely to base that planning on extrinsic cost functions. Our point here however is that these two notions are not inextricably linked. It is possible to have visual based planning without explicit preplanning of a Cartesian trajectory, and vice versa.

As an example, consider the adaptive control model of Jordan et al. (1994). The model employs a cascade of Neural Networks, including a central controller, and a forward model of the arm's dynamics and kinematics. The controller network encompasses the entire hierarchy of Figure 1-1: its inputs are the desired initial and final positions, and it outputs the temporal stream of control signals required to produce a movement. The controller specifies a set of movement criteria in extrinsic space, such as a series of via points through which the path must pass. The controller is then trained by propagating the extrinsic, or distal, errors backward through the forward models, converting them into intrinsic, or proximal errors (Jordan and Rumelhart, 1992). The feature of the model relevant for our discussion is that although the movement criteria are visually defined, the trajectory is not explicitly formulated in Cartesian coordinates. Any model which uses extrinsic error signals to drive an adaptive controller is implicitly planning in visual space.

Conversely, it is possible that explicit Cartesian end-point planning can utilize criteria based on intrinsic properties of the movement. Part II of this thesis will present evidence for the influence of the arm's dynamic properties on the movement plan. In the final chapter of this thesis, we will argue that this information is in fact used in the CNS at the level of the Cartesian end-point planner.

1.6 Plan of the Thesis

Finally, we consider a few experimental alternatives for addressing the issues introduced in this chapter and describe the course we have taken in this thesis. Observational studies were the mainstay of early research on goal directed arm movements, and they are still an essential tool for identifying interesting phenomena. With the current explosion in Virtual Reality technology, it is becoming feasible to create more complex studies, moving beyond planar point-to-point movements to more natural movements which involve interactions with the environment and fewer constraints on the arm's degrees of freedom. As a step in that direction, Part II of this thesis investigates the planning of obstacle avoidance movements, first in the horizontal plane and then with unconstrained arm movements in three dimensions.

Still, observational studies are limited, and it is important to develop move direct methods of investigating the structure of movement control. One approach has been to analyze movement error. The variable error associated with pointing movements has been used by a number of researchers as a means of identifying separate channels of control, the logic being that independent control paths should have independent noise (Soechting and Flanders, 1989b; Flanders and Soechting, 1990; Gordon et al., 1994b). Others have argued that the variability of movements should be lowest when viewed in the coordinates in which they are planned (Haggard et al., 1996). Similarly, patterns of systematic errors have used to identify the planning coordinates (Soechting and Flanders, 1989a; Gordon et al., 1994a). For example, Gordon et al. (1994a) show that when pointing to visual targets without concurrent visual feedback, there is a directionally dependent bias in movement extent that aligns with the inertial anisotropies of the arm. This result is consistent with separate channels for planning movement extent and direction, as the former channel would not be able to take into account the arm's inertia without information from the latter.

Physiological studies have also had a major impact on our understanding of motor planning. An example is the work in primate motor cortex by Georgopoulos and colleagues (Georgopoulos et al., 1986; Georgopoulos et al., 1983; Schwartz, 1994), who have shown that cell populations encode movement direction and velocity in hand centered Cartesian coordinates (although see Scott and Kalaska, 1995). Furthermore, Kalaska et al. (1990) show that while cell activity in primary motor cortex is sensitive to external loads placed on the arm, cells in area 5 of parietal cortex show a similar spatial coding which is independent of movement dynamics. These results are consistent with a hierarchical model such as those discussed in Section 1.3.

Most recently, a number of researchers have employed perturbation techniques in an attempt to gain more direct insight into the structure of movement control. The logic of these studies is to perturb one feature of the movement and look for compensatory changes in behavior. If such adaptation occurs, one can argue that the features of the movement restored by the adaptation are planned by the CNS superordinate to those aspects which changed with the adaptation. For example, a number of researchers have investigated pointing movements in altered dynamic environments such as elastic loads (Flash and Gurevich, 1991), skew-viscous fields (Shadmehr and Mussa-Ivaldi, 1994), and rotational Coriolis forces (Lackner and DiZio, 1994). These studies have found that after practice, subjects return to their pre-perturbation baseline trajectories (although see Uno et al. 1989). Others have artificially perturbed the visual feedback during movement, which also resulted in compensatory adaptation (Wolpert et al., 1995; Flanagan and Rao, 1995). As a whole, these studies have provided strong support for notion that movement execution is subordinate to the Cartesian trajectory plan. This thesis will make extensive use of perturbation techniques. In Part I, visual perturbations will be used to provide further support for Cartesian planning, and Part II will use both visual and dynamic perturbations to localize the origins of observed kinematic features of obstacle avoidance movements.

We now return to the two questions posed at the beginning of this chapter and discuss how this thesis will attempt to address them.

What does the CNS plan? Our approach is to use visual feedback perturbation studies as a means of directly probing the structure of the Cartesian planner. In Chapter 2, we employ a novel prism adaptation technique to investigate the relationship between the inverse kinematic map and trajectory planning. In Chapter 3 we will address the planning

of movement velocity by perturbing the visual feedback velocity while leaving the perceived path unchanged.

By what criteria? The results of Part I support the notion of visual based planning of movement, i.e. that the criteria by which the CNS plans movements are based solely on the end-point kinematics. In Part II of the thesis, however, we present a series of obstacle avoidance studies which show that the Cartesian plan is influenced by the details of the actuator. Furthermore, that information is used to optimize features of the movement which depend on the particular task at hand.

Finally, in Chapter 7 we discuss how to reconcile the conclusions of the two halves of the thesis. In doing so, we present a modified hierarchical model, in which a limited bi-directional flow of information allows the Cartesian planner to optimize more aspects of the movement than simply the Cartesian trajectory.

Part I

Vision and the Planning of Arm Movements

Chapter 2

Prism Adaptation and Trajectory Planning

2.1 Introduction

In this chapter we will address the question of the Cartesian planning of point-to-point movements. In particular, we will investigate the effects of a local reorganization of the inverse kinematic map on trajectory planning. In doing so, we hope to identify what aspects of the movement plan originate explicitly in extrinsic coordinates.

There a number of ways in which the CNS could choose a trajectory for reaching to a visual target. At a minimum, the target itself originates in extrinsic coordinates. This target could then be converted directly to intrinsic coordinates, and the remainder of the planning process can be carried out in that space. This possibility is depicted in the top row of Figure 2-1. On the other hand, it is possible that the entire trajectory is planned in extrinsic space and then converted into the appropriate intrinsic signals, as in the bottom row of Figure 2-1. And there are a number of intermediate possibilities. For example, a Cartesian path could be specified, while the timing along that path could be determined after the inverse kinematic transformation. Or, the Cartesian planner could provide only a series of control points through which the path should pass, as shown in the middle row of Figure 2-1.

The debate over the nature of the Cartesian planner has a long history. The original version of the Equilibrium Point Hypothesis (Bizzi et al., 1976) suggested that converting the

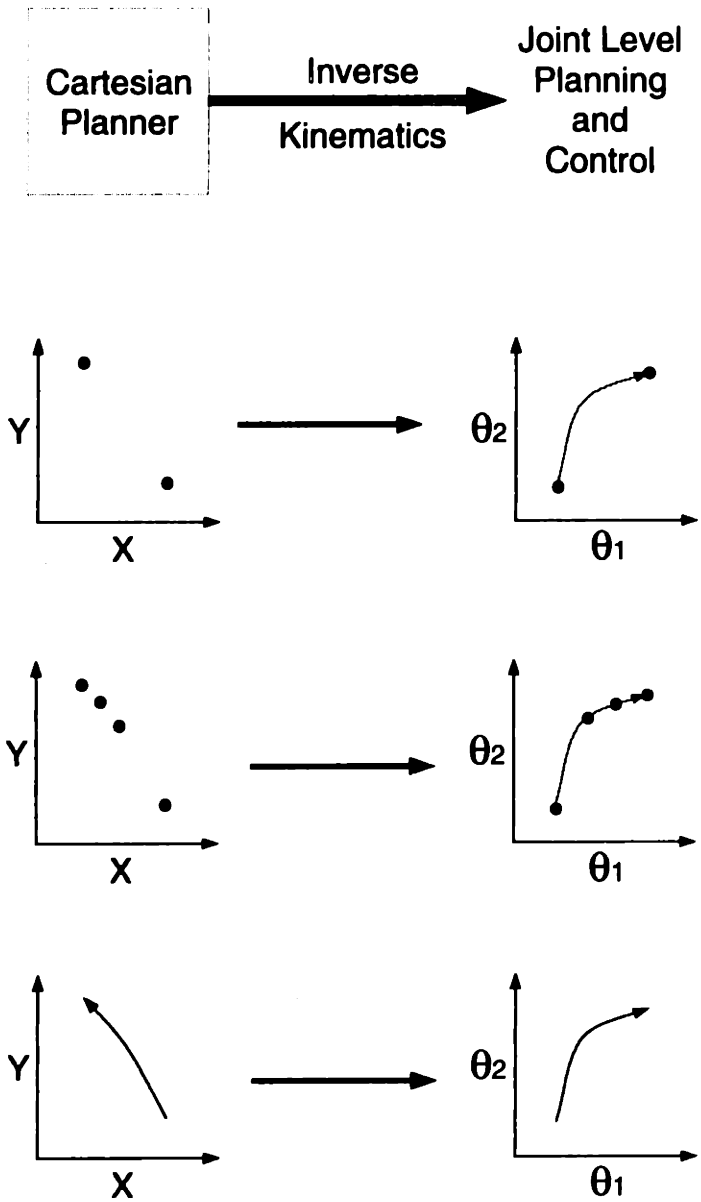

Figure 2-1: Various models of the Cartesian planner. The right hand column depicts the characteristics of the movements which are planned in extrinsic space. That plan is converted into intrinsic coordinates, and shown in black on the right hand column. The gray features in the right hand plots represent aspects of the movement which originate in intrinsic space.

target location into an appropriate arm posture is all that is required to execute movement. Investigations of the behavior of deafferented monkeys showed that this simple model was not correct (Bizzi et al., 1984), but the authors noted that their data were consistent with a model in which a series of equilibrium points were specified over time. This idea was fleshed out by Flash (1987), who proposed that an entire "virtual trajectory" was planned in Cartesian space. In all of these models, the static mapping from locations in Cartesian space to arm posture determines the shape of the trajectory.

There is a good deal of evidence for trajectory planning in Cartesian space. In addition to the observational studies showing the invariant properties of straight line paths and bell-shaped velocity profiles (Morasso, 1981; Soechting and Lacquaniti, 1981; Flash and Hogan, 1985), recent studies which have artificially perturbed either visual feedback (Wolpert et al., 1995; Flanagan and Rao, 1995) or movement dynamics (Flash and Gurevich, 1991; Shadmehr and Mussa-Ivaldi, 1994; Lackner and DiZio, 1994; Flash and Gurevich, 1996) suggest that the movement plan is superordinate to the details movement execution. These latter results will be reviewed more fully in Chapter 4, but two studies are of particular concern to the issues in this chapter.

Lackner and DiZio (1994) placed subjects at the center of rotating platform, so that when motionless they experienced only a small centrifugal force. However, when subjects attempted to point to visual targets, the effects of the Coriolis forces induced a sizable perturbation. Lackner and DiZio asked subjects to point in the dark to lit targets. They found that although it took less than 40 trials until subjects trajectories exhibited the straight paths and bell-shaped velocity profiles of the pre-rotation movements, there was a persistent bias in pointing accuracy which was not evident before the introduction of the perturbation. Immediately after the rotation stopped, subjects exhibited aftereffects in the form of path curvature in the direction opposite to the initial perturbed trajectories. This trajectory adaptation provides support for Cartesian planning model, since the CNS chooses to reorganize the lower levels of movement control in order to maintain extrinsic invariances such as straight path. However, in a follow-up study investigating the intermanual transfer of adaptation, Lackner and DiZio found contrary evidence (DiZio and Lackner, 1995). During the rotation, subjects moved only with their right arms, but the post-rotation session began with left arm pointing. The paths of these movements were straight, showing no transfer of the trajectory adaptation, but there was an error in movement end point consistent with the

residual bias seen with the right hand during rotation. After several movements this bias disappeared. Subjects then returned to right handed pointing, and surprisingly, the end point bias was gone, but the trajectory aftereffects were still evident. Lackner and DiZio's interpretation is that inverse kinematics is independent of trajectory control, with central specification of the movement end point and peripheral control of the trajectory itself.

Wolpert et al. (1995) perturbed the visual feedback during pointing movements by bowing the visually perceived trajectory out from the path while maintaining veridical feedback at the beginning and end of the movement. Subjects could have maintained their pre-perturbation trajectories and still reached the target, however they compensated for the visual perturbation by curving their movements in the direction opposite to the perturbation. These findings suggest that the CNS plans movement paths in visual space. However, Wolpert et al. (1995) does not address whether the planning is explicit or implicit. This is because their visual perturbation was "dynamic", in the sense that subjects were able to view their fingers throughout the movement. Such feedback could provide an error signal to an adaptive controller which prefers straight paths (see Section 1.5). There are other less theoretical reasons to expect that continuous feedback could have different effects than feedback restricted to the end of movement. Held and Hein (1958), showed the subjects wearing left shifting prism goggles exhibit a rightward post-exposure bias in their pointing when the exposure phase included watching self-produced motion. On the other hand, if during the exposure phase the arm is kept still, no adaptation is seen. More recently, Redding and Wallace (1992) have demonstrated that when subjects make pointing movements with prism shifted vision, the nature of their adaptation depends on the amount of visual feedback. When the finger is visible throughout most of the movement, adaptation is primarily proprioceptive (as measured by the error subjects exhibit when asked to point straight ahead). On the other hand, when the finger only becomes visible near the end of the movement, the adaptation is primarily visual (as measured by the error in subjects' assessment of the time at which moving cursor passes straight in from of them).

In this chapter, we will investigate the effects of a reorganization of the static visuomotor map on trajectory planning. The idea is to limit subjects' visual feedback to narrow bands extending perpendicularly to the direction of movement (see Figure 2-2). By choosing appropriate feedback shifts for each band, we will induce a non-linear deformation in the visuomotor map. We will then assess whether such end point adaptation effects movement

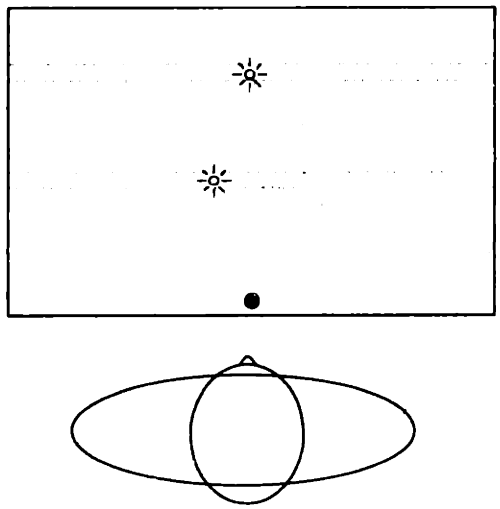

Figure 2-2: Visual Feedback for Experiment 2.1. Feedback is limited to two narrow bands. In the more proximal band, feedback is perturbed by simulating a leftward prism shift. In the distal band, subjects receive veridical feedback.

trajectories which pass through the perturbation bands.

2.2 Experiment 2.1

2.2.1 Experimental Methods

Subjects were seated at the virtual visual feedback system described in Appendix A. Direct view of the arm and hand was precluded, and the experiment was conducted in the dark. When visual feedback of finger-tip location was given, it was in the form of a 1cm radius circle of light projected onto the plane of the table using the virtual visual feedback. Target location and trial information were projected in the same manner.

Every trial began with subjects moving their right finger a fixed start position, which was marked with a tactile stimulus made from a small velcro patch. The location of the start position was along the subjects' midline, approximately 11cm in front of the subjects' eyes. Before the start of the experiment, subjects' hands were passively moved to the start position, and subjects had no difficulty returning to that position. After attaining the start position, a target circle would appear on the table as a blue 1cm radius circle. Subjects were instructed to wait in the start position, taking notice of the location of the target, until the "go signal", which consisted of a short tone and the target changing colors from blue to white. At that point, subjects were instructed to point to the target. There were

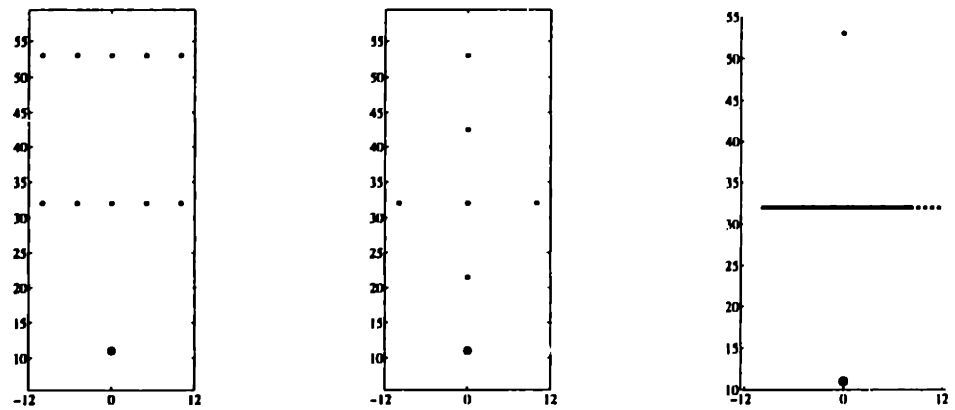

Figure 2-3: The experimental protocol for Experiment 2.1. Open circles represent targets. The gray closed circle represent the starting location. Units are cm's, with the origin at the X-Y location of the subjects eyes (approximately). (a) Training trials. (b) Test trials. (c) A left pass obstacle trial.

three kinds of trials in the experiment: training trials, test trials, and obstacle trials.

Training trials were marked by a hollow target circle. In these trials, subjects were given no visual feedback unless they were within a 2cm swath of the workspace centered at the target circle and oriented perpendicularly to the straight line path. The visual feedback could be offset in the X (transverse) direction, simulating the effects of right or left shifting prism. However unlike wearing real prism goggles, the remapping between vision and proprioception was only experience in restricted region, local in the Y (sagittal) direction. This technique is based on the methods developed in (Bedford, 1989; Ghahramani et al., 1996). Subjects were told that on training trials, they should be able to point accurately to the target, even if they had to hunt for it, and that the trial wouldn't end until they were within 2cm of the target. Training trial targets were always located either 21cm (50% mark) or 42cm (100% mark) distal from the start position (i.e. along the Y-axis). At the 50% mark feedback displacement was 6cm to the left or the right. At the 100% mark there was no displacement, i.e. veridical feedback was provided. This goal of this protocol was to force a non-linear reorganization of the visuomotor map along the sagittal direction.

Test trials were marked by a filled target circle. Subjects were given no visual feedback during a test trial, and they were instructed to move to the target "as accurately as possible in one quick movement." The trial ended when finger movement ceased, independent of the

location of the finger, at which point the target circle disappeared and a tone was sounded. Test trials served a dual purpose: the error in final position is used as a measure of end point adaptation (Held and Hein, 1958; Welch, 1971), and the shape of the trajectory is used to assess the effect of that adaptation on trajectory planning.

Obstacle trials were identical to test trials, except that subjects were asked to move around an obstacle on their way to the target location. For obstacle trials the target was always located 42cm from the start position along the Y-axis (i.e. at the 100% mark), and the obstacle was always oriented perpendicularly to the path at the 50% mark, extending 10cm to the one side of midline and across the entire other half of the workspace (see Figure 2-3(c)). If the 10cm protrusion was to the left, the trial was said to be a *left obstacle* trial, and similarly for the right.

Before the experiment began subjects were presented with a few test and obstacle trials with complete visual feedback (i.e. they could see the finger cursor throughout the course of the of the movement). This made it easier to familiarize subjects with the task, and also made it clearer what was expected of them in the obstacle trials – to make sure the finger cursor didn't hit the obstacle. Subjects were then allowed to practice several of each kind of trial under experimental conditions.

The experiment consisted of four blocks of trials, two training blocks each followed by a testing block. The training blocks were composed of 220 training trials, 22 to each of the ten target locations shown in Figure 2-3(a). Half of the targets were located at the 50% mark, half at 100%.

The testing blocks consisted of the following: 15 test trials to each of six test locations (see Figure 2-3(b)), 15 left pass obstacle trials, and 15 right pass obstacle trials. In addition, a training trial was added to every fourth test trial in order to avoid premature decaying of the prism adaptation (Welch, 1986). The total number of trials in each testing block was 166. The entire experiment consisted of 772 movements.

10 subjects participated in Experiment 2.1. All were right handed with normal or corrected to normal vision and were naive as to the purpose of the experiment. The subjects were divided randomly into two groups: Left-Right and Right-Left.[1] In Left-Right experiments, the first training set had a prism shift of 6cm to the left, and the second training set had a prism shift of 6cm to the right. In Right-Left experiments, the order was reversed.

[1] Left-Right: 2F, 3M, age range 19-33yrs. Right-Left: 2F, 3M, age range 22-26yrs.

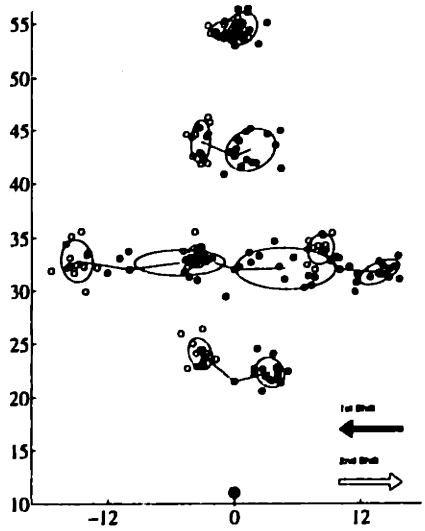

Figure 2-4: Movement end point locations for Subject JH in the Left-Right group, Experiment 2.1. Targets are markets by crosshairs. Filled circles are final positions for the first test block (left shift), open circles are for the second (right shift). Ellipses represent the 95% confidence regions.

2.2.2 Results

Before presenting the movement paths, it is necessary to show that the visual perturbation of the training blocks successfully induced the desired non-linear end point adaptation. The raw data for a single subject in the Left-Right group is shown in Figure 2-4. The circle at the bottom of this and the following figures represents the start position. Note that pointing is shifted maximally at the 50% mark, and minimally at the 100% mark, which is the desired effect. This data is summarized in Figure 2-5. The panel on the left shows the average X-axis end point error for each testing block, and the panel on the right shows the difference between the two. This latter curve is the total end point adaptation between the left and right shift phases of the experiment and will serve as the reference to which we will compare changes in movement trajectories.

The data for all subjects, averaged within the two experimental groups, is shown in Figure 2-6. The average total end point adaptation at the 50% mark was -5.5cm for the Left-Right group and 6.6cm for the Right-Left group, corresponding to 45% and 51% adaptation, respectively. At the 100% mark, there was minimal adaptation: -1.6cm (13%) and 1.9cm (16%) for the two groups. Thus, the desired effect was achieved: the adaptation is larger at the 50% mark than at the 100% mark, and there is a significant curvature in the end point

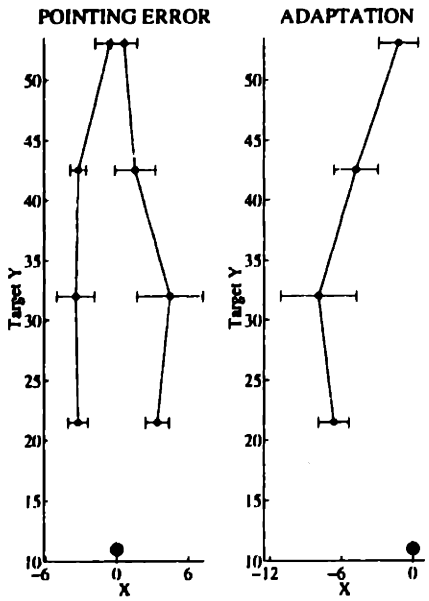

Figure 2-5: End point adaptation for Subject JH in the Left-Right version of Experiment 2.1. Error bars represent 1 standard deviation. Filled circles are for the first test block, open circles are for the second.

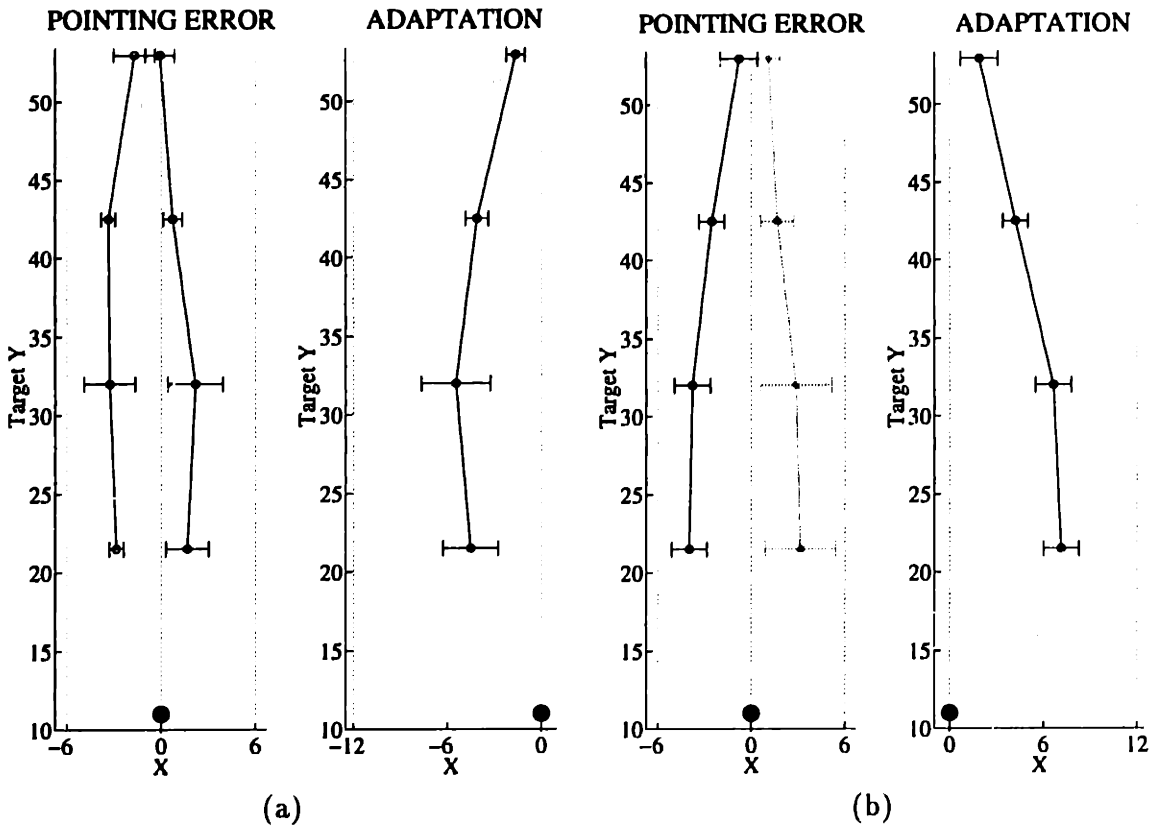

Figure 2-6: End point adaptation for Experiment 2.1. Points represent means (s.d.) over all subjects in the (a) Left-Right group, (b) Right-Left group. Filled circles are for the first test block, open circles are for the second.

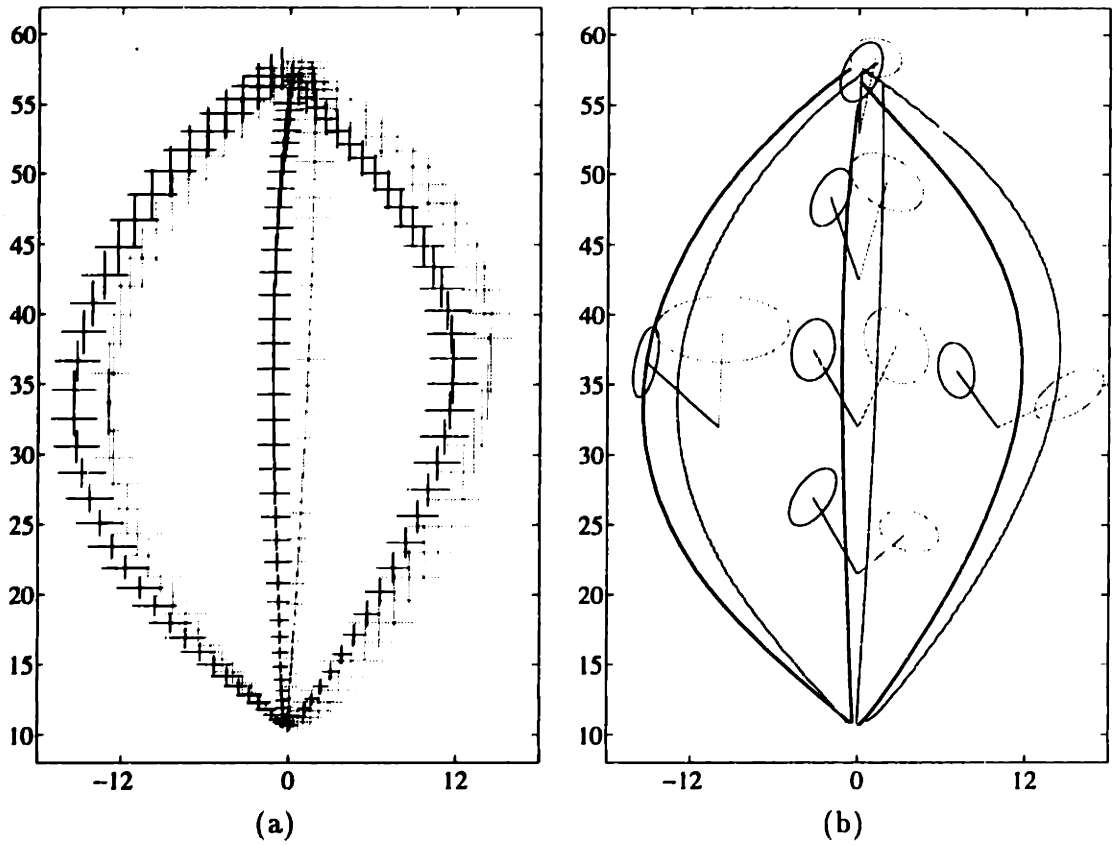

Figure 2-7: Movement trajectories for Subject MF in the Right-Left group. (a) Each cross-hair represents the mean and standard deviation at one time point. Trajectories were normalized in time before averaging. (b) Average paths along with 95% confidence ellipses for end point locations. Black is for the first test block (Left shift), Gray for the second (Right shift).

adaptation.

Figure 2-7 shows average movement trajectories for a typical subject in the Right-Left group. The paths for two testing periods show a significant difference beyond what would be expected as a result of the small shifts in end point location. Panel (b) shows the average paths superimposed upon the 95% confidence ellipses for the same subjects end point locations. Note that although the no-obstacle trajectories are clearly separated and tend toward the end point ellipses, they do not pass directly through them. This latter possibility would be predicted if path planning were completely specified in visual space and then converted to intrinsic coordinates via the same visuomotor map that is reflected in end point adaptation. We will return to this issue in the discussion at the end of the chapter.

Although Figure 2-7 shows clear changes in the paths between the two phases of the

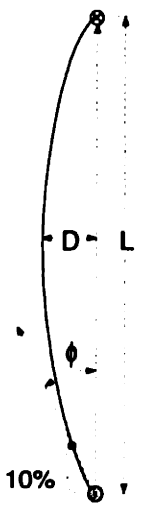

Figure 2-8: Measures of path curvature for Experiment 2.1.

experiment, the fact that there is some end point adaptation at the 100% mark makes it more difficult to interpret these changes. To overcome this problem, we will define two measures of path curvature which are independent the overall direction of the movement, as shown in Figure 2-8. The *linearity index* of a movement is the ratio of the maximum deviation from the line connecting the start and end of the movement to the length of that line, D/L (Atkeson and Hollerbach, 1985). The quantity D is signed: negative for leftward deviation, positive for rightward deviation. The *initial angle*, ϕ, of the movement is the angle between the start-to-finish line and the line connecting the start of the movement to the path at 10% of the total path length. Clockwise differences are defined as positive, so that the sign of ϕ will agree with the sign of the linearity index.

In the case of obstacle trials, the initial angle of movement is not a sufficiently sensitive test of adaptation: as Figure 2-7 shows, even when there is a significant difference in the deviation from straight line, the initial angles are roughly the same due to the overall high degree of curvature. For these trials we used as a second measure of adaptation the obstacle *clearance*, defined as the distance along the X axis from the obstacle to the path at the 50% mark. The clearance is positive when the path passes to the right of the obstacle tip, negative when it passes to the left. This convention was chosen so that the sign of the clearance would agree with the other two measures of path curvature.

The path statistics described above were calculated for each obstacle trial (left obstacle and right obstacle) and for each test trial to the 100% mark (no obstacle). Positive values of the linearity index and initial angle correspond to the path bowing out to the right,

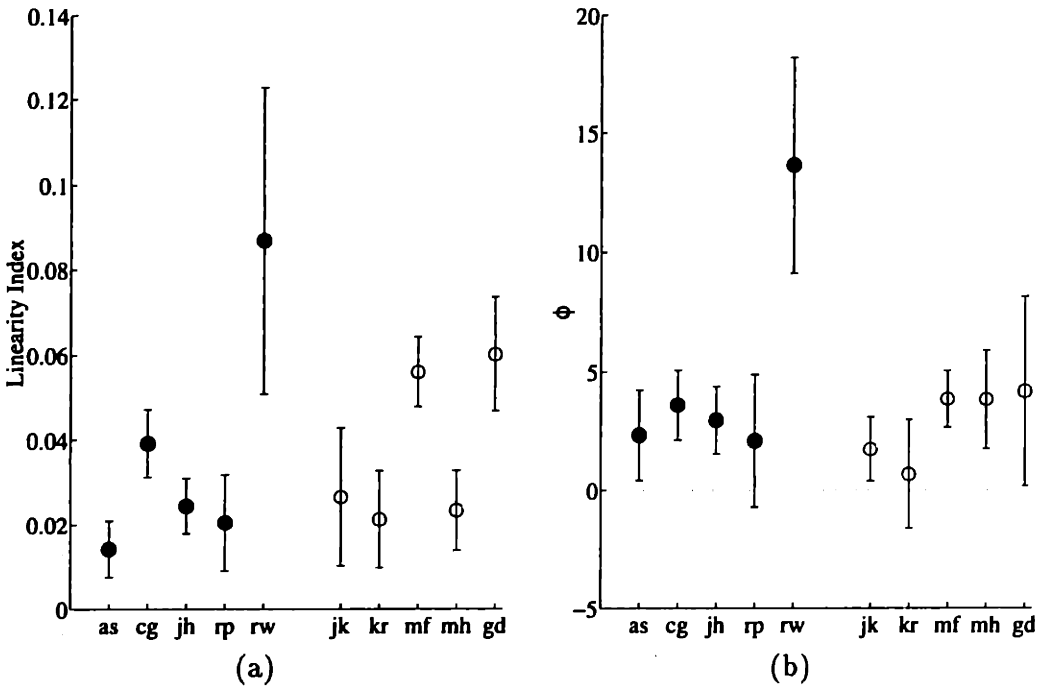

Figure 2-9: Trajectory Adaptation in no obstacle test trials, Experiment 2.1. Mean (s.d.) difference in no obstacle linearity index and initial angle between Left Shift and Right Shift test blocks for each subject. Filled circle: Left-Right, Open circle: Right-Left.

which we would expect to be the result of trajectory adaptation to the leftward prism shift. Conversely, the rightward shift should make these measures more negative. For each subject and each obstacle condition, we present the difference in the value of the statistic between the Left Shift test block and the Right Shift test block. Positive differences in all measures are a sign of trajectory adaptation.

Trajectory adaptation in no obstacle trials can be seen in Figure 2-9. The change in linearity index is significantly positive for every subject, with a mean (s.e.) over subjects of 0.037 (0.007). The initial angle adaptation is also positive for every subject, mean (s.e.) 3.8°(1.1°).

Adaptation in the right obstacle condition can be see in Figure 2-10. The change in both in linearity index and clearance are positive for all but one subject and are typically significantly greater than zero. The mean (s.e.) adaptation is 0.09 (0.01), linearity index, and 3.7cm (0.7cm) clearance.

Finally, adaptation in the left obstacle condition can be see in Figure 2-11. Here, four subjects (two in each experimental group) show a negative change in the linearity index

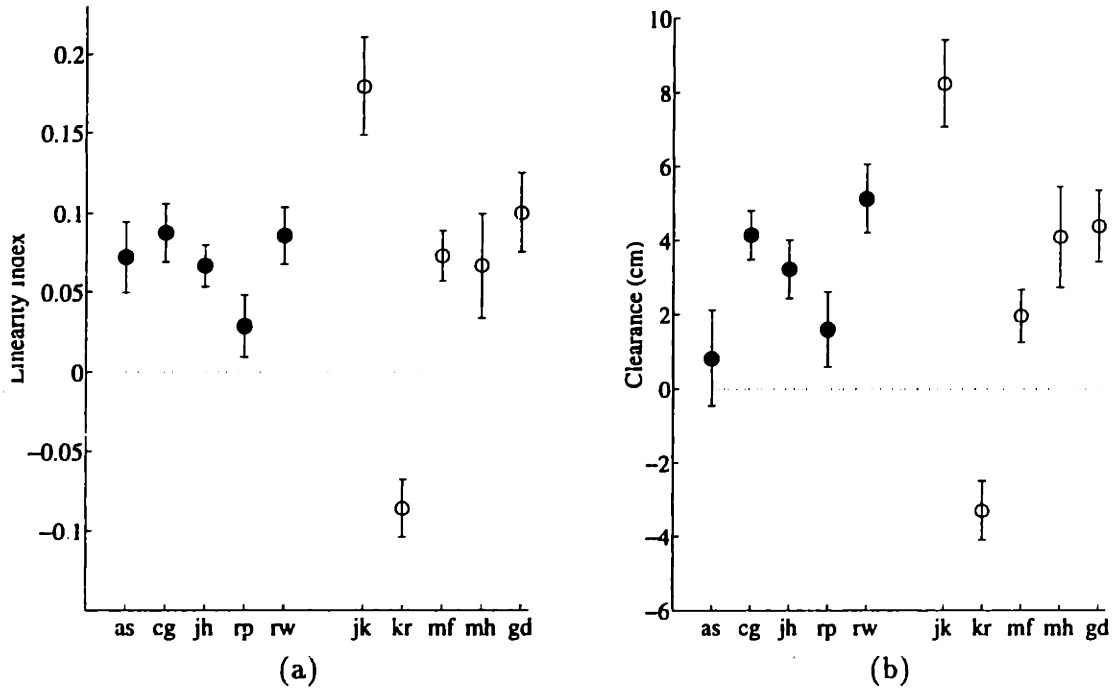

Figure 2-10: Trajectory Adaptation in right obstacle, Experiment 2.1. Mean (s.d.) difference in no obstacle linearity index and clearance between Left Shift and Right Shift test blocks for each subject. Filled circle: Left-Right, Open circle: Right-Left.

between the left shift and right shift test phases, the opposite of what would be expected as a result of the prism shift. Two of those subjects (one in each experimental group) also showed negative change in the clearance. Nonetheless, the average across subjects for both measures of adaptation were significantly positive: 0.048 (0.008) linearity index and 2.6cm (0.5cm) clearance.

Figures 2-9 to 2-11 show an unambiguous change in curvature between the two testing phases. In order to assess how much of that change is due to the visual perturbation, we performed analyses of variance on these data. For the no obstacle condition, a 2-way anova on linearity index with one between subjects variable, Experimental Group, and one within subjects variable, test phase (Left Shift, Right Shift), resulted in a significant main effect for test phase ($F(1,8)=22.8, p= 0.001$), with a large effect size $R^2= 0.96$. No other effects were significant. In the obstacle case, we performed a 3-way anova on clearance with one between subjects variable, Experimental Group, and two within subjects variables, test phase (Left Shift, Right Shift) and obstacle direction (Left, Right). This analysis resulted in a significant interaction between prism and obstacle ($F(1,8)=14.8, p= 0.005$), $R^2= 0.94$. No

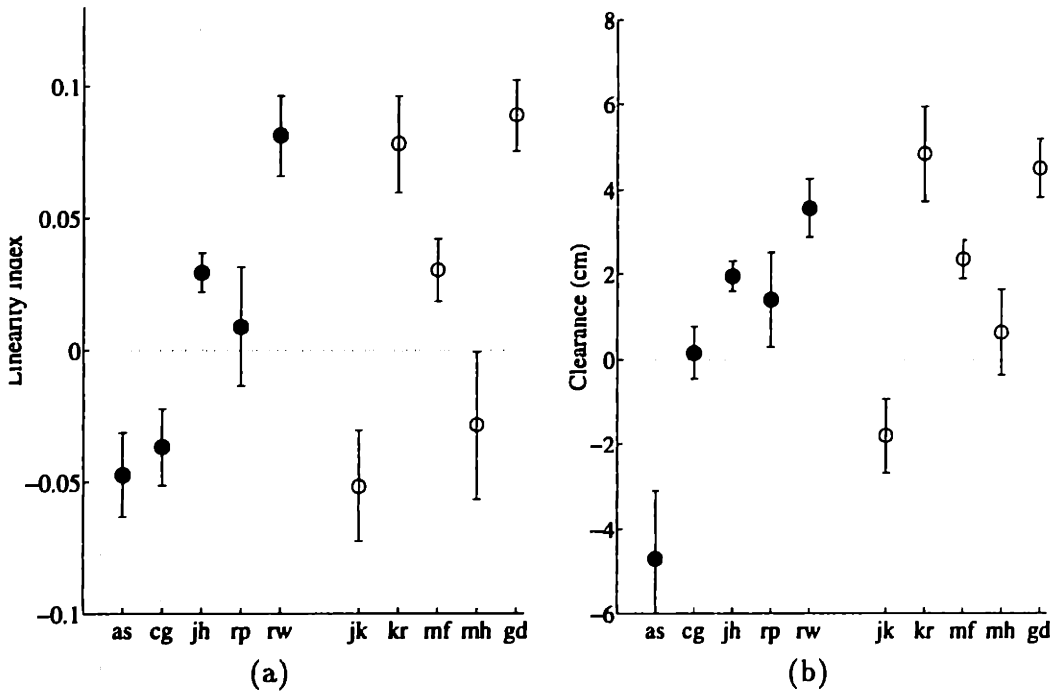

Figure 2-11: Trajectory Adaptation in left obstacle trials, Experiment 2.1. Mean (s.d.) difference in no obstacle linearity index and clearance between Left Shift and Right Shift test blocks for each subject. Filled circle: Left-Right, Open circle: Right-Left.

other effects were significant. In both anovas, the effects are consistent with the hypothesis that trajectories adapt to follow the change in the end point visuomotor map. Furthermore, qualitatively similar results were found when the other measures of curvature.

2.3 Discussion

The main result of this chapter is that movement end point adaptation due to spatially localized visual perturbations affects changes in movement path. When the transverse component of the end point error depends non-linearly on the distance along the sagittal direction, sagittal pointing movements exhibit a similar, though reduced, non-linear deformation. In other words, the trajectory follows the inverse kinematic map.

Evidence for Explicit Cartesian Planning

The dependence of the movement path on the organization of the static visuomotor map suggests that the path is explicitly planned in Cartesian space. This extends the conclu-

sions of other recent visual perturbation studies (Wolpert et al., 1995; Flanagan and Rao, 1995). In previous studies, visual feedback was available throughout the movement. To illustrate the significance of this fact, consider again the model of Jordan et al. (1994) (c.f. Section 1.5). The feature of the model relevant here is that although the movement criteria are visually defined, the movement plan does not make explicit use of the inverse kinematics (i.e. it is a model of implicit visual planning). Such a model would be expected to exhibit adaptation when the perturbed feedback is available throughout the movement, as the visually perceived trajectory no longer satisfies the controller desiderata. However, it would not necessarily be expected to exhibit the adaptation seen in this study, as there was no visually perceived path to drive the error cascade.

Returning to the various models of the Cartesian planner discussed at the beginning of this Chapter, these results are inconsistent with a minimal model in which only the initial and final positions of the movement are specified extrinsically. Distinguishing between the preplanning of the entire path and a discrete set of control points is difficult, but the data do address the issue. We noted above that the path adaptation was much smaller than the end point adaptation. If we measure the maximum path separation between the average Left and Right phase no obstacle trials, we find a mean (s.d.) separation of 2.8cm (1.4cm) across subjects. Comparing this to a mean 50% mark end point adaptation of 6.0cm (2.4cm), we would be tempted to conclude that there was about a 47% transfer from end point adaptation to movement path. However, it is important to note that the maximum path separations did not occur at the 50% mark. In fact, for every subject the point of maximum separation was greater than 60% along the path, with a mean (s.d.) of 78% (8%) over subjects. If we compare the path separation and end point adaptation at the point of maximum separation,[2] we see a larger effect, with an average of 69% transfer from end point to path. Furthermore, across subjects there is a highly significant correlation between the maximum separation and the end point adaptation at that point. This relationship can be seen in the scatter plot of Figure 2-12(a). For comparison, Figure 2-12(b) shows no significant correlation between path separation and end point adaptation at the 50% mark.

These observations are consistent with a model of planning in which only a discrete set of

[2]To calculate end point adaptation at the point of maximum path separation, values from measured points were linearly interpolated along the Y-axis.

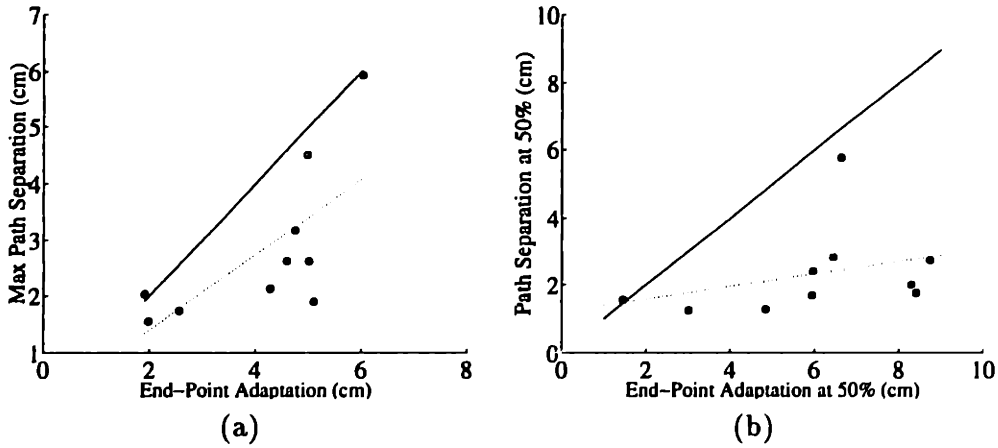

Figure 2-12: The relationship between path and end point adaptation in Experiment 2.1. (a) Maximum path separation between Left and Right phase no obstacle trials vs. end point adaptation at that point. (a) Path separation vs. end point adaptation at the 50% mark. The solid line is $X = Y$. The dashed line is least squares best fit to the data.

control points is chosen in Cartesian space. Numerous researchers have argued that pointing movements are composed of a series of progressively smaller submovements (Crossman and Goodeve, 1983; Meyer et al., 1982; Milner, 1992). These models predict that the first subunit would terminate well beyond the 50% mark of a movement. If each submovement were intrinsically planned, with only the initial and final locations specified in extrinsic space, we would expect to see the pattern of path adaptation described above.

Generalization of Prism Adaptation

An ancillary result of our experiment is the nature of the generalization of the end point remapping to points outside those viewed during the exposure phase. As our findings bear directly on a recent debate in the literature, it is worth discussing them here. Bedford (Bedford, 1989) argues that changes in the visuomotor map are constrained to be linear. Her experiments require subjects to point with a rod fixed at the proximal end along a horizontal arc centered at the subject's head. In three of her four experiments, only one or two exposure points are given, and a linear mapping would be consistent with the exposure. In her last experiment, subjects are exposed to a prism shift at three locations. The magnitude of the shift was not a linear function of the angular position of the points, yet Bedford found that post-exposure pointing errors were roughly a linear function of angular location. However, there was also a significant "leveling off in the regions outside training", i.e. the shift decayed

beyond the region of exposure (Bedford, 1989). This latter effect was found to dominate when subjects pointed freely in the horizontal plane. (Ghahramani, 1995; Ghahramani et al., 1996) showed local adaptation of the visuomotor map, that is exposure at one point led to aftereffects which decayed with distance from the exposed location. Our results are inconsistent with Bedford's claim that visuomotor remapping is restricted to linear transformations, as can be seen in Figure 2-6. On the other hand, the local adaptation we observed agrees with the findings of Ghahramani and colleagues.

In summary, we have shown that a reorganization of the visuomotor end point map results in a corresponding adaptation in the movement path. These results provide evidence for the explicit planning of arm movements in extrinsic Cartesian space and for the use of the static end point map in converting that plan into intrinsic motor commands.

Chapter 3

The Effect of Visual Feedback on Movement Velocity

3.1 Introduction

In Chapter 2 we provided evidence for the Cartesian planning of movement path. We now want to address the issue of the temporal component of movement. Are movement velocities also preplanned by the CNS, or they an emergent property of the lower levels of the control hierarchy?

As discussed in the Chapter 1, invariances in human movement, across subjects and across a variety of conditions, suggest that the relevant attributes are planned by the CNS. This argument has been applied to the planning of velocity profiles in both point-to-point arm movements and rhythmic drawing and tracing behavior to argue for the planning of velocities. Point-to-point movements tend to exhibit bell-shaped velocity profiles (Morasso, 1981), even when moving at different speeds and while under inertial load (Soechting and Lacquaniti, 1981; Atkeson and Hollerbach, 1985). When the path of a pointing movement is curved, for example to avoid an obstacle, it still exhibits stereotypical velocity profiles, reminiscent of the superposition of bell shaped segments with boundaries at the high curvature regions (Abend et al., 1982; Morasso, 1983). A different regularity in velocity profiles holds for rhythmic movements such as drawing and handwriting: the tangential velocity varies with the inverse of the instantaneous curvature of the path (Viviani and Terzuolo, 1982). Lacquiniti et al. (1983) formulated the 2/3 power law to account for this observation. The

power law states that the velocity of the end-point is explicitly determined by the curvature through the relationship $V = KC^{-\frac{1}{3}}$.[1] This relationship implies that the trajectory is completely determined by the desired path, up to an overall scaling of tempo. The various versions of the 2/3 power law can account for the observed velocity profiles of a wide range of cyclic and drawing movements (e.g. Lacquaniti et al., 1983; Viviani and Cenzato, 1985; Viviani and Flash, 1995).

However, these observations do not distinguish whether the regularities seen in the velocity profiles of human movements are planned by the CNS, or whether they are an emergent property of lower levels of the control hierarchy, including the inertial and viscoelastic properties of the arm. Current researcher is divided on whether the velocity of movement is centrally specified.

For point-to-point movements, optimal control models such as minimum jerk (Hogan, 1984; Flash and Hogan, 1985) and minimum torque change (Uno et al., 1989) posit that the CNS implicitly plans the velocity of movement. Others have modeled complex hand and arm movements by the composition of temporally overlapping submovements with stereotyped symmetric velocity profiles (Morasso et al., 1983; Milner, 1992). On the other hand, the Equilibrium Point Control Hypothesis holds that the velocity profile of pointing movements are due, at least in part, to the viscoelastic properties of the arm (Mussa-Ivaldi et al., 1985; Flash, 1987; Bizzi et al., 1992). Finally, a recent model by Jordan et al. (1994) shows that the stereotyped velocity profiles seen in reaching movements can emerge from a hierarchically organized adaptive controller whose error criteria are purely path dependent.

For rhythmic movements there is a similar dichotomy of opinions. The most prominent model is the 2/3 power law, which is usually interpreted as describing a centrally imposed constraint on the movement trajectory. However, a recent computational study has shown that the relationship between curvature and velocity can be explained by the dynamic properties of the arm (Gribble and Ostry, 1996).

The resolution of this issue is not likely to come from more observational studies and the modeling of their data. Even if models such as minimum jerk and the 2/3 power law can account for most of the existing experimental data, we can not be sure that they are not merely descriptive, a concern that is heightened by studies such as (Gribble and Ostry,

[1] Note that the "2/3" refers to the exponent in the relationship between angular velocity and curvature, which translates to a exponent of -1/3 for tangential velocity.

1996). Yet showing that observed invariances can be accounted for by the arm's dynamic properties does not rule out the possibility that the CNS maintains those properties at the higher level as well. In fact, it is a plausible argument that since the planner evolved in conjunction with the plant, and we should expect that the movements which are most easily executed are those which the CNS chooses.

These concerns have been dealt with effectively in the investigation of path planning through the use of perturbation studies. The results of Chapter 2 and similar experiments have provided strong support for the notion of Cartesian path planning. Here we employ a similar strategy in the investigation of velocity planning. We will perturb the perceived velocity of subjects' movements without substantially altering the path and measure the degree to which they adapt their behavior in order to bring their visually perceived velocities back to the pre-movement baseline. We present two experiments focusing on both curved, cyclic movements and obstacle avoidance movements. We find that in the case of rhythmic movements, subjects do not adapt their velocity profiles in response to changes in the strength of the power law of the visual feedback. However, adaptation does occur in response to a velocity skewing perturbation in obstacle avoidance reaching movements.

3.2 Velocity Feedback Perturbations in Rhythmic Movement: Experiment 3.1

The 2/3 power law specifies that the tangential velocity of movements should vary according the curvature of the path. If the law reflects the planning constraints employed by the CNS, we would expect that changes to the relationship in the visually perceived velocity of movements should engender a subsequent modification of behavior to compensate for those changes, i.e. adaptation. The strategy of this experiment is to artificially modify the strength of the dependence of visual feedback velocity on path, either by flattening the perceived velocity or strengthening its peaks and valleys. We then look for adaptation in the behavior of the subject, both with and without visual feedback.

The experiment consisted of three phases: pre-perturbation, perturbation, and post-perturbation. If the variations in velocity are planned by the CNS, we would expect a change in behavior during the perturbation phase which should dissipate during the post-perturbation phase.

In addition to monitoring motor performance, we tested the affects of the velocity perturbation on the perception of motion velocity. Viviani and Stucchi (1992) asked subjects to adjust the velocity of a cursor moving around an ellipse or a pseudo-random scribble so that the velocity was constant. In fact, subjects were changing the exponent of the power law, with a value of zero being the target value. They found that subjects were consistently biased in the direction of the 2/3 power law and argued that this effect reveals both that the perceptual mechanism has access to the motor control processes responsible for the movement constraint and that for some reason motion which obeys this constraint looks constant. We reasoned that if Viviani and Stucchi's interpretation was correct and feedback perturbation altered the law of movement, then it should also alter the perceptual mechanism. Thus, we tested subjects with a modified version of their task after each of the three phases of the experiment.

3.2.1 Methods

14 subjects participated in this experiment. Subjects were randomly divided into two groups,[2]whose treatments differed in the direction of the perturbation used. All subjects were right handed, had normal or corrected to normal vision, and were naive as to the purpose of the experiment.

The experiment was conducted with the virtual visual feedback apparatus described in Appendix A. Movements were performed in the dark, and subjects did not have direct view of their arm and hand, but received visual feedback in the form a 1cm radius circle of light whose virtual image could be located at the position of the finger tip or at some offset from that location. The position of the finger was monitored with a Northern Digital Optotrak infrared position monitoring system at 144 HZ, twice the refresh rate of the VGA projector.

The experiment consisted of two kinds of trials, motor and perceptual. These will be described in the following sections.

Motor Trials

In motor trials, subjects were asked to trace their finger along the outline of an ellipse projected onto the virtual plane of the table. The figure was centered 30cm in front of

[2]Group one: 1M, 4F, age range, 19-31yrs. Group one: 2M, 7F, age range, 18-40yrs.

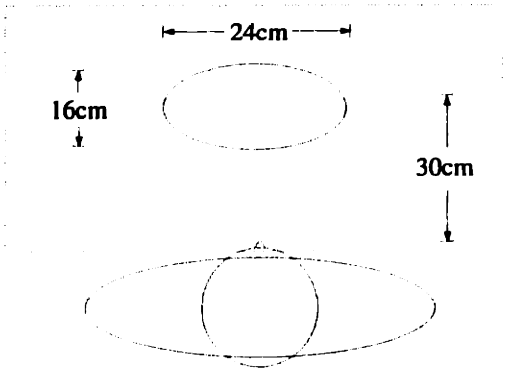

Figure 3-1: The experimental design for Experiment 3.1.

the subjects' eyes along the midline, with a major axis of 24cm and a minor axis of 16cm. The arrangement is shown in Figure 3-1. Subjects were instructed to move smoothly and continuously around the ellipse and were told that accuracy was not important. This latter instruction was given to avoid having subjects make intermittent corrective movements, which typically display many small velocity peaks. Subjects were told that the goal of the experiment was to learn to move around the ellipse at a certain tempo, which would be held constant throughout the experiment. When a trial began, a small white circle appeared at the rightmost point of the ellipse. Subjects were instructed move into this "starting circle" and wait while they heard a series of 5 equally spaced tones which defined the target tempo. The tones sounded every 1500ms. The fifth and final tone was higher pitched, signalling subjects to begin moving. The purpose of introducing the target tempo was to attempt to hold constant the overall timing of the movements across the experiment. Pilot studies indicated that subjects tended to increase the rate of movements during the experiment, and we wanted to avoid this confounding variable. Setting a target tempo has the additional benefit of encouraging subjects to pay attention to the rate of movement, which could heighten the effect of any perturbation to the perceived velocity.

Each motor trial consisted of 10 counter-clockwise loops around the ellipse. After the final loop, a tone sounded and the screen blanked. Subjects could then rest as long as they wanted before the next trial began, though they never rested for more than a few seconds. Motor trials came in blocks of four, the first three with visual feedback (FB), the fourth with no visual feedback (NO-FB).

Visual Perturbation

Statistics on the movement velocity profiles during pre-perturbation phase were used to compute a positional perturbation as described in Appendix B. The perturbation was chosen in the following fashion: if $v(\theta)$ is the average velocity as a function of angular position during the pre-perturbation phase, and $\bar{v}$ is the mean of that profile, than the desired velocity perturbation was

$$\delta_v(\theta) = \alpha(\bar{v} - v(\theta)). \tag{3.1}$$

If the magnitude of the perturbation was $\alpha = +1$, then the cursor would appear to be moving at a constant velocity. On the other hand, if the perturbation magnitude was $\alpha = --1$, the deviations from the mean velocity would be accentuated by a factor of 2.

The two experimental groups in this study experienced perturbations with magnitudes $\alpha = +1$ and $\alpha = --1$, and they will be referred to as the +1 Group and the -1 Group, respectively.

Perceptual Trials

The perceptual trials in this experiment were adapted from (Viviani and Stucchi, 1992). Trials began with the same elliptical figure appearing on the screen as in motor trials. This time however, the finger cursor was not under the subject's direct control. The cursor traced out the path of the ellipse with a velocity profile equal to

$$v_p(\theta) = \bar{v} + \beta(\bar{v} - v(\theta)) \tag{3.2}$$

where $v(\theta)$ and $\bar{v}$ are the average velocity profile and its mean from the motor trials of the pre-perturbation phase, i.e. the quantities from Equation 3.1. The parameter β was initially set to a random value chosen uniformly from the interval $[-3, 3]$. During a perceptual trial, subjects could change the value of β with a trackball.

Before the experiment began, subjects were shown that when the trackball was rotated to the left the cursor would move very slowly around the left and right ends of the ellipse and very quickly past the top and bottom (large negative values of β). On the other hand, when the trackball was rotated to the right (large positive values of β) the cursor would display

the opposite behavior. Subjects were not given an explicit description of the relationship between the trackball position and the cursor velocity, nor were they told that the cursor velocity bore any relationship to their own movements. The task was to adjust the trackball until the cursor moved at a constant velocity around the ellipse.

Experimental Design

Each experiment began with a warm-up session in which subjects practiced the task with no feedback perturbation until they reached an error criterion,[3] but always for at least 2 blocks. During this session they were also introduced to the perceptual task. Each experiment consisted of a pre-perturbation phase (PRE) of 2 blocks, one block during which the perturbation was phased in linearly over the three FB trials, 7 perturbation blocks (PERT), and 3 post-perturbation blocks (POST). After each phase, a set of 5 perceptual trials occurred, totaling 15 perceptual trials. We will also refer to the perceptual trial sets as PRE, PERT, and POST, depending on which motor trial phase immediately preceded them.

Data Processing

To eliminate the effects of startup transients, the first 3 loops of each 10 loop trial were discarded. The raw position data was sufficiently smooth to allow the calculation of velocity by simple first differencing. For higher derivatives, the planar positions of the finger tip were fit with cubic smoothing splines ($\lambda = 0.995$, matlab routine `csaps`), and derivatives were then taken analytically from the spline fit. Curvature of movements was calculated using the equation

$$c = \frac{\sqrt{v_x a_y - v_y a_x}}{(v_x^2 + v_y^2)^{\frac{3}{2}}}$$

where $v_.$ and $a_.$ are the velocity and acceleration in the subscripted direction.

3.2.2 Results

We will begin by analyzing the Motor Trials. Typical paths and velocity profiles for a subject in the +1 Group are shown in Figure 3-2. Note difference between the feedback velocity profiles during the perturbed and unperturbed trials: the peaks and valleys of the

[3]The error criterion was to get within 300ms of the target tempo for two consecutive trials.

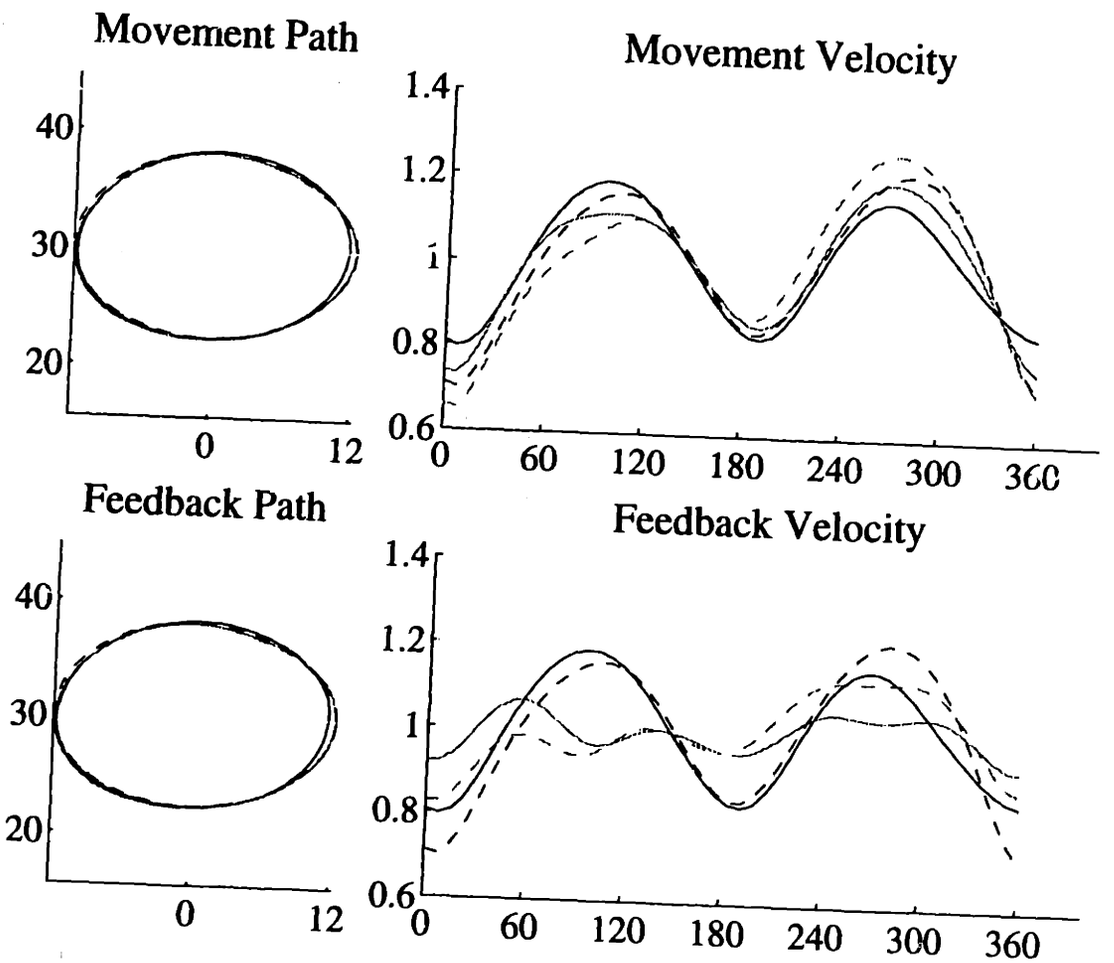

Figure 3-2: Paths and velocity profiles for subject KT in the +1 Group of Experiment 3.1. Each line represent a single block. The top rows are averages over the three FB trials in the block, the bottom row is the average for the NO-FB trial. Solid Black, the final PRE block; Solid Gray the first PERT block; Dashed Gray, the final PERT block; and Dashed Black, the final POST block.

latter are mostly suppressed in the former. The feedback is not completely flattened out because the performance is variable, and in particular changes over time (see Appendix B for further discussion of this issue). A similar array of plots can be seen for a typical −1 Group subject in Figure 3-3. Notice that here the peaks and valleys are accentuated in the perturbed feedback.

To assess the degree of adaptation, we will first examine three statistics derived from the velocity profiles and look for changes in their in values over the course of the experiment. These results show clearly that behavior is not adapted to maintain the power law. In the next section, we will present a more direct comparison the velocity profiles which will show that in fact there were no changes in behavior.

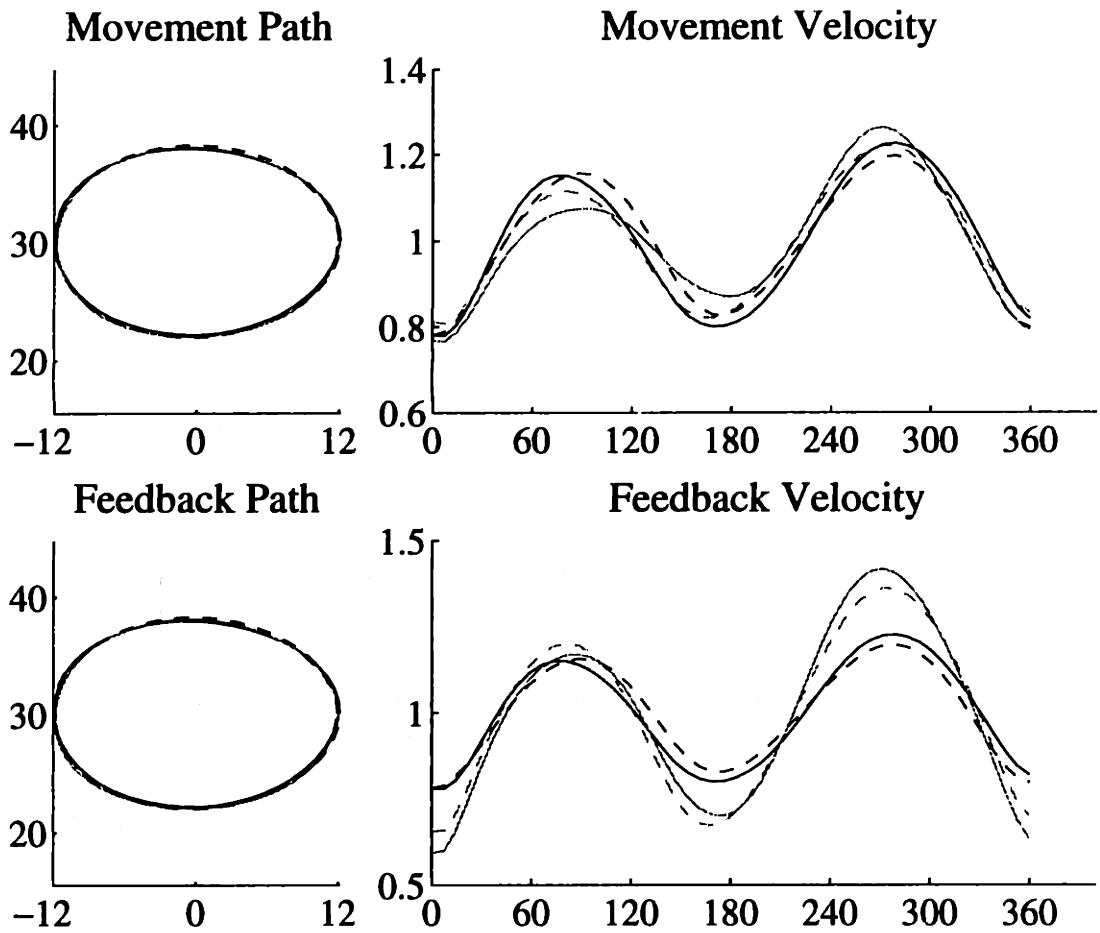

Figure 3-3: Paths and velocity profiles for subject KT in the −1 Group of Experiment 3.1. Each line represent a single block. The top rows are averages over the three FB trials in the block, the bottom row is the average for the NO-FB trial. Solid Black, the final PRE block; Solid Gray the first PERT block; Dashed Gray, the final PERT block; and Dashed Black, the final POST block.

Summary Statistics

We begin by addressing directly the issue of the 2/3 power law. In order to assess the degree to which subject adapt to changes in the perceived power law, we will consider three statistics which relate the velocity profile to the to path.

Power Law Exponent and Correlation: For each movement set, the tangential velocity and path curvature were computed for every time step and the log of the velocity was regressed on the log of the curvature. The resulting slope is the power law exponent, β, which is predicted to have the value $-1/3$ by the 2/3 power law. We also computed the correlation coefficient, r, for the regression. Note that the $\alpha = +1$ perturbation would reduce both values to zero for the perturbed visual feedback if perturbation were perfect. Conversely, the $\alpha = --1$ perturbation would be expected to increase β. If the movements exactly obeyed the power law, r would more or less double.

Peak to Valley Ratio: For each movement set, the two highest peaks and the two lowest valleys of the tangential velocity profile were identified. The velocity values of each pair were averaged, and the ratio of the peak height to Valley height was computed, PVR.

The results are summarized in Figures 3-4 to 3-9. Each plot shows the value of a single statistic for each of the 13 blocks of the experiment. The solid circles represent values for the actual movement, averaged over the three FB trials per block. The open circle represent values for the actual movement in the one NO-FB trial in each block. Finally, the squares represent the statistics for the feedback during the PERT phase. Each data point is the mean over all subjects in that appropriate experimental group, with error bars representing standard errors. The grey blocks on the plots represent the periods when the perturbation was in effect. The narrow lighter gray patch to the left lies over the one trial block when the perturbation was being phased in.

The horizontal lines in each plot provide an estimate of how much we expect the perturbation to alter the value of the statistic. To compute these estimates, the trajectories from the last PRE phase and the last POST phase trials were chosen as baselines. For each of these trials, we computed what the perturbed feedback *would have been* had it been a PERT trial. Then the summary statistics were computed on these fictive feedback trajectories. The resulting value is a measure of what the statistics would be expected to be for the perturbed feedback if subjects behavior is unaffected by the perturbation. In each plot, the black line represents the pre-perturbation baseline, the grey line the post perturbation

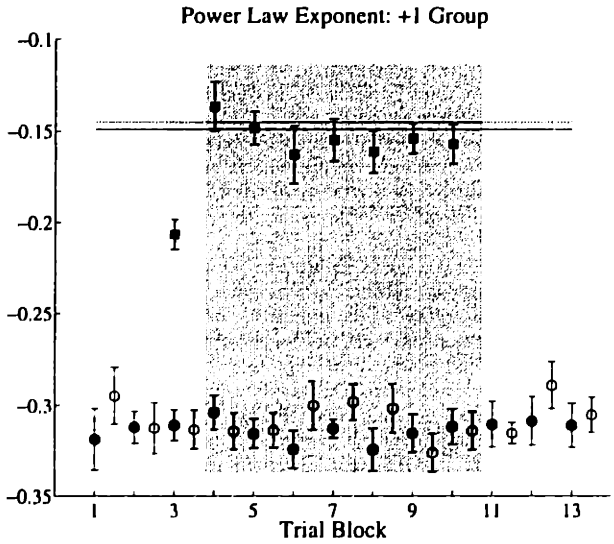

Figure 3-4: The best fit power law exponent, β, for the +1 Group, Experiment 3.1. Solid circles, FB movements. Open circles, NO-FB movements. Squares, perturbed feedback. The gray region covers the PERT phase. The horizontal lines are the PRE (black) and POST (gray) perturbation baselines (see text for details).

baseline.

+1 Group: Figures 3-4 and 3-5 show the results of fitting a Velocity/curvature power law to the movements of the +1 Group. The power law is obeyed, with a mean correlation coefficient of r=-0.83 over FB trials and r=-0.76 for NO-FB trials. The mean power law exponent over all subjects in this group was $\beta = -0.31$ both for FB and NO-FB movements. The perturbation greatly reduced the adherence to the power law of the feedback, with r=-0.59 and $\beta = -0.16$. Despite this fact, the figures show that there was no significant effect of the feedback on the behavior: the statistics for the movements remain constant throughout the experiment, and the perturbed feedback values never get significantly below the baselines.

The mean peak to valley ratio for the +1 Group was PVR=1.49 for FB trials and PVR=1.41 for NO-FB trials. The perturbation lowered this value in the feedback to PVR=1.22. Figure 3-6 shows the block by block behavior of the statistic. Here, the perturbed feedback does seem to reach a value lower than the error baselines, and it looks as if the PVR for FB movements is slightly lower during the PERT phase then the other phases. However, the there is no change in the PVR's for the NO-FB during the experiment. We will return to these data below with a more analytic test for adaptation, but the initial assessment is that there is no sign of adaptation.

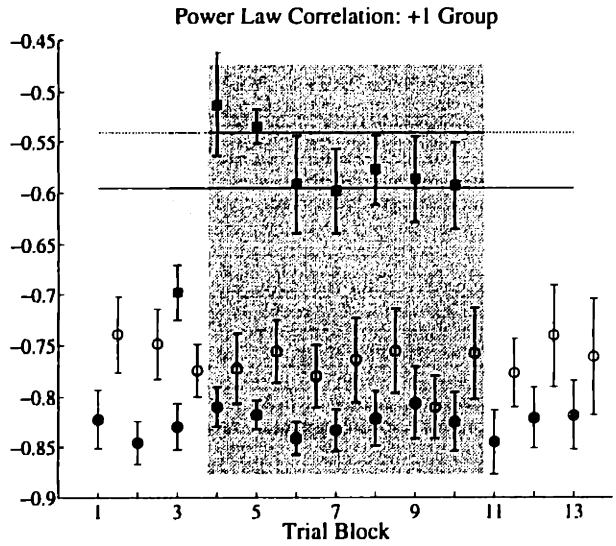

Figure 3-5: The power law correlation coefficient, r, for the +1 Group, Experiment 3.1. Solid circles, FB movements. Open circles, NO-FB movements. Squares, perturbed feedback. The gray region covers the PERT phase. The horizontal lines are the PRE (black) and POST (gray) perturbation baselines (see text for details).

−1 Group: Figures 3-7 and 3-8 show the results of fitting a Velocity/curvature power law to the movements in the $\alpha = - - 1$ group. Again, the movements obey the power law, with a mean r of -0.81 over FB trials and -0.77 NO-FB trials. The mean β over all subjects in this group was -0.30 for FB trials, -0.34 for NO-FB trials. These results are nearly identical to the values for the +1 Group. In this case, the perturbation increased the strength of the power law in the feedback. During the PERT phase, the feedback correlation increased slightly to r=-0.86 with a larger exponent of $\beta = -0.15$. Again, despite this fact, the figures show that there was no significant effect of the feedback on the behavior. The movement statistics remained roughly constant during the perturbation, and the perturbed feedback values never rise above the baselines.

The mean values of the peak to Valley ration for the -1 Group are PVR=1.45 for FB trials and PVR=1.39 for NO-FB trials, also similar to the Group 1 behavior. The perturbation increased this value in the feedback to PVR=1.85. Figure 3-9 shows the block by block behavior of the statistic. As with the +1 Group, there seems to be an initial rise in the PVR as a result of the perturbation, but the PVR returns to baseline PERT phase. The feedback PVR never falls significantly below the post perturbation baseline. Finally, the negative slope in the perturbed feedback values is part of an over all trend toward a lower PVR, which was also seen in Group 1, and will be discussed further in the next section.

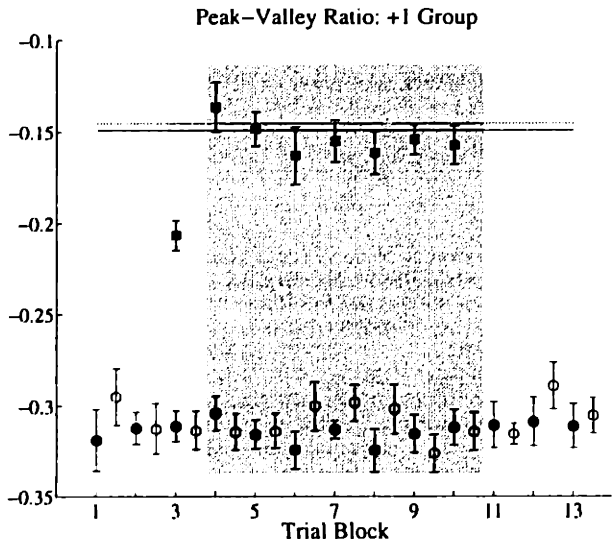

Figure 3-6: The peak to valley ratio, PVR, for the +1 Group, Experiment 3.1. Solid circles, FB movements. Open circles, NO-FB movements. Squares, perturbed feedback. See text for more details.

Again then, our initial assessment is that there is no sign of adaptation.

To quantitatively assess the statistical significance of the any changes in behavior indicative of adaptation, we performed a contrast analysis on the statistics described above (Rosenthal and Rosnow, 1985). The weighting by trial block was chosen to detect U-shaped changes in the location of the landmark over the three phases of the experiment:

$$\lambda = [\frac{1}{5}, \frac{1}{5}, 0, -\frac{1}{7}, -\frac{1}{7}, -\frac{1}{7}, -\frac{1}{7}, -\frac{1}{7}, -\frac{1}{7}, -\frac{1}{7}, \frac{1}{5}, \frac{1}{5}, \frac{1}{5}]. \tag{3.3}$$

Four separate contrasts were performed on each statistic, for FB and NO-FB trials in each experimental group. In accordance with our informal observations above, none of the 12 contrasts was significant with the exception of the PVR of the FB trials in the +1 Group, which had $t(109)=3.34$, $p= 0.0006$.

There are several reasons why the change in PVR for the +1 Group should not be taken as a sign of adaptation. First, there was an overall trend toward a lower PVR over the course of the experiment, as can be seen in Figure 3-10. A contrast analysis with linear weights supports this conclusion for all but the NO-FB trials of the +1 Group. A contrast which focuses just on the differences in PVR between the PRE and PERT phases shows no significant effect ($p= 0.47$). Thus the positive result above was due entirely to the low PVR in the POST phase. Secondly, if there was adaptation in the PVR of the movements in the

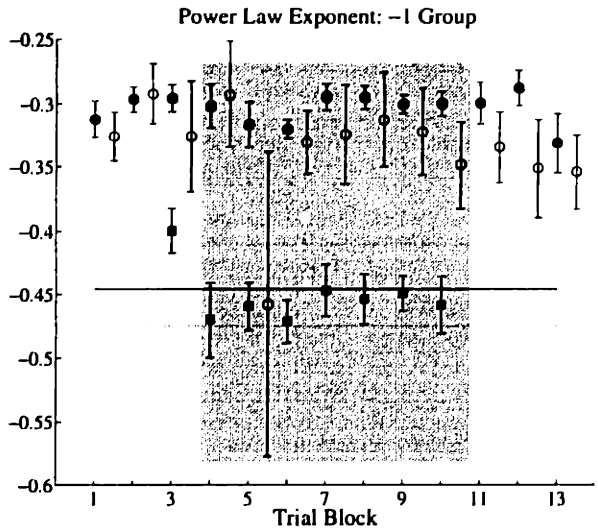

Figure 3-7: The best fit power law exponent, β, for the −1 Group, Experiment 3.1. Solid circles, FB movements. Open circles, NO-FB movements. Squares, perturbed feedback. The gray region covers the PERT phase. The horizontal lines are the PRE (black) and POST (gray) perturbation baselines (see text for details).

+1 Group, this adaptation should have carried over to the NO-FB trials, but there are no effects seen there. Finally, the other movement statistics show no sign of adaptation.

Summarizing the results of this section, there is no adaptation in the relationship between velocity profile and path, as measured by the power law fit and the peak-to-valley ratio. These results imply that the CNS does not directly plan the power law relationship observed in experimental data.

Velocity Profiles

It is possible that the CNS does explicitly plan velocity profiles of cyclic tracing, but that the criteria for the movement plan are not those which relate directly to the power law. In that case, the measures we investigated in the previous section may not capture the right aspects of the velocity profile to pick out the adaptation. Thus, we present a second, model free analysis which uses the absolute difference in normalized velocity profiles as a measure of profile dissimilarity or distance (see Figure 3-11). Adaptation will be assessed by comparing the average velocity over a block to PRE and POST phase baseline velocity profiles. The baselines are chosen to be the last block in the appropriate phase.

We will also compare feedback velocity profiles for the PERT phase to the same movement baselines. We expect these distances to be large due to the effects of the perturbation.

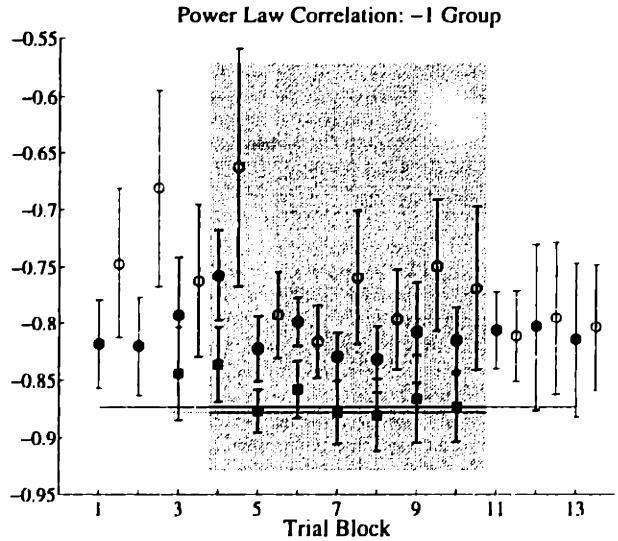

Figure 3-8: The power law correlation coefficient, r, for the −1 Group, Experiment 3.1. Solid circles, FB movements. Open circles, NO-FB movements. Squares, perturbed feedback. The gray region covers the PERT phase. The horizontal lines are the PRE (black) and POST (gray) perturbation baselines (see text for details).

A negative slope in these values over the course of the 7 PERT blocks would be a sign that the feedback velocity profiles were beginning to look more like the baseline movement profiles. This *could* be taken as a sign of adaptation. However, it is possible that the introduction of the perturbation causes transient changes in subjects behavior which disappear after subjects learn to ignore the altered feedback. While this does not constitute adaptation, it would also result in a negative slope in the feedback velocity distances. Thus, we need a different measure of what constitutes having or not having adapted to the perturbation. We will employ the same method used above for the power law statistics: we computed what the feedback of the PRE and POST baseline movements *would have been* had they been perturbed. The distance between the baseline profiles and their fictive feedback profiles serves as a threshold for adaptation: distances below those values for PERT phase feedback imply that the movement has changed in such a way as to bring the feedback closer to the baseline behavior.

Figure 3-12 shows these distance comparisons for the +1 Group, and Figure 3-13 for the −1 Group. The top row of the two figures presents the velocity profile distances for the visual feedback of FB trials. There is no significant slope, and the distances do not stray from the thresholds, implying that behavior was unaffected by the perturbation.

The middle row of the two figures presents the velocity profile distances for the move-

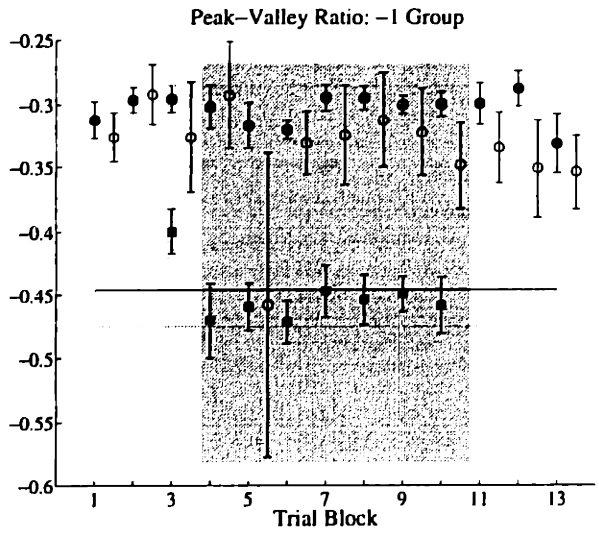

Figure 3-9: The peak to valley ratio, PVR, for the –1 Group, Experiment 3.1. Solid circles, FB movements. Open circles, NO-FB movements. Squares, perturbed feedback. The gray region covers the PERT phase. The horizontal lines are the PRE (black) and POST (gray) perturbation baselines (see text for details).

ments in the FB trials. Note that for the PRE and POST phases, these are the same as the those in the top row. Furthermore, note that two points (blocks 2 and 13) are identically zero. These are the baseline movements themselves. It is clear that movement variation during the PERT phase is well within that seen in the PRE and POST phase.

Finally, the bottom rows represent the NO-FB trials. The baseline velocity profiles are now the single NO-FB trials in blocks 2 and 13. Also, the data points for the PERT phase are the fictive perturbed feedback of the movement, making the plot analogous the Feedback plot on the first row. Again, there is no downward trend and the distances never get below the threshold.

In conclusion, the feedback velocity perturbations had no significant effects on the velocity profiles of subjects movements. Thus, we conclude that CNS does not plan velocity profiles, or at least not the aspects of the profiles which we perturbed.

Perceptual Trials

In perceptual trials, subjects viewed a cursor moving around the ellipse, adjusting a trackball until they determined that the cursor was moving at constant velocity. In fact, the cursor moved around the ellipse with a velocity profile determined by Equation 3.2, where the value of β was controlled by the trackball. A response of $\beta = 0$ corresponds to the cursor

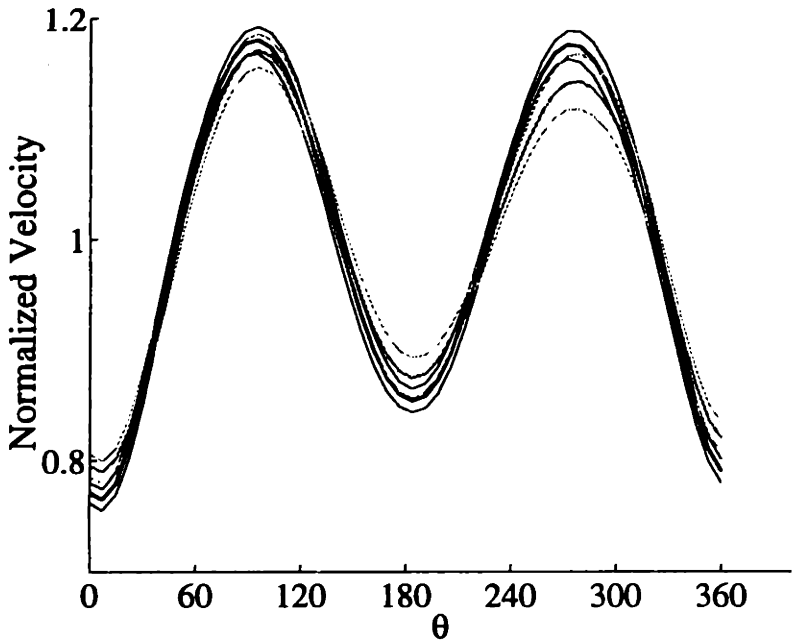

Figure 3-10: Velocity profiles and standard error for the last PRE block (black) and last POST block (grey), averaged over all 14 subjects. Note that there is an overall trend toward smoother velocity profiles as the experiment progresses.

moving at exactly uniform speed around the circle, which would be the optimal response. A response of $\beta = +1$ would correspond to subjects choosing their own average velocity profile as constant speed. Given the results of Viviani and Stucchi (1992), we expect that the pre-perturbation β responses would be significantly greater than zero. If perturbed visual feedback adapts this perceptual mechanism, then we would expect that responses during the PERT set would be different between the two groups: closer to zero for +1 Group and more positive for −1 Group.

The results for the perceptual trials are shown in Figure 3-14. Note first that in the pre-trial phase, the β responses were not significantly different from zero. However, there was a significant trend toward increasing responses as the experiment progressed, and by the end of the experiment, the responses for both groups were significantly positive.

A two-way anova was performed on the responses with 1 between-subjects factor, Experimental Group (E=+1,−1), and one within-subjects factor, Phase (P=PRE,PERT,POST). The overall mean was significantly positive, $F(1,12)=11.2$, $p< .01$, as predicted. The only other significant effect was the phase main effect, $F(2,24)=3.9$, $p= 0.034$, as discussed above. This result suggests that the feedback did not affect the responses made in the perceptual test. In fact, although the Phase by Group interaction was not significant, if we examine

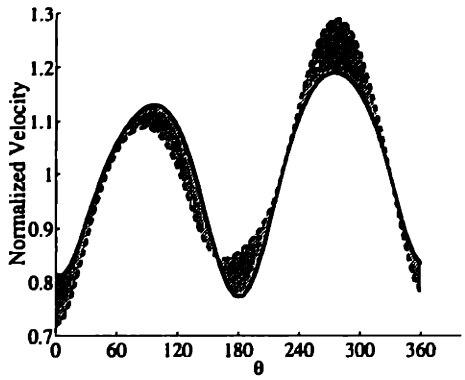

Figure 3-11: The distance measure used in Experiment 3.1 for comparing tangential velocity profiles. First, the profiles are normalized so that average value over the ellipse is unity. The area between two profiles is then taken as the distance between them.

phase-to-phase responses for each Group, we see that the trends are the opposite of what was predicted: the change in β from PRE to PERT was larger for the +1 Group than the -1 Group, and the changes from PERT to PRE go the other way. We conclude that the feedback perturbation had no effect on the subject's perception of constant velocity.

On the other hand, the significant increase in the response bias during the course of the experiment is worth noting. The duration of the experiment was approximately 45 minutes, and it might be expected that subjects would begin to lose concentration over that time. One explanation then is that subjects have the ability to accurately discriminate constant velocity, but that this discrimination requires some degree of effort, and that when the assessment is made with less care, "natural" movements look like constant velocity.

Another explanation is that the act of moving around the ellipse is responsible for the increased bias, independent of the visual feedback. This explanation may seem less likely, as Viviani and Stucchi found a large perceptual bias without asking subjects to make any movements. However, our task differed from theirs in one important respect: while they had subjects chose between movement following various power law relationships, we based our perceptual stimuli directly on subjects' behavior. Thus, if the response bias is due to perceptual penetration of the motor plan, practice could increase the effect.

3.2.3 Comments

The results of this experiment suggest that the 2/3 power law is not planned explicitly by the CNS, or at least is not planned by an adaptable mechanism. This conclusion is consistent

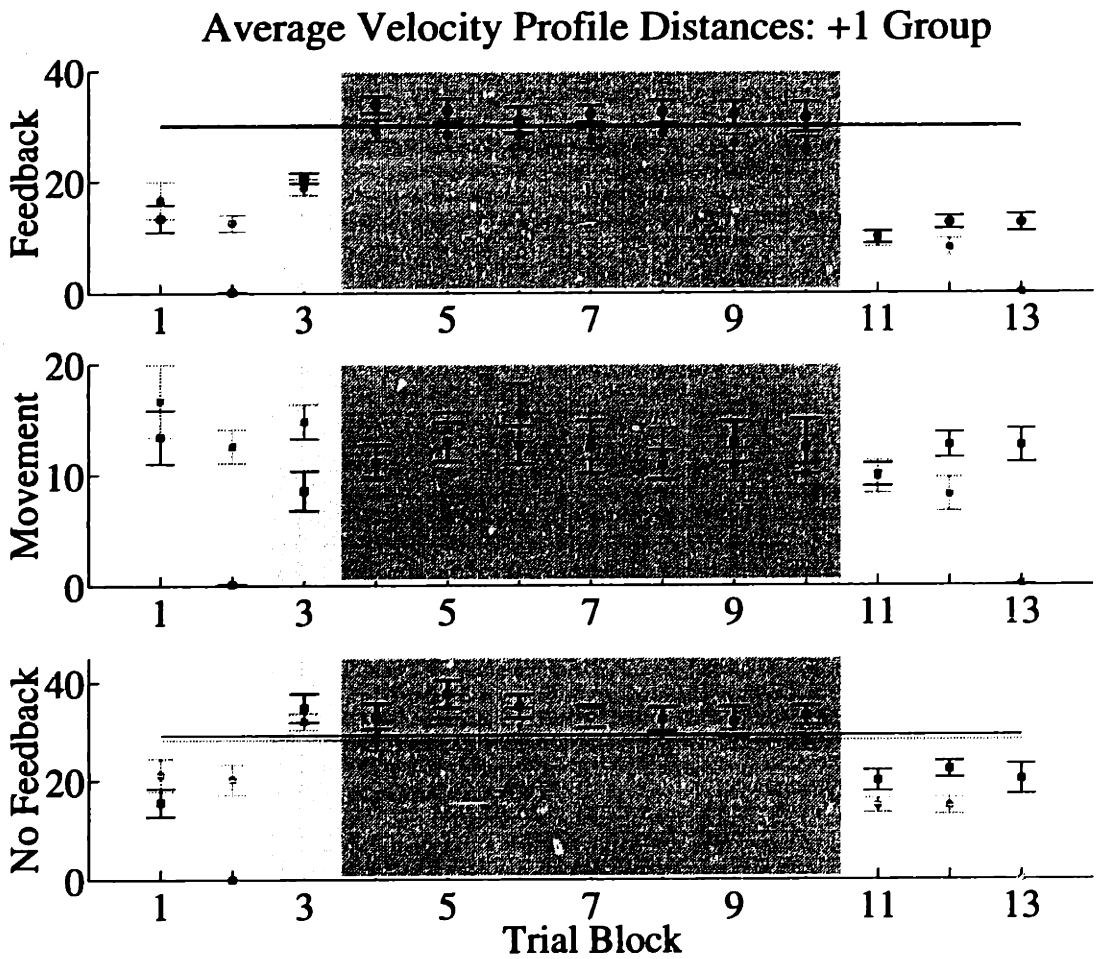

Figure 3-12: Velocity profile comparisons for the +1 Group in Experiment 3.1. The average velocity distances from the PRE (black) and POST (grey) movement baselines. The dashed lines in the top and bottom plots represent a threshold for adaptation: the distance from the movement baselines to the their fictive perturbed feedback. The gray region covers the PERT phase.

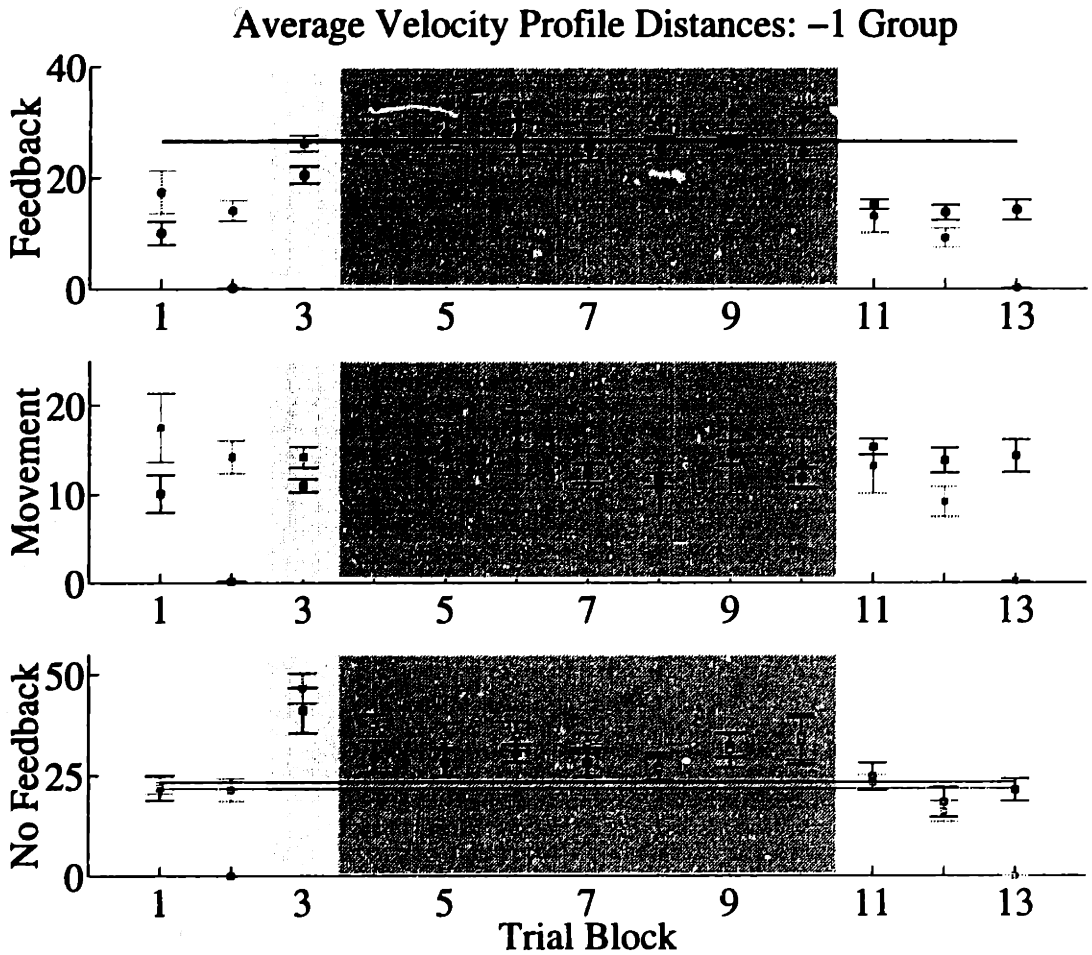

Figure 3-13: Velocity profile comparisons for the -1 Group in Experiment 3.1. See Figure 3-12 for details.

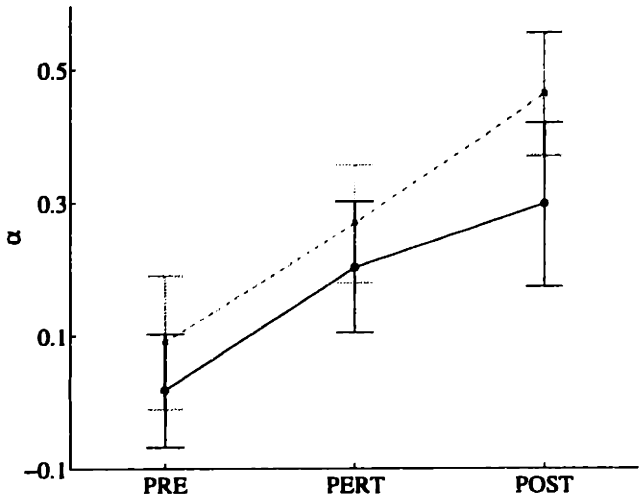

Figure 3-14: Perceptual test results from Experiment 3.1. β responses (mean and s.e. over subjects) for each phase. +1 Group, black circles; −1 Group, grey squares.

with previous results by the author (Sabes, 1996) in which a different set of perturbations was used. However, there are a number of alternative explanations of why subjects may have shown no adaptation. First, subjects were not able to view their hands, but were rather shown a white circle of light approximately 1cm in diameter which was located at the same position as the finger-tip. Perhaps this visual feedback was not adequate to induce adaptation. However, previous studies using this same virtual feedback apparatus, e.g. Wolpert et al. (1995), have found that subjects adapt the path of their movements based on positional perturbations of the feedback. Furthermore, in the following study we will show that velocity skewing perturbation of discrete obstacle avoidance movements also results in a compensatory modification of behavior.

The feedback was delivered as a spot of light on a VGA projector screen with a refresh rate of 72 Hz. Perhaps that rate is not high enough to give adequate information about the velocity profile. We argue against this objection by citing Viviani and Stucchi (1992). Their perceptual study, described above, also used a VGA monitor (refresh rate not cited), and subjects were able to make fine distinctions in velocity profiles.

Finally, it could be that the CNS does plan the velocity of these movements, but the veridical proprioceptive feedback supersedes the perturbed visual feedback. This possibility is unlikely given the vast array of literature showing that vision dominates proprioception in the perception of hand location. See Welch (1986) for a review.

In summary, we have shown that subjects do not adapt their behavior when the visual

feedback of cyclic arm movements fails to obey the 2/3 power law. We conclude that the regularities of movement which the 2/3 power law describes are not planned, implicitly or explicitly, by the CNS. There may be other aspects which are planned, and we will look at one of them in the next section.

3.3 Skew Perturbations in Discrete and Continuous Movements: Experiment 3.2

The previous study and others like them (Sabes, 1996) suggest that the velocity of movements is not planned explicitly by the CNS. However, Ghahramani and colleagues (personal communication) have preliminary evidence that subjects adapt the velocity profiles of unobstructed pointing movements in response to artificially skewed visual feedback. The interpretation of their results is somewhat unclear due to an overall reduction in the pace of movements during the perturbation period, but they are still suggestive.

We propose to investigate the differences between velocity planning in rhythmic and discrete movements directly. The goal of the experiment was to match the two conditions as closely as possible, and look for differential responses to the perturbation, which would suggest different control mechanisms for the two classes of movements. We adopted an obstacle avoidance paradigm, as it allowed us to have subjects make ellipse-like paths which were similar between the two conditions.

3.3.1 Methods

8 subjects participated in this experiment. Subject were divided into equal two groups,[4] whose treatments differed in the direction of the perturbation used. All subjects were right handed, had normal or corrected-to-normal vision, and were naive as the purpose of the experiment. The experiment was conducted with the virtual visual feedback apparatus described in Appendix A, in the same manner as Experiment 3.1 (c.f. Chapter 3.2.1).

There were two kind of trials, continuous (CT) and discrete (DS). CT trials began with a blue sagittally oriented, 8cm long bar-shaped obstacle appearing in the workspace, 30cm in the front of the subjects eyes along the midline. Two end circle circles also appeared 7cm to either side of the center of the obstacle. This arrangement is shown in Figure 3-15.

[4] +Skew Group: 2M, 2F, age range 16-26yrs, -Skew Group: 4M, age range 19-24yrs.

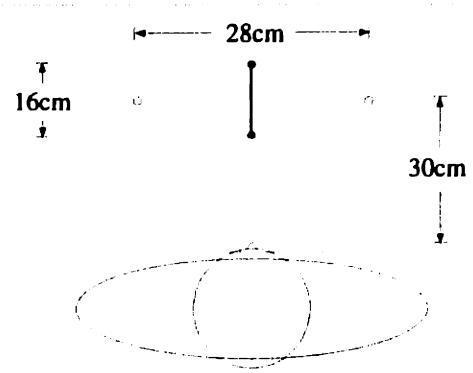

Figure 3-15: The experimental design for Experiment 3.2.

Subjects were asked to move smoothly and continuously around the obstacle in a counter-clockwise direction, passing through the end circles. Otherwise, the instructions for this experiment are identical to those given for the motor trials in Experiment 3.1. In particular subjects were told that the goal of the experiment was to learn to move around the obstacle at a certain tempo (1500ms per loop), which was presented to them through a series of tones before each trial. A CT trial consisted of 14 loops around the obstacle.

DS trials began with the same visual display as in CT trials, except the obstacle was red, and the end point circles were alternately red and white. When an circle was white, it was the current target. After subjects successfully pointed to the target, it turned white and an 800ms delay period began, during which S's were required to remain in the current circle. At the end of the delay, a tone was heard and the other circle turned white, marking it as the current target. Subjects were asked to point from target to target reaching above the obstacle on the right-to-left movements and below the obstacle on the left-to-right movements. This resulted in a piecewise, counter-clockwise circumnavigation of the obstacle. As in the CT condition, subjects were told that the goal of the experiment was to learn to move around the obstacle at a certain rate. Here, the target rate was 1000ms for each movement, and subjects were made aware of the target rate by a low tone which sounded 1000ms after movement onset. A high tone sounded at the completion of each movement. Each tone lasted 35ms, and any portion of the two tones which overlapped was heard as a middle pitched tone. Subjects were told that their task was to get the time of the high and low pitched tones to match. A DS trial consisted of 10 movements in each direction. This means that the two trials conditions would result in approximately the same time of feedback exposure in the two conditions if subjects achieve the target rates.

As in Experiment 3.1, trials came in blocks of four, the first three with feedback throughout the trial, and the fourth with no visual feedback. After each trial, subjects could rest as long as they wanted before the next trial began. Each experiment consisted of a pre-perturbation phase of 2 blocks, one block where the perturbation was introduced linearly over three feedback trials, 8 perturbation block, and 3 post-perturbation blocks. Additionally, before each experiment subjects practiced with no perturbation until they reached an error criterion as in Experiment 3.1, but always for at least 2 blocks. During a single experiment, all the trials were either CT or DS. Each subject participated in two experiments in the same session, one with each trial condition. The order of the experiments was randomized.

Visual Perturbation

During the feedback trials of the pre-perturbation phase, statistics were collected about the subject's velocity profiles. Between the pre-perturbation phase and the perturbation phase, these statistics were used to calculate the average velocity profile over the path. This profile was used to calculate the velocity skewing position perturbation as described in Appendix B. The magnitudes of the skewing was chosen to attain a preset angular shift in the velocity peak over a single loop (a movement pair for the DS case). The shift was 45° for the CT case and 20 for the DS case. These magnitudes were chosen to give roughly equal maximum displacement in the positional dependent perturbation. The angular displacement for CT trials was chosen to be so much larger in an attempt to roughly equalize the size of the perturbations. The skew transformation has less and less effect as the velocity profile gets flatter. Since the velocity profiles of rhythmic movements are much flatter than those of discrete pointing movements (which necessarily go to zero at the end points), it was necessary to choose a larger skew for CT movements. The average (s.d.) maximum angular displacement for perturbations used in the experiment was 12.1° (3.1°) for CT sessions and 15.9° (1.7°) DS session.

The 8 subjects that participated in the experiment were divided randomly into two, one receiving a rightward skewing perturbation (+Skew Group), the other a leftward skewing perturbation (-Skew Group).

Data Processing

To eliminate the effects of startup transients, the first 3 loops of each 10 loop trial were discarded. The sampled position data was sufficiently smooth to allow the calculation of velocity by simple first differencing. For higher derivatives, the planar positions of the finger tip were fit with cubic smoothing splines ($\lambda = 0.995$, matlab routine `csaps`), and derivatives were than taken analytically from the spline fit. Curvature of movements was calculated using the equation

$$c = \frac{\sqrt{v_x a_y - v_y a_x}}{(v_x^2 + v_y^2)^{\frac{3}{2}}}$$

where $v_.$ and $a_.$ are the velocity and acceleration in the subscripted direction.

Calculation of the extrema of the CT velocity and curvature profiles proceeded as follows. First, the trajectory over an entire trial was segmented into loops, and the average velocity for a trial was computed as a function of angular position. Next, the two highest local maxima and lowest local minima were identified. If these peaks and valleys were interleaved, i.e. there was a peak between the two valleys and vice versa, then the process was finished. If the extrema were not interleaved, the lowest point between the maxima and the highest point between the minima were identified. The "depth" of these two new extrema was defined as the minimum of the absolute difference in velocity or curvature from that point to the neighboring extrema. The deeper the of the two new extrema was kept, and finally, if it was a peak (valley) then the lower (higher) of the two old peaks (valleys) was discarded.

3.3.2 Continuous Movement Results

The effects of the perturbation on the velocity of the visual feedback in CT trials can seen in Figure 3-16. The plots show the average velocity profiles for actual movements and perturbed feedback over the perturbation phase of an experiment. It is seen that the primary effect of the perturbation is to rotate the perceived velocity profile about the obstacle center. In order to determine the amount of effective rotation, we calculated the cross correlation of the movement and feedback velocity profiles, and identified the angle of the peak. The mean (s.d) velocity rotations were $+26.4°(8°)$ for the +Skew Group and $-25.6°(12.7°)$ for the -Skew Group.

Figures 3-17 and 3-18 show sample paths and velocity profiles for a single subject in the +Skew Group and -Skew Group respectively. It can be seen from these figures that the

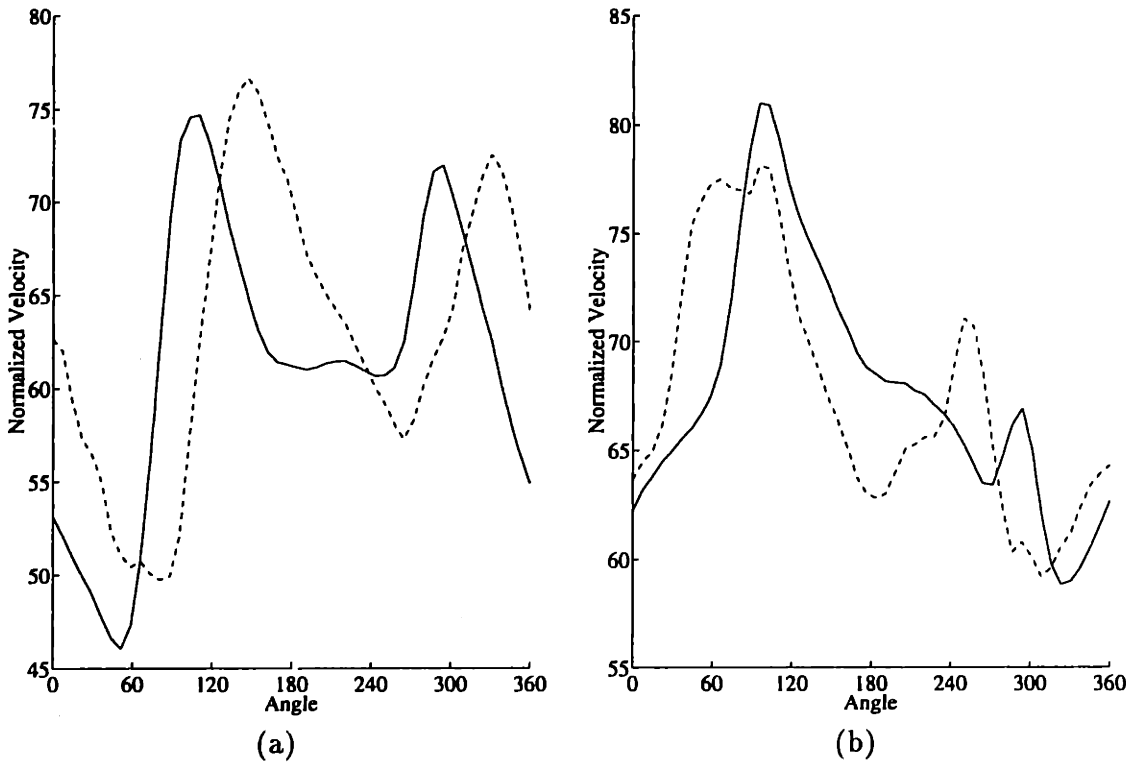

Figure 3-16: Effects of skew perturbation on continuous movements in Experiment 3.2. The normalized velocity profiles are averages over all feedback trials during the perturbation phase.

velocity profiles are much more variable than those in Experiment 3.1. This is primarily due to the fact that subjects chose paths with low eccentricity: mean (s.d.) major to minor axis ratios were 1.17 (0.1) over subjects and trials. This fact complicates the interpretation of the data from the CT trials in this experiment, as the statistics such as the power law exponent and Peak to Valley ratio were too noisy for analysis.

However, since the major effect of the perturbation was to rotate the velocity profile, we can look directly at the locations of the peaks and valleys of the movement and feedback velocity profiles and see if they change over the course of the experiment. The predicted adaptation would be to rotate the velocity profile in the opposite direction of the perturbation in order to maintain the relationship between path and velocity. However, since the path was not constrained, subjects could also adapt to the perturbation by rotating the path, but leaving the velocity profile unchanged. In this case, the rotation should be in the same direction as the perturbation.

The velocity and curvature extrema for each of the 13 no feedback trials are shown in Figures 3-19 and 3-20 for the +Skew and -Skew Groups, respectively. In general, the first

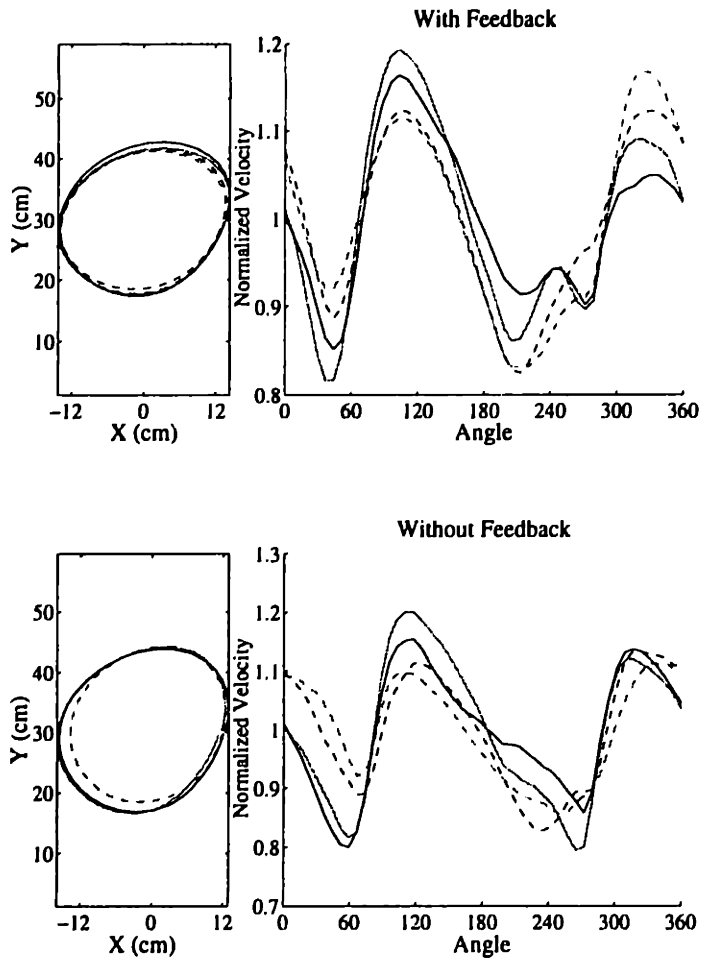

Figure 3-17: Experiment 3.2: Paths and velocity profiles for continuous movements, subject MG in the +Skew Group. Each line represents a single block. Top row, average over three FB trials. Bottom row, average for one NO-FB trial. Solid Black, the final PRE block; Solid Gray the first PERT block; Dashed Gray, the final PERT block; and Dashed Black, the final POST block.

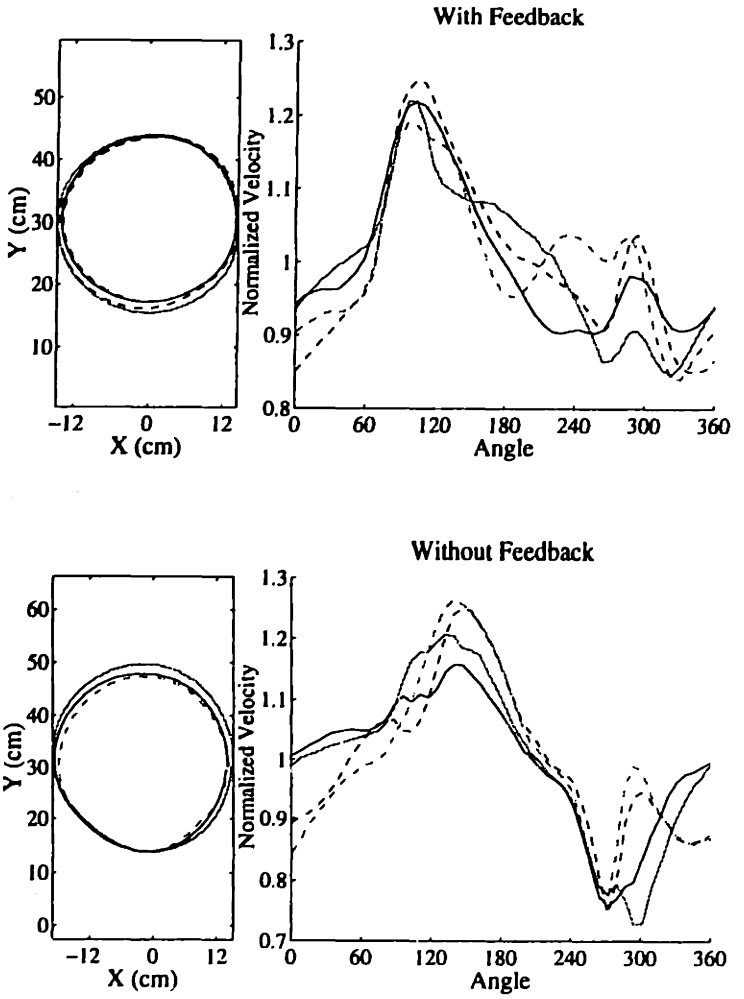

Figure 3-18: Experiment 3.2: Paths and velocity profiles for Continuous Movements, subject NP in the -Skew Group. Each line represents a single block. Top row, average over three FB trials. Bottom row, average for one NO-FB trial. Solid Black, the final PRE block; Solid Gray the first PERT block; Dashed Gray, the final PERT block; and Dashed Black, the final POST block.

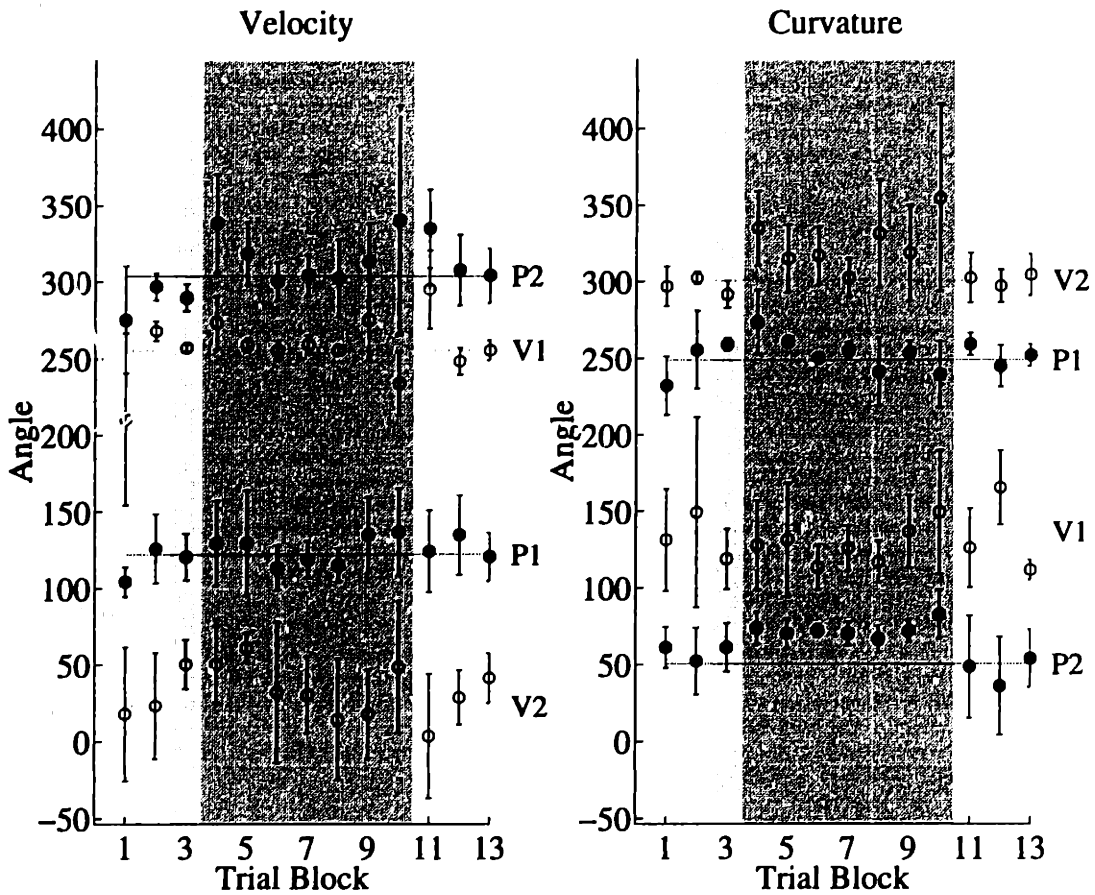

Figure 3-19: Velocity and curvature extrema for the +Skew Group in Experiment 3.2. Solid circles represent maxima, open circles minima. Error bars are one standard deviation. The horizontal lines mark the means of the 5 PRE and POST phase trials.

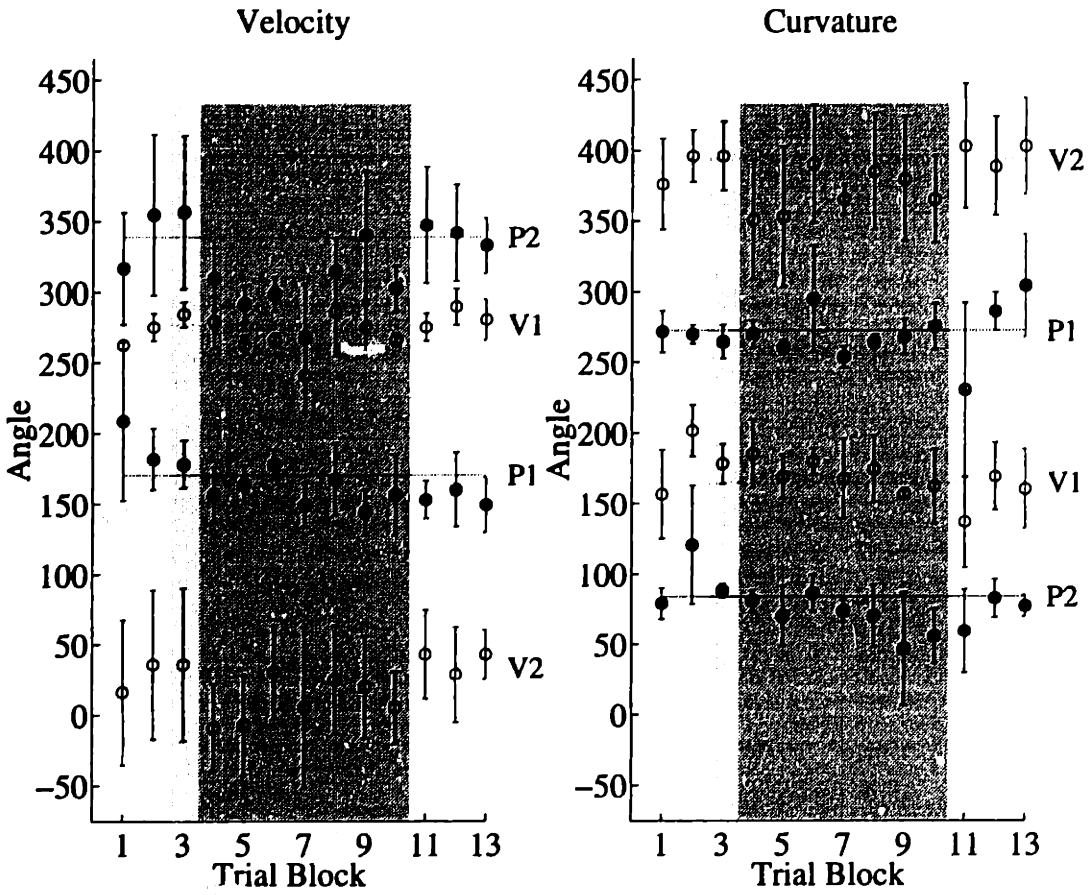

Figure 3-20: Velocity and curvature extrema for the -Skew Group in Experiment 3.2. Solid circles represent maxima, open circles minima. Error bars are one standard deviation. The horizontal lines mark the means of the 5 PRE and POST phase trials.

velocity peak and valley (P1 and V1) were relatively stable across trials and subjects, while the second set of velocity extrema were much more volatile. The curvature profiles tended to be rather flat with sharp peaks, making exact localization of the minima difficult.

Beginning with the +Skew Group, none of the velocity extrema in Figure 3-19 appear to adapt. However, curvature P2 and V2 both appear to adapt in the direction of the perturbation, as would be predicted if subjects alter their path in attempt to counteract the effects of the perturbation. Figure 3-20 shows a shift of the second velocity peak (P2) for the -Skew Group, but it is in the direction of the perturbation, the opposite of what would be expected from an attempt to counteract the effects of the perturbation. The changes in path curvature are not as clear as above, but there seems to be a slight shift of P2 and V2 in direction of the perturbation, as seen in the +Skew Group.

To assess the statistical significance of the changes described above, we performed a contrast analysis on the velocity and curvature extrema location (Rosenthal and Rosnow, 1985). The weighting by block was the same as that used in Experiment 3.1, Equation 3.3, and was chosen to detect U-shaped changes in the location of the landmark over the three phases of the experiment. For the +Skew Group, the only significant contrasts were in path curvature P2 ($t(39)=3.03$, $p= 0.002$) and V2 ($t(39)=2.30$, $p= 0.01$), in accordance with informal assessment above. For the -Skew Group, the curvature P2 and V2 shifts were marginally significant ($p= 0.06$ and $p= 0.07$ respectively). Also, the shift in velocity peak P2 was significant ($t(39)=2.41$, $p= 0.01$), but in the opposite direction to what would be predicted for adaptation. Again, these results concur with our initial assessment.

We performed the same statistical tests on the velocity and curvature extrema of the feedback trials, and none of the landmarks showed any significant shifts in location over the course of the experiment.

These results suggest that there may have been some attempt counteract the effects of the perturbation by rotating the path shape in the direction of the perturbation. This would have the effect of reducing the misalignment of curvature and velocity profiles induced by the perturbation. However, these results must be interpreted with caution. The location of the curvature minima were difficult to ascertain. Furthermore, the very low eccentricity of the paths made for volatile velocity and curvature profiles. The apparent shift in the second velocity peak of the -Skew Group is probably a result of this noise. Finally, no changes were evident in the feedback condition.

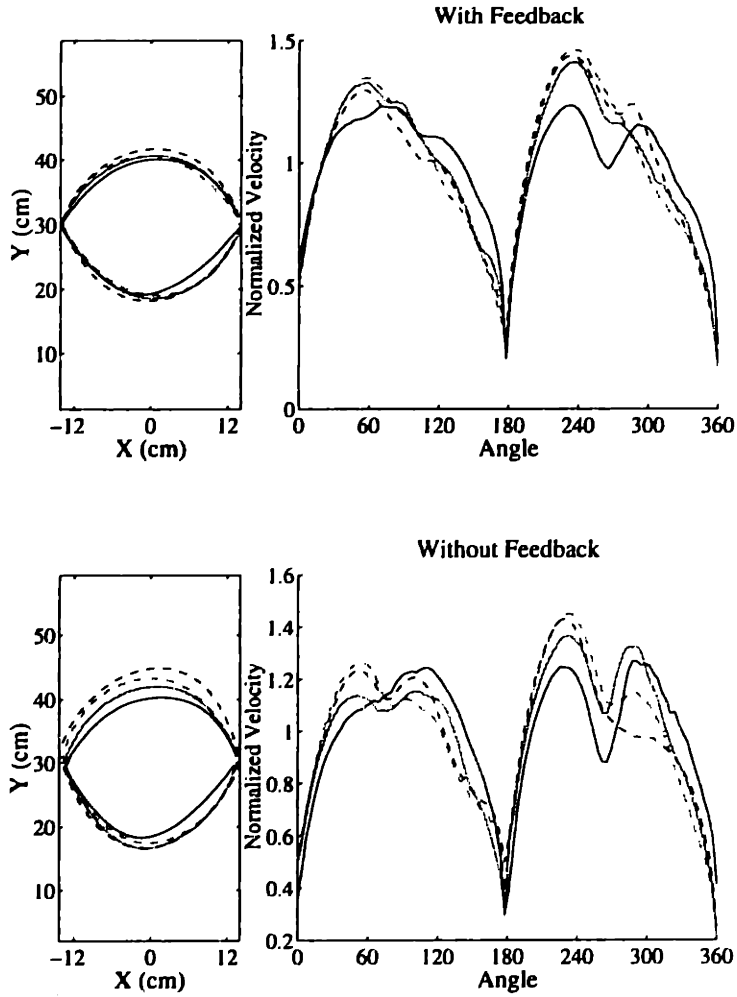

Figure 3-21: Experiment 3.2: Paths and velocity profiles for Discrete Movements, subject MK in the +Skew Group. Each line represents a single block. Top row, average over three FB trials. Bottom row, average for one NO-FB trial. Solid Black, the final PRE block; Solid Gray the first PERT block; Dashed Gray, the final PERT block; and Dashed Black, the final POST block.

3.3.3 Discrete Movement Results

In the case of discrete movements, skewing the velocity of the visual feedback resulted in a significant adaptation in subjects behavior when the feedback was removed entirely. Figures 3-21 and 3-22 show sample paths and velocity profiles for a single subject in the +Skew Group and -Skew Group respectively.

In order to assess the degree of adaptation, we measured the skew in the feedback and movement velocity profiles throughout the experiment. Given a velocity profile as a function

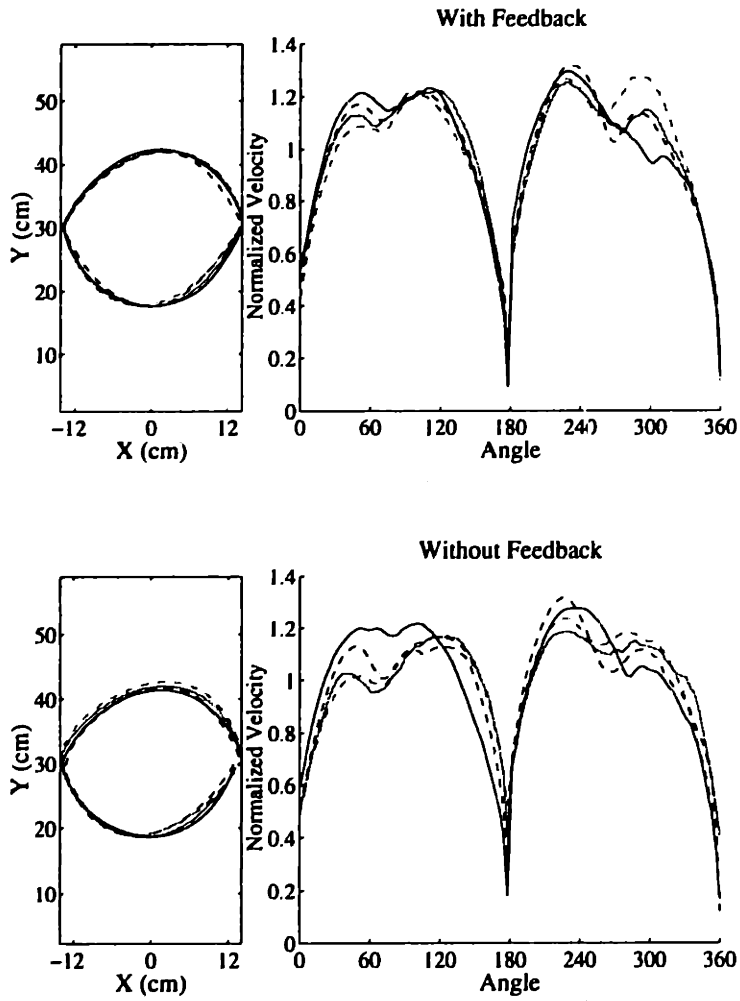

Figure 3-22: Experiment 3.2: Paths and velocity profiles for Discrete Movements,subject MO in the +Skew Group. Each line represents a single block. Top row, average over three FB trials. Bottom row, average for one NO-FB trial. Solid Black, the final PRE block; Solid Gray the first PERT block; Dashed Gray, the final PERT block; and Dashed Black, the final POST block.

of the angular position, $v(\theta)$, the skew was computed using the equation,

$$\text{Skew} = \frac{1}{Z} \int \sigma^{-\frac{3}{2}} (\theta - \mu)^3 v(\theta)\, d\theta$$

where the normalization Z, mean μ, and variance σ^2 are given by,

$$\begin{aligned} Z &= \int v(\theta)\, d\theta \\ \mu &= \frac{1}{Z} \int (\theta - \mu)\, v(\theta)\, d\theta \\ \sigma^2 &= \frac{1}{Z} \int (\theta - \mu)^2 v(\theta)\, d\theta. \end{aligned}$$

The limits of integration were $[0°, 180°]$ for Leftward movements and $[180°, 360°]$ for Rightward movements. Note that the skew is a dimensionless quantity which is 0 for symmetric velocity profiles, negative for leftward skewed profiles and positive for rightward skewed profiles.

The skew was computed on the average velocity profile for movements in each direction over a single trial (i.e. the average over 10 movements). Skew data is presented by trial blocks; for data on feedback trials, the values are averages over the three feedback trials in a block. Figure 3-23 shows the skew results averages over all subjects in the +Skew Group. First, note that the perturbation does indeed skew the feedback in the negative (rightward) direction. The horizontal bars in each plot represent the average movement velocity skew for the PRE and POST phases. For both leftward and rightward movements, the velocity of the movements in feedback trials (lefthand plots) during the PERT phase exhibit a trend toward more positive skew, i.e. in the direction which compensates for the perturbation. In the no feedback trials this trend is much larger – except for the final leftward block, every block during the PERT phase has skew significantly larger than the PRE/POST mean.

Similar results are shown for the -Skew Group in Figure 3-24. Again note that the perturbation skew the feedback in intended direction. Here we also see that for both leftward and rightward movements, the velocity of the movements in feedback trials (lefthand plots) during the PERT phase exhibit a trend compensating direction, more negative skew. Again, this trend is larger in the no feedback trials.

We would now like to quantitatively assess the magnitude of the adaptation described above. As a measure of the magnitude of the perturbation, we took the difference between

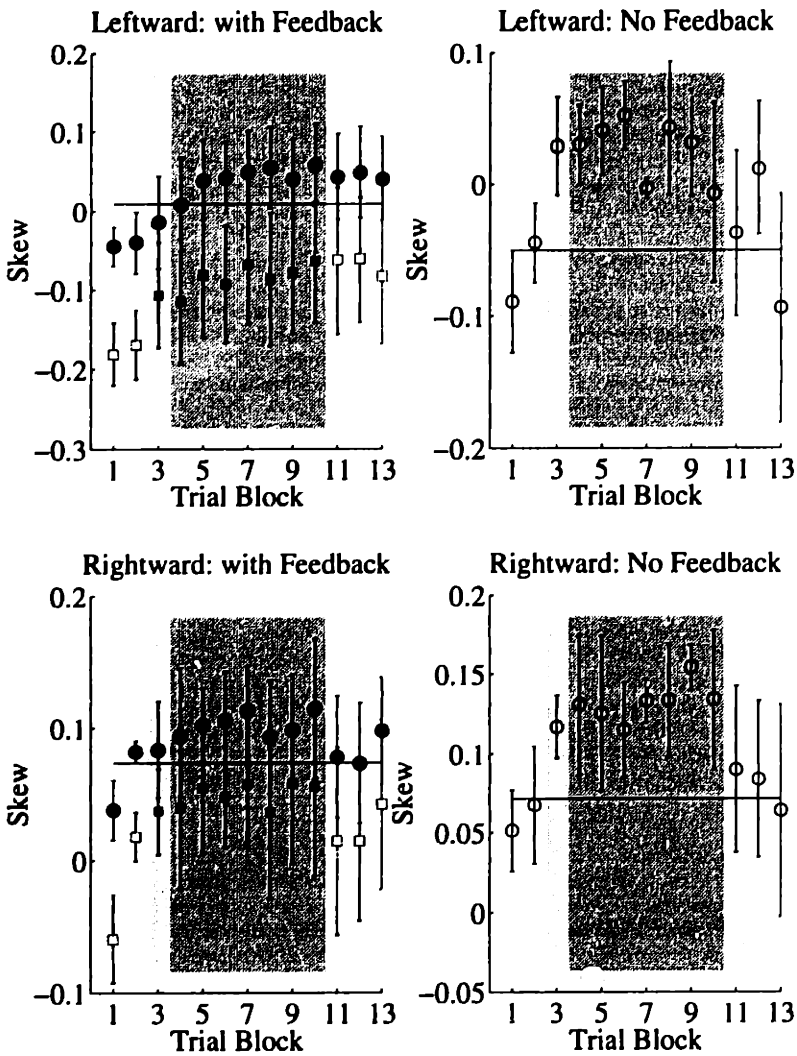

Figure 3-23: Skew results for the +Skew Group in Experiment 3.2. The upper plots are for rightward movements, lower plots for leftward movements. Horizontal lines represent the mean skew for movements over the PRE and POST phase. Solid circles, movement skew on Feedback trials; Open circles, movement skew on No Feedback trials; Solid squares, feedback skew during PERT phase; Open Squares, fictive perturbation feedback skew for PRE and POST phase.

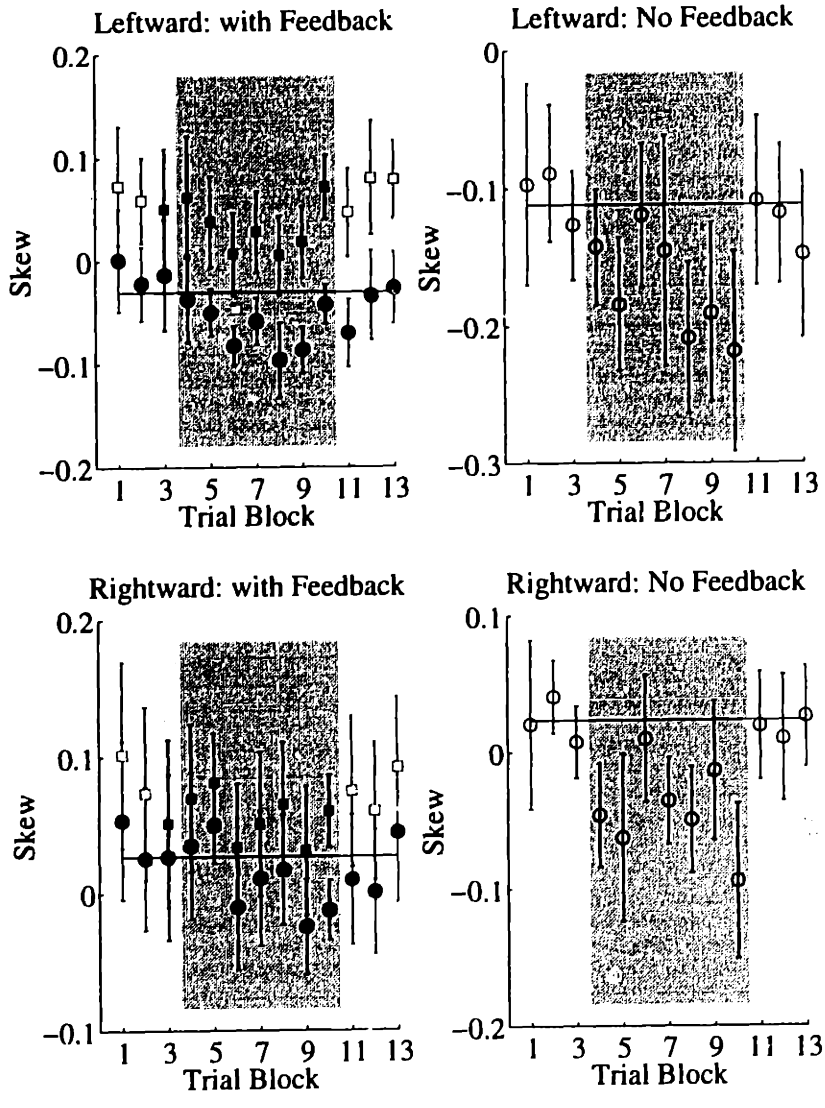

Figure 3-24: Skew results for the +Skew Group in Experiment 3.2. The upper plots are for rightward movements, lower plots for leftward movements. Horizontal lines represent the mean skew for movements over the PRE and POST phase. Solid circles, movement skew on Feedback trials; Open circles, movement skew on No Feedback trials; Solid squares, feedback skew during PERT phase; Open Squares, fictive perturbation feedback skew for PRE and POST phase.

Experimental Group	Feedback Condition	Perturbation Magnitude	Skew Compensation	Percent Adaptation	Contrast	
					t(39)	p
+ Skew	Feedback	-0.094	-0.031	33%	1.21	0.12
	No Feedback	-0.10	-0.069	69%	3.13	0.002
- Skew	Feedback	0.076	0.026	34%	1.12	0.13
	No Feedback	0.069	0.063	92%	2.17	0.02

Table 3.1: Adaptation results for discrete movements in Experiment 3.2

the average skew of the fictive perturbed feedback of the PRE and POST movements and the average skew of the actual PRE and POST phase movements:

$$\text{Perturbation Magnitude} = < \text{Skew}_f >_{\text{PRE/POST}} - < \text{Skew}_m >_{\text{PRE/POST}}, \qquad (3.4)$$

where the subscripts on "Skew" refer to (m)ovemnt or (f)eedback, and the subscripts on the angular brackets (average) refer to the phases over which the averages are taken. As a measure of compensation, we took the difference between the movement velocity skew in the PERT phase and the movement skew in the PRE and POST,

$$\text{Skew Compensation} = < \text{Skew}_m >_{\text{PERT}} - < \text{Skew}_m >_{\text{PRE/POST}}, \qquad (3.5)$$

Finally, the percent adaptation is taken to the amount of the perturbation which was compensated for:

$$\text{Percent Adaptation} = \frac{\text{Skew Compensation}}{\text{Perturbation Magnitude}}.$$

The results of this analysis are presented in Table 3.1. Inspection of

To assess the statistical significance of the adaptation, we performed a contrast analysis on the velocity skew data using the same weighting as in Equation 3.3. Remember that this weighting was designed to detect U-shaped changes in the velocity skew over the three phases of the experiment. The contrast was significant for both directions of movement in the case of no feedback. Interestingly, the contrasts were not significant for the feedback trials. The results of the contrast analysis are shown in Table 3.1. Note that although the adaptation was not significant for the trials with feedback, it was significant for the no-feedback trials.

Note that both of the preceding analyses were performed with the Leftward and Rightward movements combined. As noted above, the baseline velocity skewing was different for the two directions of movement, so we reanalyzed the data for each direction separately. The results of both analyses were very similar to those described above, and so they will not be presented here. Also, the same results were found if we used angular location of the peak tangential velocity of the movements as the dependent variable instead of skew.

Given the results of the CT movement trials, we must make sure that the changes in skew seen over the course of the experiment are not due to changes in path. We will analyze only the no-feedback trials, as these are where the skew adaptation was most prominent. For each Subject we calculated the mean paths for both the perturbation trials and the non-perturbation trials. These paths for all 8 subjects are shown in Figure 3-25. Note that the changes do not appear to be in any systematic direction. The mean and maximum of the distance between the perturbation and non-perturbation paths were computed as a measure of the change in path possibly resulting from the perturbation. The mean (s.d) of those measures over all subjects was 0.50cm (0.27cm) mean distance, 0.87cm (0.49cm) maximum distance. Only two subjects (KR, AP) showed mean path changes over 0.50cm or peak path changes over 1.0cm. Figure 3-25 shows that for the most part, these peak path differences were within the statistical noise.

Despite the fact that most subjects exhibited no significant change in DS paths between the perturbation and non-perturbation trials, one might wonder whether the few subjects that did exhibit large path changes could be responsible for the overall skew effects details above. To allay those concerns, we compare the Percent Adaptation and contrast analysis L-statistic[5] to the peak path change for each subject and each movement direction. In fact, for every subject in both movement direction the L-statistic had the sign predicted by skew adaptation: negative values for the +Skew Group and positive values for the -Skew Group. Thus, for clarity these absolute value of the L-statistic is presented. These comparisons are shown in Figure 3-26.[6] Both measures of adaptation do show an increasing trend as a function of path change, and the trend is statistically significant for the case

[5]The L-statistic is the sum of the block by block skews, each multiplied by it respective weighting. In this case, large negative values support adaptation for the +Skew Group, large positive values for the -Skew Group.

[6]The outlier in Percent Adaptation deserves comment. Subject AP exhibit an exceptionally large shift in skew for rightward movements during the perturbation period which overcompensated for the feedback shift by almost a factor of 6. This effect was not due to a single outlier trial.

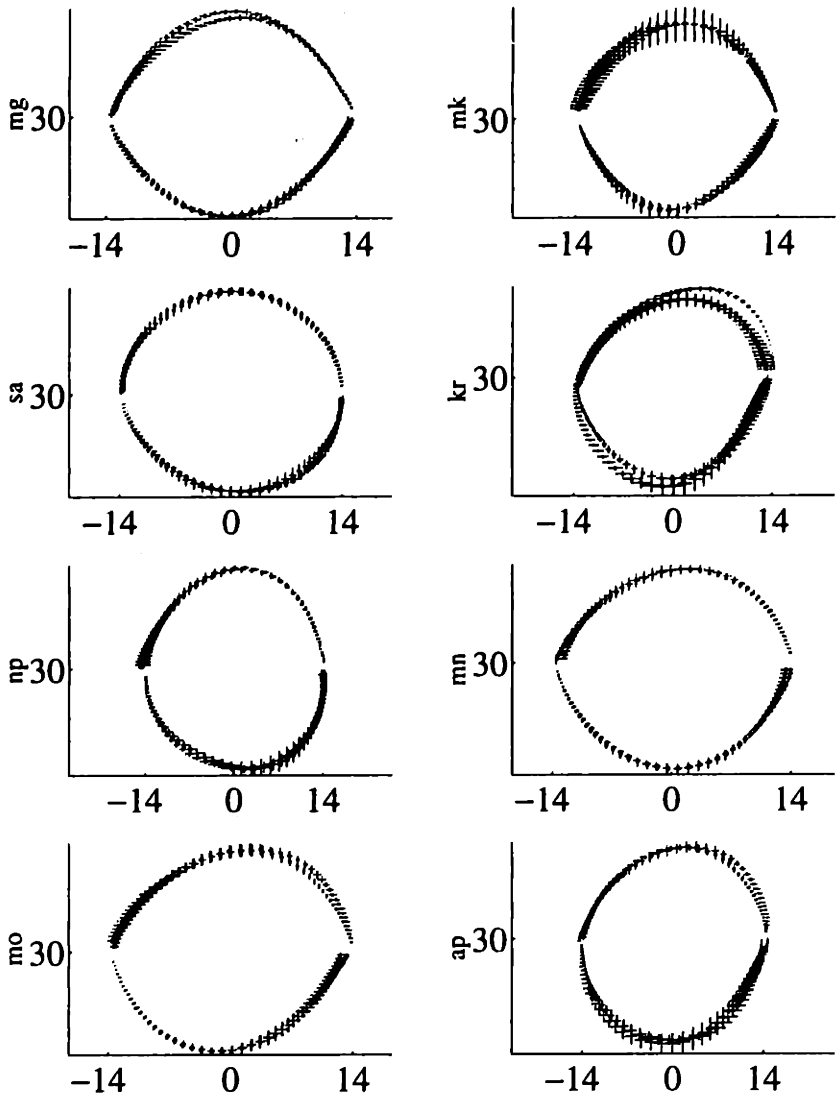

Figure 3-25: Average paths for No Feedback trials in Experiment 3.2. The error bars represent one standard deviation, all units are cm. Black, average path over all PRE and POST blocks. Grey, average over all PERT blocks. The subjects initials are shown on the Y axis; the top four plots comprise the +Skew Group, the bottom four the -Skew Group.

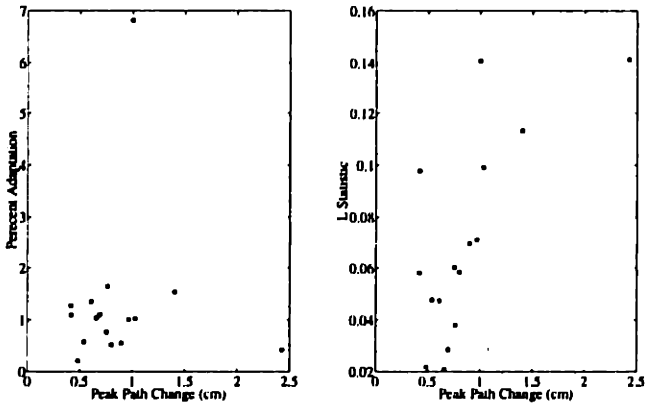

Figure 3-26: Skew Statistics as a Function of Path Change Experiment 3.2. Each point represents one movement direction for one subject: Open circle, leftward movements, Closed circle, rightward movements. (a) Percent Skew Adaptation. (b) Absolute Value of the L-statistic.

of the L-statistic. Thus, we recomputed our contrast analysis using only those subject by movement direction pairs which showed a peak path change of less than 0.75cm (leaving four of eight data sets for each experimental group). The +Skew Group still show a significant adaptation, with $t(39)=1.84$, $p= 0.04$. The adaptation for the -Skew Group is no longer significant, $t(39)= 0.97$, $p= 0.17$. If the acceptable peak path change is raised to 0.9cm, the six of the eight data sets are used and the analysis again gives significant results, $t(39)=2.15$, $p= 0.02$.

Finally, there is some concern that the changes in velocity skew described in this section may be subsidiary to overall changes in movement tempo. In fact, although subjects were fairly good at maintaining the target tempo (mean (s.d.) movement time was 1040ms (30ms) and 1030ms (40ms) for the two experimental groups), there was a trend for longer movement times in the no-feedback movements of the +Skew Group and shorter movement times in the no-feedback movements of the -Skew Group. These results can be seen in Figure 3-27.

To assess the extent to which the Skew adaptation was a result of the change in movement time, we calculated the adjusted skew by regressing the velocity profile skew on movement time. This regression was performed separately for each experimental group. We then analyzed the adjusted skew data using the same contrast analysis described above. The results were consistent with the results for the unadjusted skew: +Skew Group, $t(39)=1.57$,

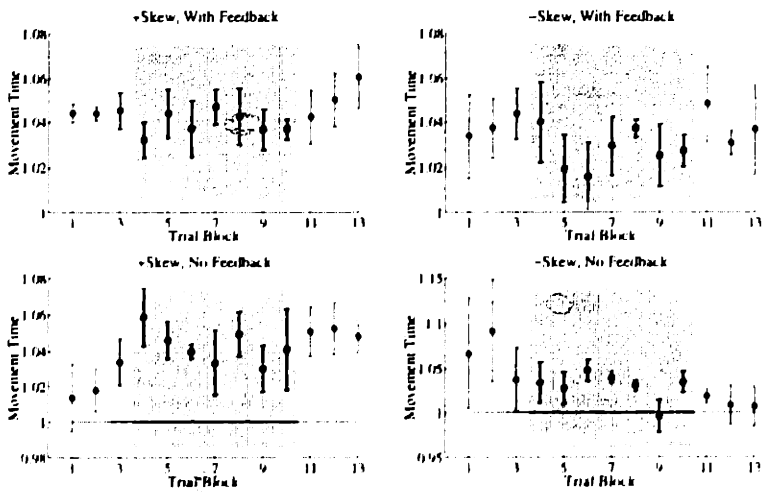

Figure 3-27: Movement Time for Experiment 3.2. Each point represents the mean and standard error over subjects for the average movement per block. The horizontal lines at 1.0s represent the target tempo. (a) +Skew Group, (b) Skew Group.

p= 0.06 with feedback, t(39)=2.84, p= 0.004 without feedback; Skew Group, t(39)=1.02, p= 0.16 with feedback, t(39)=2.09, p= 0.02, no feedback.

3.3.4 Comments

The results of these two experiments are strikingly different. In the CT case, the perturbation induced a small shift in path for feedback trials, but no effects persisted during no feedback trials, and so no adaptation would be said to have occurred. On the other hand, there was a clear and sizable adaptation to the skew perturbation in the case of discrete obstacle avoidance movements.

As mentioned above, the perturbations in the CT and DS sessions were not perfectly matched, in that the qualitative effects of the skew were different for two types of movements and the maximum positional perturbation was larger for the DS case by about 30%. However, if we compare the perturbations by their effect on the actual velocity profiles in the experiment, they compare more closely. The distance between the movement and feedback velocity profiles of the two perturbations (as defined in Figure 3-11) differs by less than 10%.

3.4 Discussion and Conclusions

There are two main findings in this chapter. First, the production of rhythmic arm movements is insensitive to large perturbations in the visual feedback. In particular, when the visual feedback violates the 2/3 power law, no attempt is made to change the movement trajectory in order to restore adherence to the law in perceived trajectory (Experiment 3.1). The small shifts in path exhibit in the CT movements of Experiment 3.2 were only present for feedback trial, suggesting that they are merely only on-line corrective procedures as opposed to the result of an adaptive central control mechanism.

If the 2/3 power law is not planned by the CNS, why does it seem to be obeyed across a wide range of movements? We suggest that the law is an emergent property of the arm's controller and its dynamics. This possibility is supported by recent computational modeling showing that the 2/3 power law behavior can result from the equilibrium point dynamics of the arm (Gribble and Ostry, 1996).

In contrast to those findings, we see that discrete pointing movements are susceptible to perturbations in the feedback velocity. In particular, when the feedback is artificially skewed, subjects adapt their behavior by skewing their movements in the opposite direction. This adaptation persists in trials where there is no feedback at all. These results provide evidence that both the path and velocity of goal directed movements is pre-planned. It should be noted that the study does not directly address the issue of the coordinate frame in which velocity planning occurs. However, these findings support the notion of a central, adaptable, trajectory planner.

Part II

Dynamics and the Planning of Arm Movements

Chapter 4

Obstacle Avoidance

4.1 Introduction

The manner by which the CNS translates visually defined tasks into a motor plan and then executes that plan in the face of uncertainty is not well understood. Given a set of externally defined constraints for a particular movement, such as an initial and final location and some potential obstacles in the workspace, the CNS must choose from the infinite number of trajectories which satisfy those constraints. The planning process could proceed hierarchically, first specifying the trajectory of the end-point, such as the hand or index finger, and then choosing joint kinematics which attain that end-point trajectory, and so on. This strategy is attractive, as it allows the higher levels of control structure to ignore the kinematics and dynamic details of the actuator, freeing it to solve the sufficiently difficult task of planning the extrinsic kinematics of the movement.

This model, which I will refer to as visual or extrinsic planning, has a strong tradition in the literature. As discussed in Chapter 1, early observations of pointing movements revealed invariances in the extrinsic kinematics across subjects and experimental conditions(Morasso, 1981; Soechting and Lacquaniti, 1981; Abend et al., 1982). The maintenance of such extrinsic kinematic features as straight lines and bell shaped velocity profiles has been widely interpreted as evidence that they are planned by the CNS.

More recently the visual planning model has experience a resurgence of support from a variety of visual and dynamic perturbation studies. Shadmehr and Mussa-Ivaldi (1994) show that subjects will adapt to an externally applied, velocity dependent, force field in such a way as to bring the end-point trajectories back to the pre-perturbation baseline,

despite the fact that the dynamics of the movements, and hence the motor commands needed to attain them, have changed radically. Lackner and DiZio (1994) placed subjects in a rotating environment, exposing them to velocity dependent Coriolis forces. They found that even when there are no visual or tactile cues of the dynamic perturbation, subjects still adapt their behavior back to baseline. Wolpert et al. (1995) perturbed the visual feedback during pointing movements by bowing the visually perceived trajectory out from the path while maintaining veridical feedback at the beginning and end of the movement. Thus, if subjects had continued making the same movements as before the perturbation, they still would have reached the target, which was the only stated goal of the task. Instead, subjects compensated for the perturbation by curving their movements in the other direction, showing that the CNS "cares about" the Cartesian properties of the movement, even at the expense of a joint level plan. In a remarkable display of how far this preference can be pushed, Flanagan and Rao (1995) showed that after prolonged exposure to artificial visual feedback which represented the location of the arm in joint coordinates, subjects alter their movements to make straight lines in joint space. The surprising result is not the particular form of the visual perturbation, but rather that the CNS is willing to so radically reorganize the movement plan to maintain straight lines in visual space.

There are however some suggestions in the literature that the visual planning model cannot account for salient features of reaching and pointing movements. A variety of researchers have shown that various characteristics of arm movements can be captured by models in which the planning of arm movements is performed in intrinsic kinematic coordinates, i.e. joint level planning (Soechting and Lacquaniti, 1981; Cruse, 1986; Kaminsky and Gentile, 1986; Soechting and Flanders, 1989a; Flanagan and Ostry, 1991; Desmurget et al., 1995). Other evidence suggests that dynamics play a role in the planning as well. Uno et al. (1989)show that when subjects are asked to make movements through via points located symmetrically on either side of the straight line from initial position to target, the paths taken on each side are not symmetric. These difference can not be accounted be accounted for by a Visual Planning model, but Uno et al. showed that the minimum torque change model predicts the path asymmetries.

As discussed in Chapter 1, we feel any conclusions from these studies are premature – being based on an overly restrictive set of movements. The question of interest is how the CNS extracts from the extrinsic environment and visually specified task the intrinsic

kinematic and dynamically relevant information, and by what criteria *relevant* is defined. In almost all of the literature cited above, the visually specified task is completely unconstrained, short of the initial and final positions themselves. This fact cuts both ways. It strengthens the argument for at least partial Visual Planning, since the CNS is free to choose *any* path, yet it chooses those that maintain extrinsic properties. On the other hand, it is not clear whether this is a general strategy which can be employed in more complex tasks.

In Section 1.4, we introduced the a class of models based on the principle of optimal control. Most such models that have been proposed are essentially models of smoothness or efficiency, either extrinsically (Flash and Hogan, 1985; Wann et al., 1988) or intrinsically (Hasan, 1986; Uno et al., 1989) defined. Nelson (1983) argues for a combination of optimization criterion, weighted according to the task at hand. We subscribe to this point of view. But in addition to the wholly intrinsic or end-point kinematic criteria, we hypothesized that adding extra constraints would bring to light new criteria which depend directly on those constraints. As an experimental paradigm for exploring this hypothesis, we chose to investigate the planning of obstacle avoidance movements.

There is some preliminary work in the literature on obstacle avoidance in human arm movements. Abend et al. (1982) asked subjects to move around a linear obstacle protruding into the straight line path. They found that the resulting trajectories displayed high curvature, low velocity regions near the tip of the obstacle, as if subjects had segmented the task into two parts – getting past the obstacle and then getting to the target. Flash and Hogan (1985) showed that this behavior could be captured by the minimum jerk model if a via point constraint was introduced, i.e. a location in space through which the trajectory is constrained pass. This model leaves open the question of how the via point would be chosen. Finally, Dean and Brüwer (1994) conducted a more comprehensive study along the lines of Abend et al. (1982). They found that the obstacle clearance and maximum deviation from straight line both varied over location in the workspace and orientation of movement. They noted that this result was inconsistent with a strict visual planning model.

We set out to look at obstacle avoidance movements with a dual purpose in mind, to determine whether visual planning model holds for a wider class of movements, and to see what criteria the CNS uses to satisfy additional constraints on the movement. To accomplish these goals, we proposed the following experiment. Subjects are asked to move around a

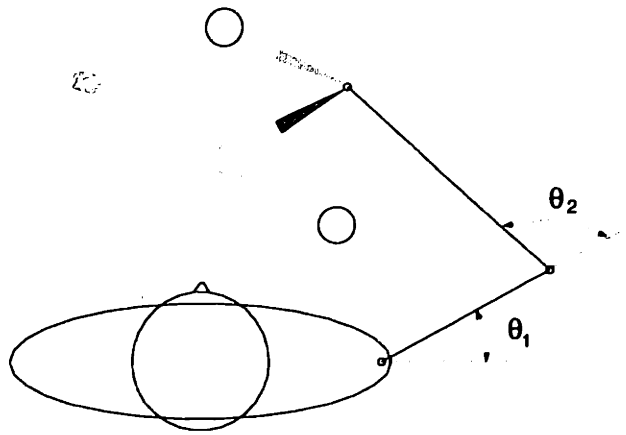

Figure 4-1: The Obstacle Rotation Experiment in 2D. The figure shows the position of the subject relative to the virtual image. The triangular obstacle and circular start and target locations are shown for two different trials, one in black, one in grey. The center of the obstacle, which remains fixed throughout the experiment, is chosen to lie at a prespecified location in the subject's joint coordinates.

virtual obstacle at various orientations. From trial to trial the obstacle tip remains fixed in space, while the obstacle orientation and the initial and final positions of the movement are rotated around that fixed point (see Figure 4-1). The result is that the object places constraints on the movement which are isomorphic up to rotation about the obstacle. If movements are planned in visual space, the resulting trajectories should be identical, modulo the rotation and any noise due to the controller. On the other hand, systematic variations in the trajectories as the presentation angle is varied would suggest that the movement plan is not based entirely on the extrinsic coordinate frame, but takes the details of the actuator, either kinematic or dynamic, in account. Furthermore, the nature of any such variation will tell us about the criterion by which the class of movements is planned. In the next section we will show that such movements do exhibit systematic variations. In the following section, we propose two models to account for the variations and compare them to the experimental data.

4.2 Obstacle Rotation in the Horizontal Plane: Experiment 4.1

4.2.1 Methods

Experiment 4.1 was conducted with five right handed male subjects, ages 18-28yrs, with normal or corrected to normal vision who were naive as to the purpose of the experiment. Subjects were strapped into a chair, insuring that their shoulders were fixed in space, and the height of the chair was adjusted so that the table was just below shoulder height. Subjects rested their right arms on the table, and their right wrists and index fingers were fixed in a fully extended posture. The net result was that movements made with the right hand were constrained to planar, two degree of freedom (shoulder and elbow rotation) motions.

This experiment employed the virtual visual feedback system described in Appendix A. The position of subject's finger tip and the angles of their shoulder and elbow joints were monitored at 144 Hz with a Northern Digital Optotrak infrared position monitoring system. Subjects wore one IRED (Infrared Emitting Diode) marker on their finger tip, and a rigid body containing six markers on their upper arm. All experiments began with a calibration procedure in which the position of the shoulder and elbow with respect to the rigid body were determined. This allowed us to calculate the shoulder and elbow angles as well as the location of the finger tip at every time step. Subjects' view of their arm was blocked by a mirror reflecting a VGA projection screen which provided them with virtual visual feedback in the form of a 1cm diameter white filled circle, located at the position of tip of the index finger. Obstacles and start and target locations were similarly displayed.

Each trial began with the a white (start) circle, blue (target) circle, and a yellow triangular obstacle appearing in the workspace. Subjects were instructed to move their finger tip into the white circle and wait for the start signal. After 800ms, a tone sounded and the target circle turned white – the signal to go. Subjects were instructed that at that point, they should reach around the obstacle tip to the target circle, making sure to avoid hitting the obstacle with their finger. If the finger tip collided with the obstacle, a low tone was sounded and the trial restarted. Otherwise, when the subject's finger tip came to rest in the start circle, a high tone was sounded and the screen blanked before the next trial. Subjects were given no further instructions, except to move naturally and comfortably. The dimensions of the virtual objects in the workspace are shown in figure Figure 4-2.

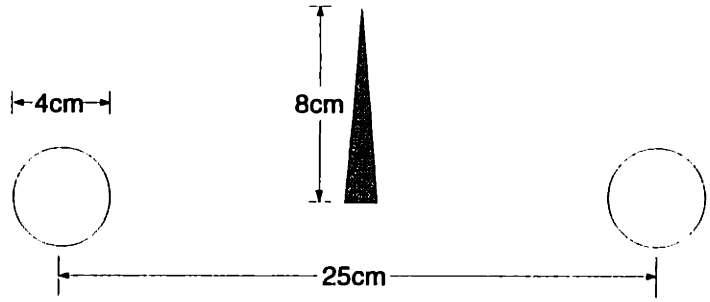

Figure 4-2: Dimensions of the visual scene for Experiment 4.1.

For each experiment, a joint configuration was chosen in advance, and once the kinematics of the arm were determined, the location of the obstacle tip was set to correspond to that location in the subject's joint space. Given the location of the obstacle tip, the layout of each trial was fully determined by a *presentation angle* ϕ, which corresponded to the orientation of the obstacle with respect to the positive x-axis, i.e. rightward. If the presentation angle was $\phi = 90°$, for example, the obstacle pointed away from the subject. Trials occurred in pairs. The identities of the start and target circles were switched within the pair, but the presentation angle was held fixed. An experiment consisted of 150 trial pairs with presentation angles randomly chosen from a uniform distribution over the circle.

All five subjects participated in two sessions, one at each of two joint space locations for the obstacle tip: Position 1, $\theta = (30°, 110°)$; and Position 2, $\theta = (75°, 75°)$.

Data Analysis

The sampled position data was sufficiently smooth to allow the calculation of velocity by simple first differencing. For higher derivatives, the planar positions of the finger tip were fit with cubic smoothing splines ($\lambda = 0.995$, matlab routine **csaps**), and derivatives were than taken analytically from the spline fit. Curvature of movements was calculated using the equation

$$c = \frac{\sqrt{v_x a_y - v_y a_x}}{(v_x^2 + v_y^2)^{\frac{3}{2}}},$$

where $v_.$ and $a_.$ are the velocity and acceleration in the subscripted direction.

4.2.2 Results

If the visual planning model were correct, there should be no systematic variations in the trajectory as the presentation angle is varied, except for the rotation itself and any effects

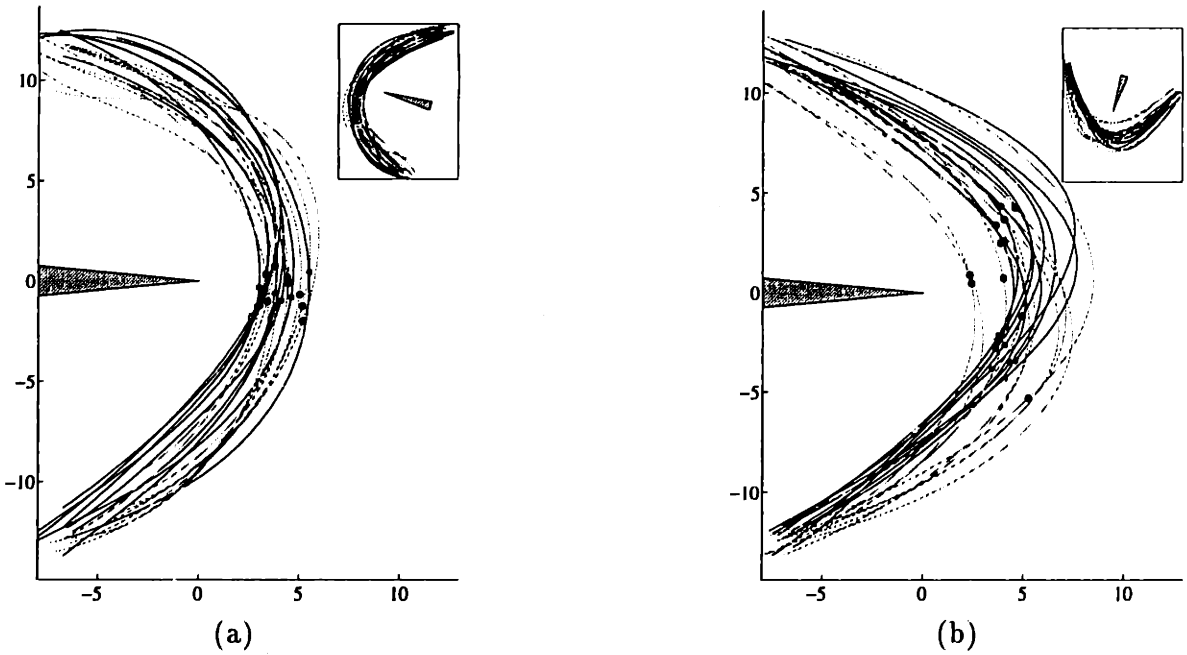

Figure 4-3: Sample paths from subject JM at the of the obstacle rotation experiment with center at Position 1. Black paths are clockwise movements, grey counterclockwise. The circles mark the point of closest approach to the obstacle tip, i.e. the near points. The presentation angles for the trials in the two figures are 90°, but the paths have been rotated into a canonical position for comparison. The insets show the actual orientations of the movements.

due to perceptual anisotropies. On the other hand, if the planning of obstacle avoidance movements depends on the kinematic or dynamic details of the arm, then we would expect additional asymmetries.

Figure 4-3 shows two sets of paths rotated into a canonical orientation. The presentation angles for the trials in the two figures were approximately 90° apart. The circles in the picture represent the "near points", where the paths come closest to the obstacle. There are marked differences between movements at the two presentation angles. Those in the left hand panel are fairly symmetric, with the near points clustering along the line of the obstacle. But when the presentation angle is shifted 90°, the paths become much less symmetric. In particular, the near points tend to cluster to one side or other of the obstacle. These differences in movement path at orthogonal presentation angles was characteristic of all the subjects in the this experiment: at some angles the paths tended to be symmetric at other angles the paths tended to be more skewed.

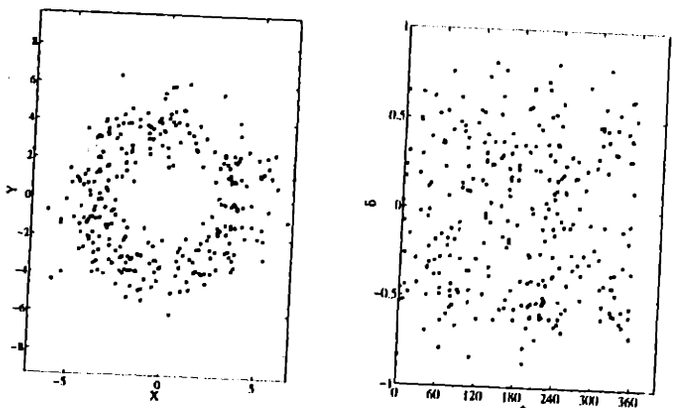

Figure 4-4: Hypothetical near point data for Experiment 4.1 showing no systematic variation. (a) Near points relative to the obstacle tip. (b) Near point angle, δ_{NP}, vs. presentation angle.

We will now make these informal observations more quantitative, by focusing a set of trajectory landmarks, and presenting a formal model which fits the experimental results. The purpose of the rest of this section is to convince the reader that the path variations described above are a general and robust property of the obstacle avoidance movements investigated in this study. In the following section (4.3), we present a model of trajectory planning which will incorporate the formal model below and provide an intuitive explanation of the movement asymmetries described here.

We begin by defining four trajectory landmarks: the near point (NP); the apex or point of maximal deviation from the straight line path (AP); the location of the local minimum of velocity (VM), if there is one; and the location of the peak of curvature (CP). If planning is carried out in Cartesian space, the symmetry of the task would predict that the position of any of these landmarks relative to the obstacle should be independent of the presentation angle, ϕ. Since ϕ was chosen uniformly from $[0°, 360°]$, the landmark locations should be uniformly distributed about the circle as well. Figure Figure 4-4(a) shows hypothetical near point locations which are consistent with the visual planning model. On the other hand, if the details of the actuator do influence planning, then the landmarks should not be distributed uniformly – for example they might cluster at certain angles around the obstacle tip. This is exactly what is seen in Figure 4-5, which shows near point locations for two subjects in the experiment.

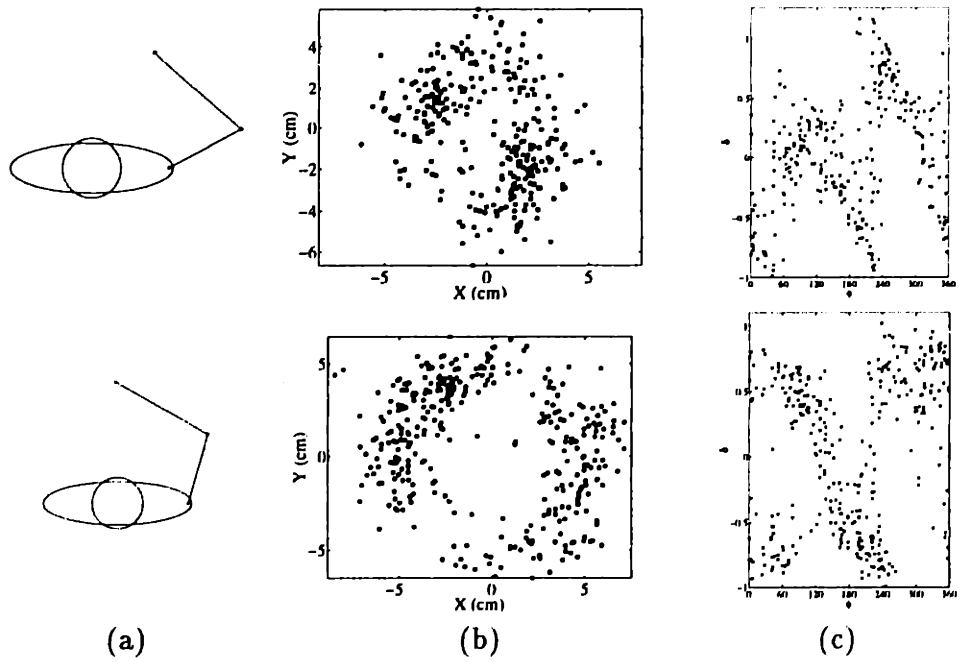

Figure 4-5: Sample near point results for Experiment 4.1. (a) The arm configuration for each experiment. (b) Location of the near points relative to the obstacle tip (center point of the experiment). (c) Dependence of the near point angle on the presentation angle. Top row: Subject JM at Position 1. Bottom row: Subject NT at Positon 2.

The non-uniformity of the near point and other landmark distributions can be seen more clearly by making explicit the dependence of their location on ϕ. We begin by defining an angle, δ, for each landmarks the difference between the presentation angle and the angle of the landmark from the obstacle tip. Figure 4-6 illustrates the case of the near point angle, δ_{NP}. Note that the δ are difference angles, that is they represent the angular distance which the landmark lies off presentation direction. If planning is based solely on extrinsic criteria, there should be no systematic dependencies of the δ on the presentation angle. Such is the case in Figure 4-4(b), which is a scatter plot of δ_{NP} versus ϕ for the same hypothetical data discussed above. On the other hand, if the details of the actuator do influence planning, we would expect that the δ would vary as the direction of the movement varies. Figure 4-5(c) shows a striking dependence of δ_{NP} on ϕ for two subjects' data.

Similar results are seen for the other three landmarks. Figures 4-7 and 4-8 show δ versus ϕ plots for all four landmarks for two different subjects. There is a clear dependence of landmark angle on presentation angle in every case, but there is a particularly simple and suggestive order to the near point and apex plots. These appear to be piecewise

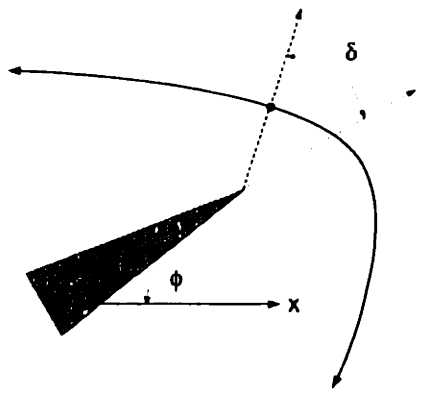

Figure 4-6: Definition of the near point angle, δ_{NP}, for the obstacle rotation experiment. The other landmark angles are similarly defined.

linear with negative slope. This form means that the zero crossings can be thought of as attractor points: as the presentation angle decreases from the zero crossing value, δ becomes positive, bringing the landmark back towards the zero crossing direction, and similarly for larger presentation angles. These attractor angles, which are located 180° apart, define an axis toward which the near points will cluster, as can be seen in the left hand plots of Figures 4-7 and 4-8. We define the variable ω to be the angle of the attractor that lies in the range $[0°, 180°]$, and we will refer to both the angle ω and the axis which it defines as the *preferred axis.*

We will now make these observations more formal. Given a data set, we can fit a piecewise linear model as described above using nonlinear least squares regression. The model for the regression is,

$$\delta = b\,\mathrm{smod}_{\pi}(\omega - \phi) + \varepsilon, \tag{4.1}$$

where ε is zero mean normally distributed noise and $y = \mathrm{smod}_{\pi}(x)$, the "signed mod", is defined as the y in the interval $[-\pi/2, \pi/2]$ such that $y - x = n\pi$ for some integer n. The parameter ω is the location of the zero-crossings, i.e. it is the preferred axis. If the presentation angle is near ω, then the predicted delta is small, and the landmark will lie near the line of the obstacle. On the other hand, when the presentation angle is far from ω, the model predicts that the landmark will get pulled to one side of the obstacle toward ω. The slope, b, determines the strength of the attraction.

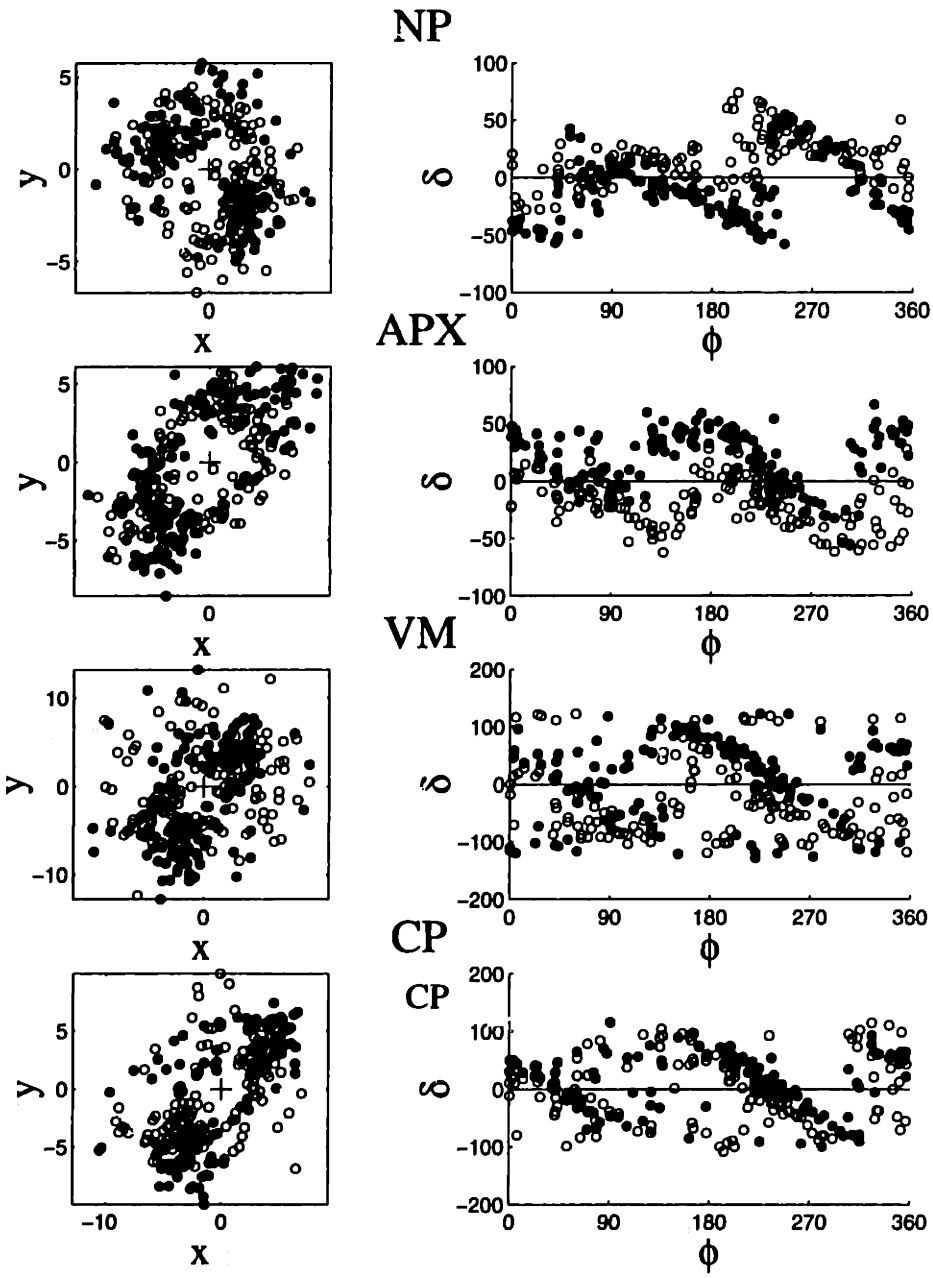

Figure 4-7: Landmark locations and angles for Subject NT in Position 1. From the top: near point, apex, velocity minimum, and curvature peak. Solid circles represent clockwise movements, open circles counterclockwise.

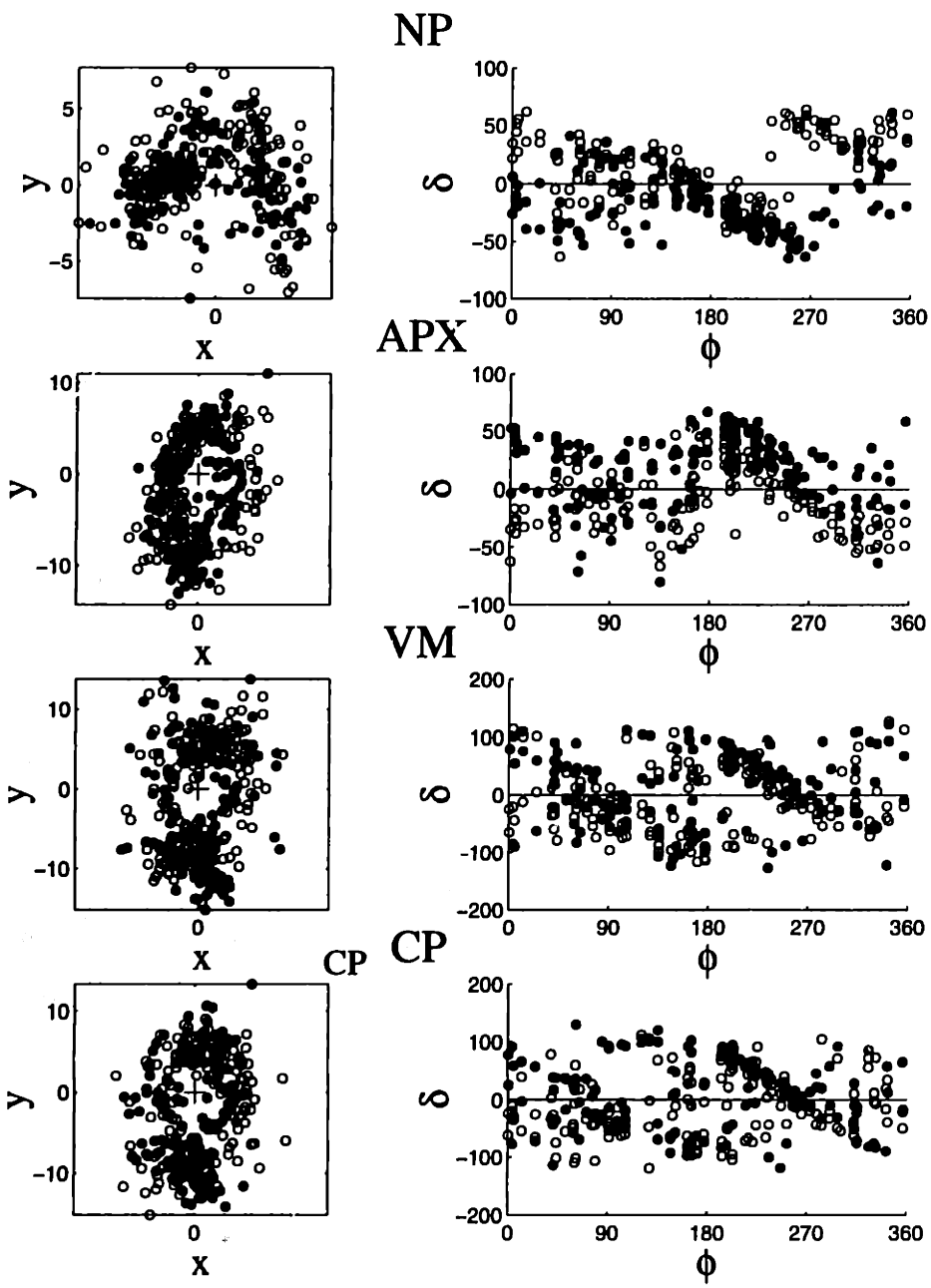

Figure 4-8: Landmark locations and angles for Subject PB in Position 2. From the top: near point, apex, velocity minimum, and curvature peak. Solid circles represent clockwise movements, open circles counterclockwise.

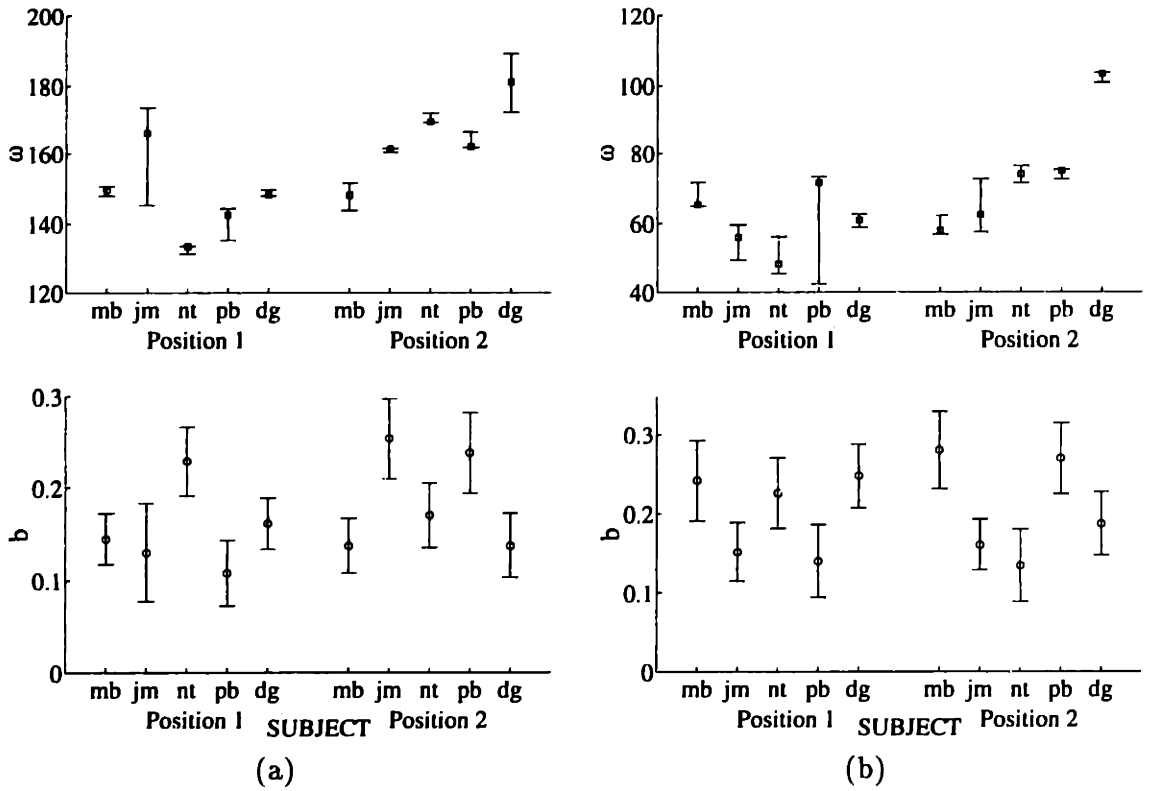

Figure 4-9: Regression results for Experiment 4.1. The top row is the preferred angle ω for each subject and each position, the bottom row is the regression slope, b. (a) Near Point Angle regression, (b) Apex Angle Regression.

The regression was computed by minimizing the square error with coordinate descent.[1] Confidence intervals for the preferred axis were derived using the fact that the difference in log likelihood between the optimal ω^* and some other ω is approximately distributed as χ^2 (McCullagh and Nelder, 1989). Thus the $1-\alpha$ confidence interval is:

$$\omega \in \{\omega \mid l(\delta, \phi|\omega) - l(\delta, \phi|\omega^*) < \chi^2(1-\alpha, 1)\}, \tag{4.2}$$

where $l(\delta, \phi|\omega)$ is the log likelihood of the data, given ω, which in this case is equivalent to the sum square error. Standard errors for the b are computed as in the case of linear regression. Also note that b plays the same role regarding hypothesis testing here as in the case of linear regression: if the b is significantly different from zero, the model is supported by the data, and the null hypothesis that the δ do not depend on ϕ is rejected.

Figure 4-9 shows summary results of the near point and apex angle regressions. Note

[1] Given the preferred axis, ω, the slope, b, is easily calculated as the correlation between δ and $\text{smod}_\pi(\omega - \phi)$. Standard one dimensional root finding techniques can then be used to optimize ω, given b.

that for every subject in both locations, the regressions have significantly positive slopes. Furthermore, the preferred axis for a given joint configuration is roughly constant across subjects.

With these analyses, we have shown that there are consistent asymmetries in obstacle avoidance trajectories as the orientation of the movement varies. Landmarks such as the near point and apex of the movement cluster at a preferred axis in space, independent of the presentation angle. We defer further interpretation of these results until after presenting a model for the planning of obstacle avoidance movements.

4.3 A Stability Model

In the previous section it was observed that the trajectory near points tend to cluster at opposite poles of the obstacle center. Comparing Figures 4-5 (a) and (b), we notice that the clusters roughly align with the orientation of forearm. This observation suggests that the planner chooses the near point location based at least indirectly on the arm's configuration as it approaches the obstacle.

What properties of the arm would make one location more desirable for the near point than others? We hypothesize that the answer to this question lies in the notion of stability. Since the only constraint on the movement, other than the start and target points, is to avoid colliding with the obstacle, it would be desirable to choose a path which maximizes the stability of the arm with respect to the obstacle. This notion will be made more formal in the next two sections, which introduce two notions of stability, one dynamic and one purely kinematic.

4.3.1 Kinematic Stability: Manipulability

The first definition of stability is based only on the kinematics of the arm. We are interested in how sensor or actuator noise propagates from joint angles to end-point position. Assume that either the joint actuators or sensors are noisy, with the independent noise at each joint having a variance, σ^2. Then the resulting noise in either achieved or sensed end-point position can be derived as follows:

$$\mathrm{Var}(d\mathbf{x}) \;=\; E(d\mathbf{x}\, d\mathbf{x}') \;\approx\; E(J\, d\theta\, d\theta'\, J')$$

$$= J\,\mathrm{Var}(d\theta)\,J' = \sigma^2 JJ',$$

Where $J(\theta) = \nabla_\theta \mathbf{x}$ is the Jacobian of the arm at the specified joint configuration. The approximation on the first line holds as long as the noise is sufficiently small in magnitude. The matrix

$$M(\theta) = J(\theta)\,J'(\theta)$$

reshapes the joint noise into end-point noise, and can thus be thought of as a measure of directional stability: assuming equal noise at each joint, it is more difficult to position or sense accurately along the major eigenvector of M than along its minor eigenvector. [2]

Yoshikawa (Yoshikawa, 1990) calls the matrix M manipulability, and discusses its relevance to the design of robot manipulators. His main point is that the eigenvalues of the matrix corresponds to the end-point velocities achievable for a given magnitude of joint velocity. Thus, in designing artificial manipulators, it is desirable to attain M with a large determinant (greater "manipulability"), and a small condition number (more uniform "manipulability").[3] Our use of the matrix here is different, as it focuses on the adverse effects of manipulability. As an eigenvalue of M grows, it become possible to attain larger end-point velocities along the corresponding eigenvector with the same joint velocities, but it also requires more precise joint control and sensing to achieve the same accuracy in end-point control and sensing. Here we focus on how the CNS might use the information contained in M to best to take advantage of (or cope with) non-isotropic manipulability.

In Experiment 4.1 the arm is constrained to planar, two-joint movements, as discussed in Section 4.2.1, and so the analytic form of the Jacobian is

$$J = \begin{bmatrix} -l_1 \sin\theta_1 - l_2 \sin(\theta_1+\theta_2) & -l_2 \sin(\theta_1+\theta_2) \\ l_1 \cos\theta_1 + l_2 \cos(\theta_1+\theta_2) & l_2 \cos(\theta_1+\theta_2) \end{bmatrix},$$

where l_1 and l_2 are the lengths of the upper arm and forearm respectively. This equation allows us to compute the manipulability matrices from the experimental data, and several examples are shown in the dashed curves of figure Figure 4-10.[4]

[2] Note that since M is by definition symmetric, its eigenvectors are guaranteed to be an orthogonal basis of the end-point cartesian space.

[3] The determinant of a matrix is the product of its eigenvalues. The condition number is the ratio of the largest to smallest eigenvalue.

[4] A symmetric matrix defines an ellipse (or ellipsoid in three dimensions) whose axes are the eigenvectors,

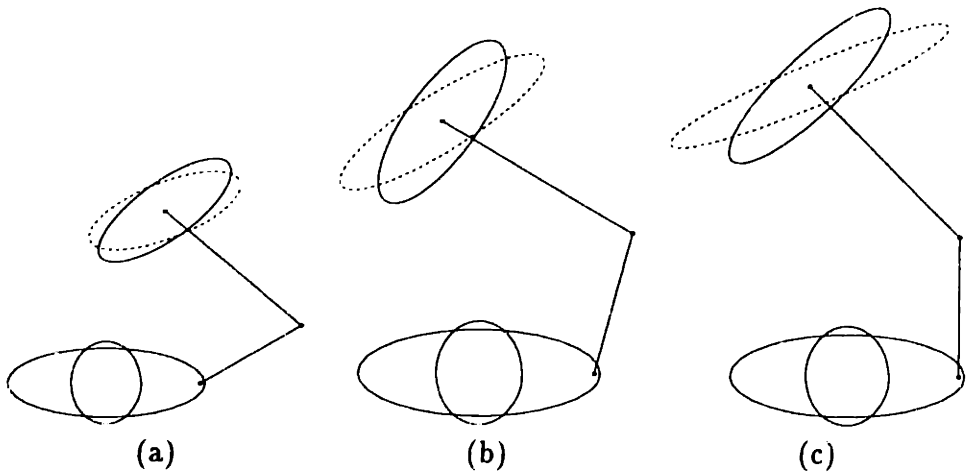

Figure 4-10: Manipulability (dashed) and mobility (solid) ellipses for a sample subject at various joint locations. (a) 30°, 110°, (b) 75°, 75°, (c) 90°, 45°.

4.3.2 Dynamic Stability: Mobility

We can also define stability based not on kinematic noise, but on the response of the arm to dynamic perturbations. One such measure such is the end-point mobility matrix

$$W(\theta) = J(\theta)\, I^{-1}(\theta)\, J'(\theta),$$

where $I(\theta)$ is the inertia matrix of the arm. W is the inverse the of the joint inertia matrix (the joint mobility matrix) transformed into the cartesian space (Hogan, 1985). The matrix relates forces at the end-point to the resulting acceleration, assuming the arm is initially at rest:

$$\mathbf{a} = W(\theta)\,\mathbf{f}, \text{ if } \mathbf{v} = 0.$$

As in the previous section, the eigenvectors are easily interpreted; the major eigenvector is the direction along which force perturbations have the largest effect.

Hogan (1985) shows that the CNS can take advantage of excess degrees of freedom in the arm to modulate the inertial properties at the end-point. In a striking example, he treats the arm as a 3 degree of freedom manipulator in the horizontal plane (shoulder, elbow, and wrist rotation), and shows that with this single extra degree of freedom the direction of

---

each with a length equal to its eigenvalue. In this case, we plot the ellipse corresponding to $M^{\frac{1}{2}}$, which describes the standard deviation of end-point noise if the joint noise is uniform. $M^{\frac{1}{2}}$ has the same eigenvectors as M and its eigenvalues are the square roots of M's eigenvalues.

greatest mobility can be rotated up to 90°. Here we propose that the CNS could use this same inertial information to choose the end-point locations of critical landmarks in the a movement, such as the point of nearest approach to an obstacle.

Again, the Jacobian is easily calculated from experimental data, but direct measurements of the inertia of the arm were not available for the subjects in Experiment 4.1. Instead, we used a simple model, which assumes that the links are point masses, m_1 and m_2, located some fixed fraction along the link length, a and b. The resulting inertia matrix is

$$I(\theta) = \begin{bmatrix} m_1 a^2 l_1^2 + m_2 l_1^2 + m_2 b^2 l_2^2 + 2 m_2 b l_2 l_1 c\theta_2 & m_2 b l_1 l_2 c\theta_2 + b^2 l_2^2 \\ m_2 b l_1 l_2 c\theta_2 + b^2 l_2^2 & m_2 b^2 l_2^2 \end{bmatrix}, \qquad (4.3)$$

where $c\theta_.$ and $s\theta_.$ are the sines and cosines of the respective angles. All parameters values except link lengths were adapted from the classic 1955 Dempster study, as referenced in (LeVeau, 1992). A variety of other values were tried, and the change had little effect on the quantities of interest here. The resulting mobility matrix estimates for one subject in several arm configurations are shown in solid lines in Figure 4-10.[5]

Stability and Obstacle Avoidance

For both of the matrices introduced in the preceding sections, the minor eigenvector represents the most stable direction, i.e. the one in which less unexpected movement is seen. Conversely, the major axis represents the least stable direction. This relationship is the key to following discussion. Since the comments apply equally well to both matrices, they will be referred to collectively as stability matrices.

To understand how a stability matrix relates to movement planning, consider the examples of Figure 4-11. The upper panel shows a possible path around an obstacle whose presentation angle is along the x-axis. The stability matrix for that orientation is shown as an ellipse centered at the obstacle tip. Would stability considerations deem this a good path? The region around the obstacle tip is expanded in the figure to the right, which shows that the line from the obstacle to the near point lies along the minor axis of the mobility ellipse. Since the arm is most vulnerable to collisions when it is closest to the obstacle, it is desirable for the arm to be relatively stable along the perpendicular to the path when

[5] As with the manipulability matrix, we present the ellipse corresponding to $W^{\frac{1}{2}}$. As Hogan (1985) points out, the resulting ellipse corresponds to lines of equal Kinetic Energy in momentum space.

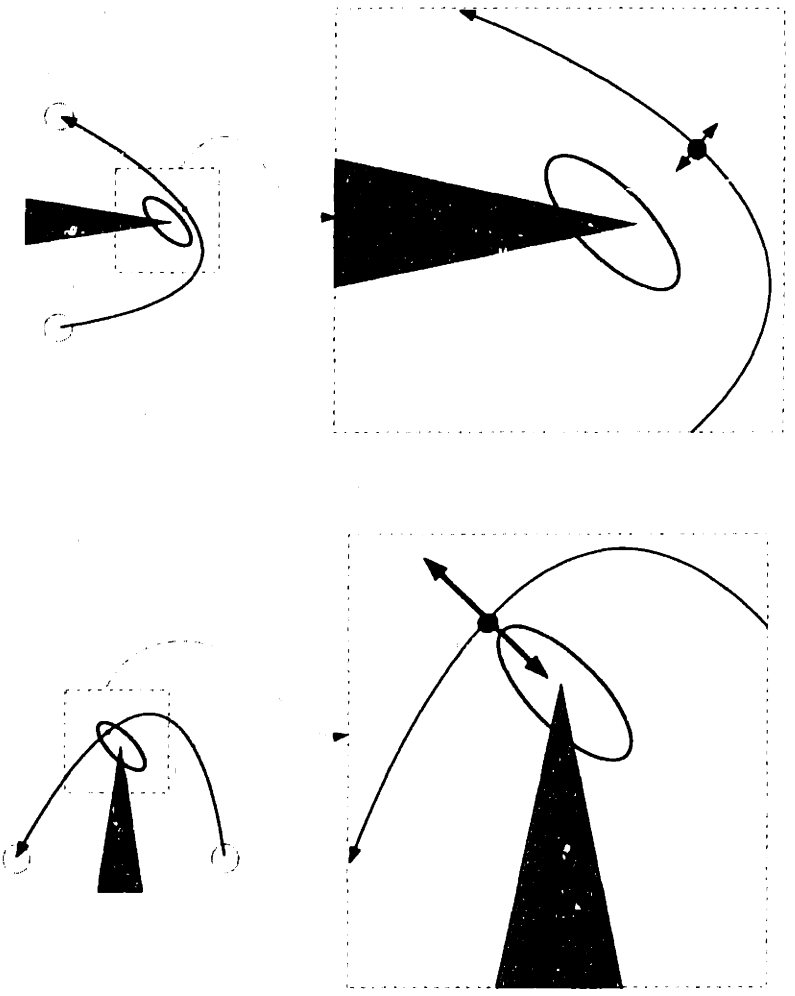

Figure 4-11: The relationship between a stability matrix and obstacle avoidance planning. The figure shows two paths identical up to a 90° rotation. The ellipses represent the stability matrix at the obstacle tip. For a discussion, see the text.

passing the near point. In this example, that criterium is maximally satisfied, as the path perpendicular is the direction in which the arm is most stable to perturbations.

The lower panel of Figure 4-11 shows an obstacle centered at the same location, but rotated 90°. The path displayed here is also the same as above, but rotated to achieve the start and target points. The near point now lies along the major axis of the mobility matrix. This means that when the finger tip comes closest to the obstacle, the arm is maximally susceptible to perturbations along the direction that will lead to a collision. For this presentation angle, then, the same near point angle is a poor choice. A more symmetric path with a δ_{NP} closer to zero would be preferable.

There are a few points to note about the preceding discussion. First, the comparisons were made based on the shape of the stability matrix at the obstacle center, not at the actual location of the finger tip. While this is a simplification, it is justifiable given that both the mobility and manipulability matrices change slowly over the workspace. Secondly, the interpretation of the mobility matrix as the acceleration response to a force perturbation is only in the static case. Nonetheless, the orientation of the mobility matrix is a dynamically relevant variable.

These considerations can be turned into a simple model of near point placement: the minor axis of the mobility or manipulability ellipse represents a preferred axis, in the sense of Section 4.2.2, for the near point. In order to minimize the risk of collision, the planner alters the trajectory of the arm to bring the near point closer to this maximally stable axis. Formally, the model is equivalent to the piecewise linear model of Equation 4.1, except that we now identify the preferred axis ω with the with minor axis of the stability matrix. Two examples of the near point location and resulting paths predicted by this model are shown in Figure 4-12.

4.3.3 Comparison of the Model and the Results from Experiment 4.1

We will now re-examine the results from Experiment 4.1 in light of the models presented above. Figure 4-13 shows raw near point data, preferred axes, and model predictions for two subjects. In both cases, the mobility minor axis is almost aligned with the near point preferred axis. The manipulability ellipse is also oriented in roughly the same direction. A summary of the comparison for all 10 data sets, i.e. for each subject and each joint configuration, is shown in Figure 4-14. Recall that the obstacle center locations were chosen

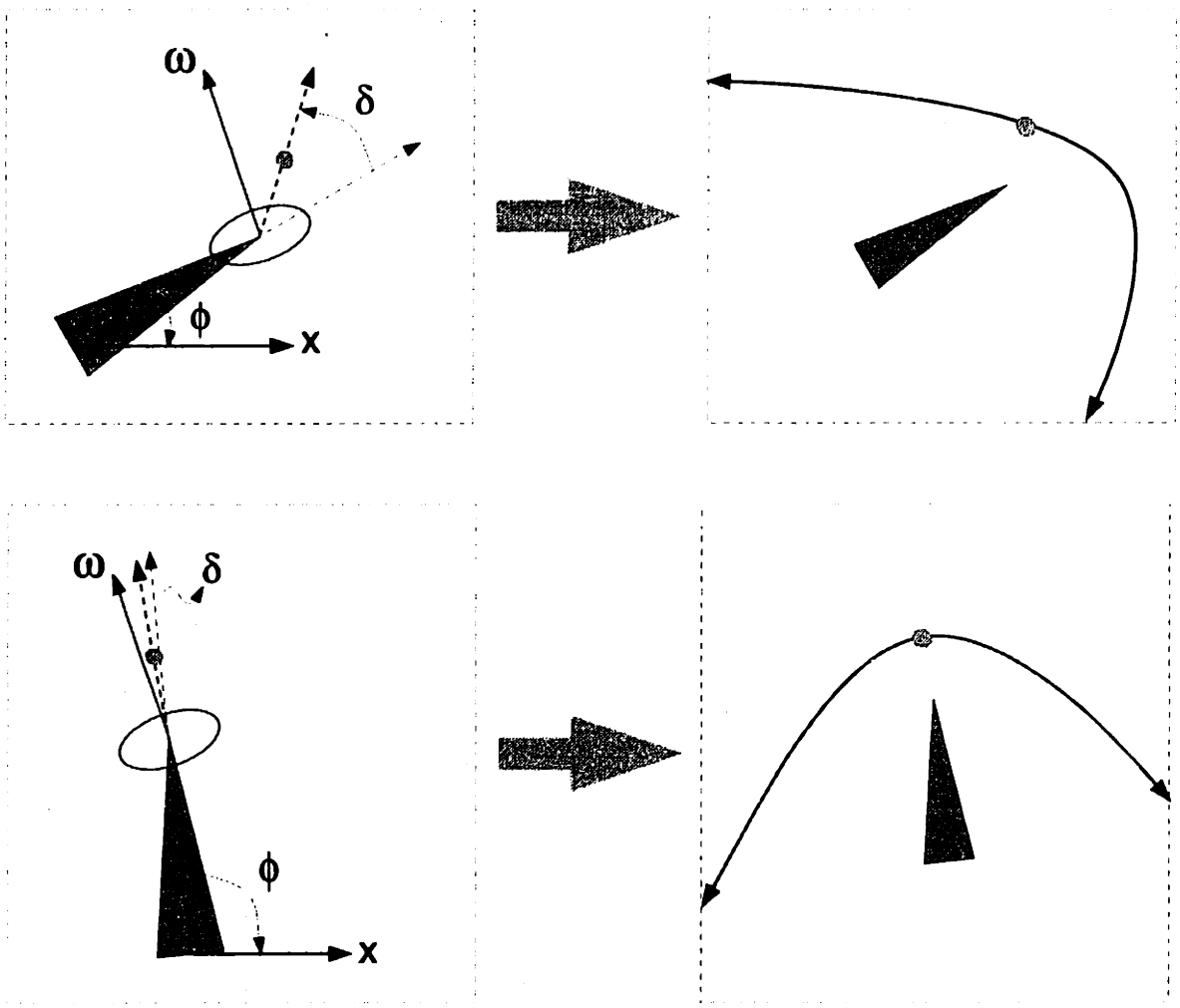

Figure 4-12: Predictions of the stability model of obstacle avoidance planning. Sample near point placements and paths for two presentation angles.

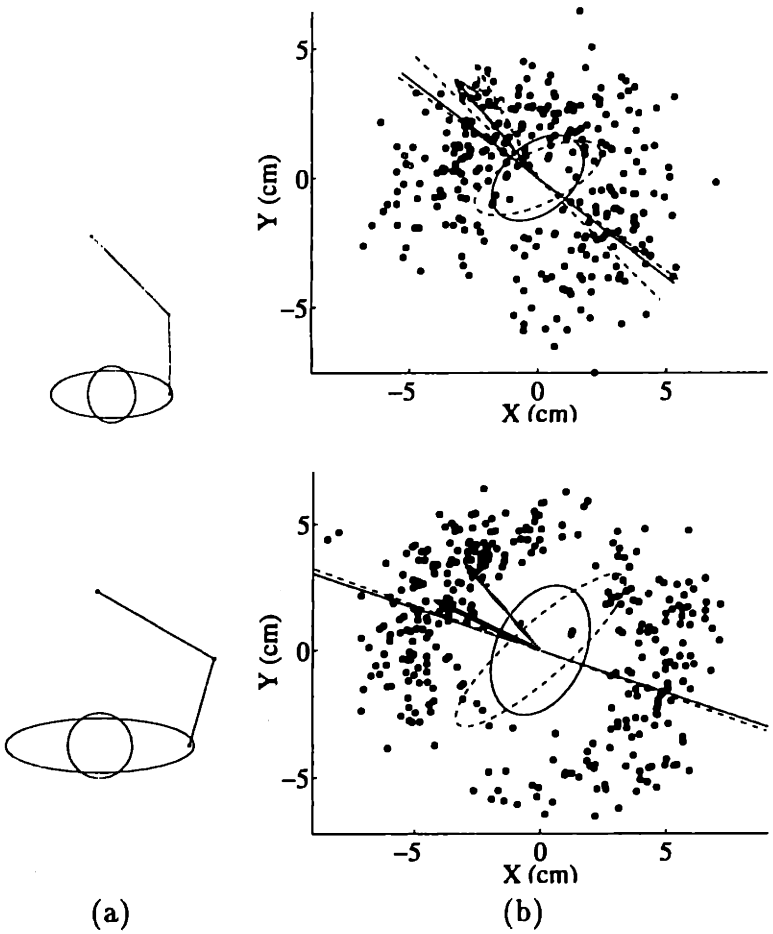

Figure 4-13: Near point data, preferred axes and model predictions for Experiment 4.1. (a) The arm configuration for each experiment. (b) Black lines represent the least squares preferred axis and 95% confidence intervals. The manipulability (dashed) and mobility (solid) ellipses with arrows representing their minor axes, manipulability in grey. Top row: Subject PB at Position 1. Bottom row: Subject NT at Positon 2.

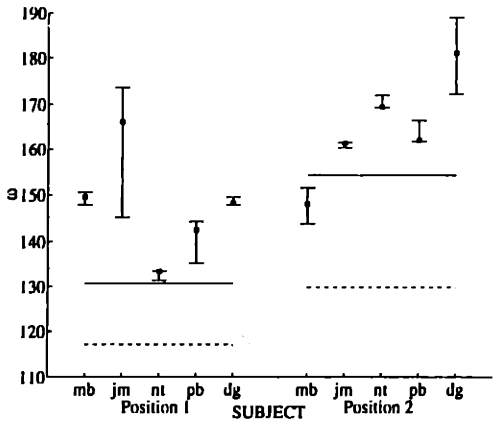

Figure 4-14: Summary of model predictions and experimental results for Experiment 4.1. The preferred angles are shown with the calculated mobility and manipulability minor axis angles.

to lie at a two specified locations in joint space. The orientation of the two stability matrices does not vary much from subject to subject at these configurations, and so a single line is used to represent the values for all subjects at a given position. Note that the scale of the plot is small – it covers only 80° of the 180° range of possible axis values. The figure shows that the mobility matrix prediction is within 10° to 20° for all but a couple of data sets. This agreement is quite good considering the overly simplistic model used to estimate the inertia of the arm. The manipulability prediction performs marginally worse. Also note that for each subject, the preferred axis at the first joint configuration is significantly lower than the preferred axis at the second orientation, a feature which both models predict.

The model suggests another comparison. Since the arm is less stable along directions off the preferred axis, it would be prudent to allow more clearance when passing near to the obstacle at those angles. In fact, the data show a significant dependence of the obstacle clearance (i.e. the distance from the near point to the obstacle) on the near point angle. Examples of this phenomenon can be seen in Figure 4-15. Regressions of Clearance on $|\delta_{NP}|$ were highly significant with $p < .001$ for all but one data set, for which the p-value was 0.02. The mean (s.d.) of the regression slopes was 2.17 (27) cm/rad. This is fairly large given that the average clearance over all data sets is 3.62cm (0.24cm) and the absolute values of δ_{NP} lie roughly in the range of zero to one. However, the effect was not all that strong, with mean a R^2 statistic of 0.16 (0.03).

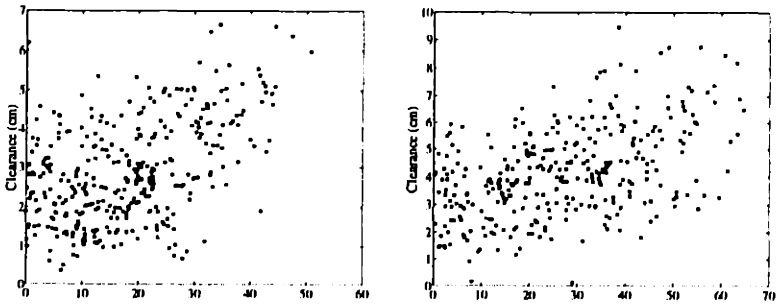

Figure 4-15: Clearance as a function of near point angle for Experiment 4.1. (a) Subject MB at Position 1, (b) Subject PB at Position 2.

4.3.4 Discussion

The important distinction between the kinematic and dynamic models does not lie in the formal definitions of the manipulability and mobility matrices. In fact, the two matrices are quite similar both in their analytic form and in the values they take for the human arm. As discussed above, the manipulability matrix can be interpreted as the Covariance matrix of end-point position if the joints have independent, equal magnitude noise. Relaxing this restriction is the same as introducing a new factor to the end-point noise,

$$M(\theta) = J(\theta)\, V_\theta\, J'(\theta),$$

where V_θ is the joint covariance matrix. The form of M is now even more similar to the mobility matrix.

The interesting distinction between the models is the nature of the information they utilize for planning arm movements: purely kinematic or both kinematic and dynamic. The observational studies of this chapter do not decisively distinguish between the possibilities, but we will return to this issue in the next chapter.

4.4 Conclusions

In this chapter we have introduced the obstacle rotation paradigm, which is designed to probe the criterion used by the CNS in planning kinematically constrained arm movements. This experiment revealed a striking asymmetry in the paths of simple obstacle avoidance

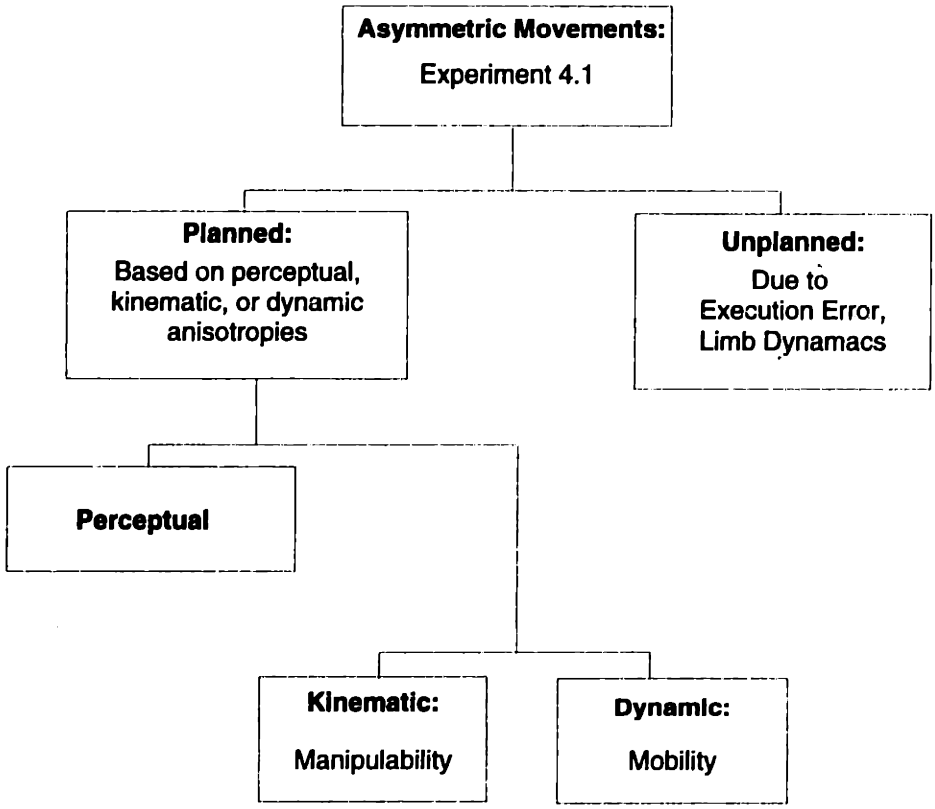

Figure 4-16: A graphical representation of the possible origins of the trajectory anisotropies in the obstacle rotation experiment.

movements. These effects could be due to a number of factors, and the possibilities are outline in Figure 4-16. We begin by assuming that the movements are planned, in the sense of Chapter 1. That is, the kinematic variations in the movements are represented in the central command signal. In this case, there must be some criterion by which the CNS chooses the path to take at each presentation angle. Those criterion could be based on any combination of perceptuo-visual cues, kinematics of the actuator, and dynamics of the actuator, as shown on the left branch of Figure 4-16. The comparisons of Section 4.3.3 show that both the kinematic manipulability model and the dynamic mobility model predict qualitatively the results of Experiment 4.1, although the mobility model shows closer agreement with the data. We will return to this comparison in the next chapter, when we measure the mobility matrix in three dimensions and compare the measurements with a 3-D version of the obstacle rotation experiment. The results of this chapter do not address the possibility that a perceptual anisotropy could be responsible for the movement asymmetries of Experiment 4.1. This concern will be resolved in the next chapter.

Finally, we consider the right branch of Figure 4-16. It is possible that the results of

Experiment 4.1 are due entirely to low level dynamic factors and not to a central planning mechanism. We defer this issue until Chapter 6, when we present two experiments which rule out a low-level explanation of Experiment 4.1.

Chapter 5

A Role for Dynamics in Motor Planning

5.1 Introduction

In this chapter, we present two experiments which continue the investigation of obstacle avoidance movements begun in Chapter 4. In particular, we will present a three dimensional version of the obstacle rotation experiment and a follow-up study directly measuring the relevant mobility matrices.

There were several motivating factors for conducting the obstacle rotation experiment in three dimensions. First, a major limitation of literature on goal directed arm movements is the restriction to planar movements. Most of those studies, including Experiment 4.1, involved interaction with a planar surface or 2 degree-of-freedom manipulandum. This fact places these movements into the domain of compliant control (Hollerbach, 1982), where an entirely different strategy may be used for planning movements. This is a particularly important point for our case, as we are trying to make an argument about the way that the CNS interacts with a *particular* object, namely the obstacle, and so additional constraints could color our results. In the present study, subjects' arms were completely unconstrained and movements were performed in a variety of orientations.

Also, we wanted to investigate whether the phenomena seen in Experiment 4.1 could be the result of a perceptual, rather than motor, anisotropy. We will tackle this issue with an intermanual comparison of obstacle avoidance movements; perceptual explanations would

predict no difference between the two sets of movements.

Finally, the Phantom 3-D Haptic Interface Device was available for directly measuring the mobility matrices of subjects under the same conditions as those in the obstacle rotation experiment.

5.2 Obstacle Rotation in Three Dimensions: Experiment 5.1

5.2.1 Methods

Experiment 5.1 is a three dimensional version of the Experiment 4.1 with unconstrained arm movements. Five subjects, two left handed and three right handed, participated in the experiment. All subjects all had normal or corrected to normal vision. The author was a subject, and two of the remaining subjects (DW, SG) were also either involved in the project or aware of the purpose of the experiment.

An Optotrak was used to monitor the position of an IRED marker mounted on the tip of subjects' index fingers, and the positions were read by an SGi Indigo 2 at 200 Hz. When subjects used their right arms, two additional markers were placed at the elbow and shoulder. The arrangement of the apparatus precluded measuring the joint positions for the left arm. Subjects were seated with their heads constrained by a chin rest and a pair of field-sequential stereo glasses, both of which were mounted on the frame of the apparatus. This arrangement allowed accurate 3D visual feedback of the finger location as well as the placement of virtual target spheres and obstacle cylinders in a workspace which was approximately 30cm in diameter centered 28.8cm below eye level (at the level of the virtual image of the screen) and 35cm in front of the subject, along the midline.

Before each experiment, the visual feedback system was calibrated to insure that the absolute positions determined by the Optotrak were in register with the perceived 3D location of the visual feedback. Calibration consisted of having subjects point to 30 randomly positioned target cubes uniformly distributed about the workspace of the experiment. The visual coordinates were fit to the absolute positions with a linear regression, and the fit was validated by testing at 10 more points. Only subjects whose RMS validation error was below 8mm were used in the experiment.

The experiment was divided into blocks during which the cylindrical obstacle was fixed in space at the workspace center (the *center point*), with it's length lying along either the X-

axis (transverse direction), Y-axis (sagittal direction), or Z-axis (vertical). Within a block, the start and target points were always located in the plane which passes through the center point perpendicular to the obstacle. The presentation angle determined the orientation of the start and target points relative to the obstacle. Examples of the virtual visual scene are shown in Figure 5-1(a).

As in Experiment 4.1, trials came in pairs with start and target points switched within the pair. A trial block consisted of 120 randomly ordered movements pairs with presentation angles located at 3 degree increments. Each subject participated in 2 sessions, one for movements with each hand. The sessions, which were on different days, consisted of three blocks, one in each plane. The order of the sessions and blocks with a session were randomized.

5.2.2 Results

Subjects in Experiment 5.1 exhibited a significant and systematic variation in the movement paths as a function of presentation angle, further supporting the findings of Experiment 4.1. Note that for a given experimental block, all the rotations of the visual scene are about the obstacle, and the obstacle remains fixed in space. The movements for any obstacle orientation lie primarily in a single plane – the fronto-parallel, horizontal, and sagittal planes for X, Y, and Z axis conditions, respectively. Furthermore, motion along the third direction does not change the distance to the obstacle. Thus, for our analysis movements are projected onto the plane perpendicular to the obstacle, and the presentation and near point angles are defined as in Experiment 4.1. Figure 5-1 shows sample near point data for three subjects in three different planes of movement. The data show the same asymmetries seen in the previous experiment. Furthermore, the plot of near point angle versus presentation angle is nearly piecewise linear with a negative slope, suggesting that within each plane there is a near point preferred axis. The figures also show the results of the preferred axis regressions.

The results of Experiment 5.1 are summarized in Figure 5-2, which shows the near point axis regressions for all subjects and all conditions. With only one exception (Subject CS, Z-plane, left hand), all near point regressions were significant. Furthermore, within an experimental condition, there was no more than about a 30° spread for the preferred angles across subjects (with the exception of Subject CS, Z-plane).

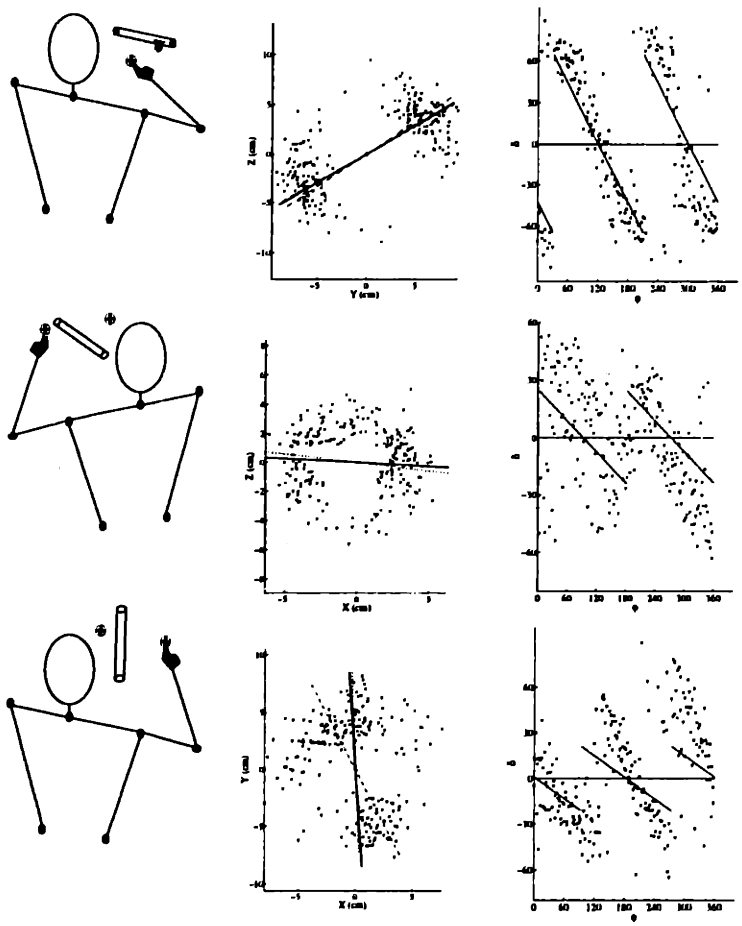

Figure 5-1: Sample Near Point Results for Experiment 5.1. (a) Orientation of the obstacle. (b) Near Points locations relative to the obstacle center. The radial lines represent the near point preferred axes and 95% confidence intervals. (c) Near Point angle vs. Presentation Angle. The model prediction is shown as well. Top: Subject TF, Right hand movements in the X (sagittal) plane. Middle: Subject CS, Left hand movements in the Y (frontal) plane. Bottom: Subject SG in the Z (horizontal) plane.

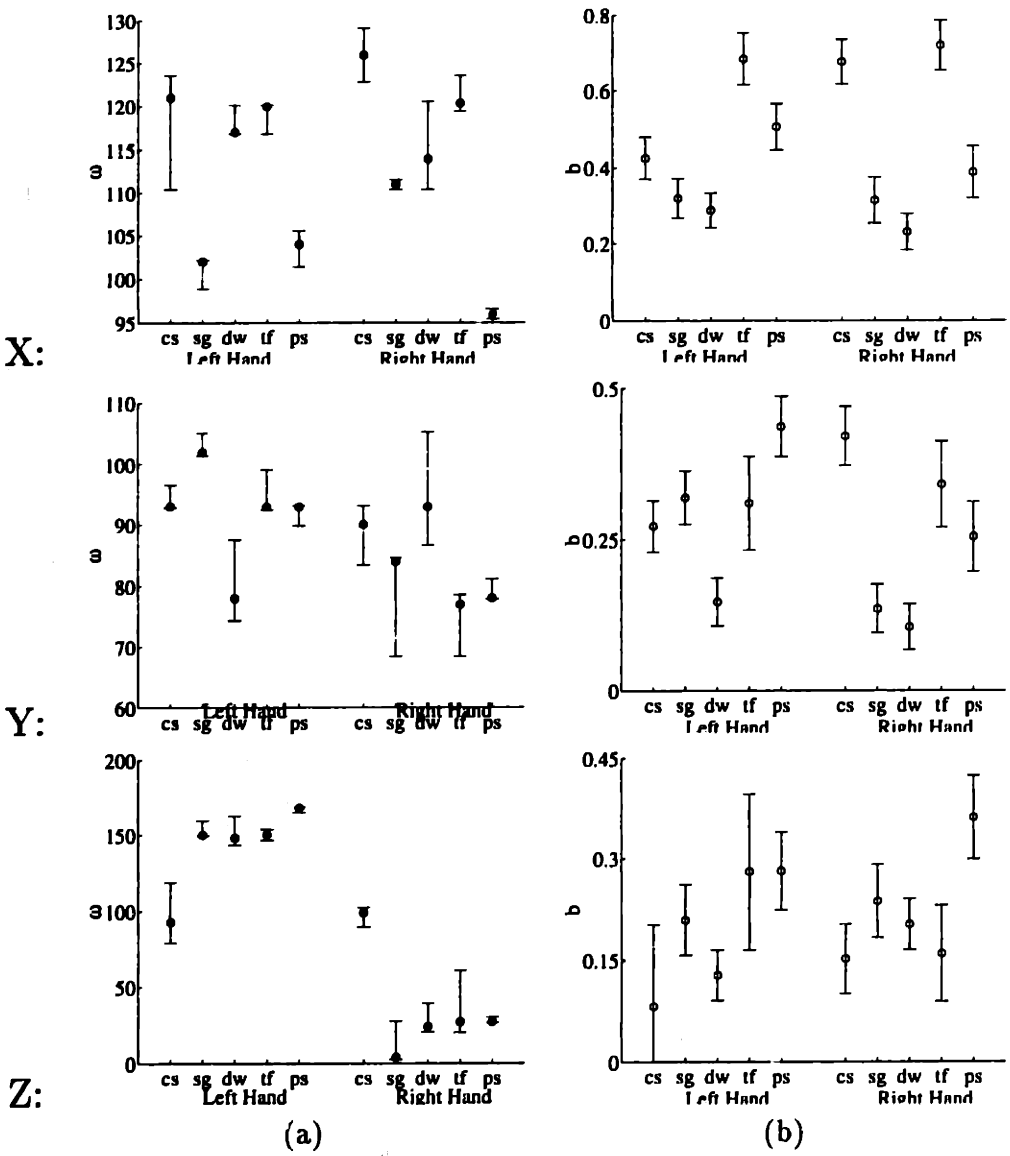

Figure 5-2: Near Point Angle Regressions for Experiment 5.1. Each row represents one plane of movement, labeled at the left. (a) Near point preferred axis, ω, for each subject and each arm. (b) Regression slope, b.

Left Hand vs Right Hand

One explanation for the trajectory asymmetries seen in these experiments is that there are anisotropies in the perceptual system which lead to different movement plans at different orientations. There is some experimental evidence suggesting that such perceptual distortions can effect the trajectory of pointing movements: Wolpert et al. (1994) showed that there is a correlation between perceived curvature and movement curvature in point-to-point movements. In order to control for this possibility, we compare subjects' behavior with their left and right hands. If the effects are perceptual in origin, then we would expect that they would be the same for both the left and right hand movements. On the other hand, if the effects are due to control processes which are dependent on either the arm's kinematic or dynamic properties, then we would expect intermanual differences in behavior. In fact, as our experiments were centered along the midline, we can predict that the asymmetries for one arm should be the mirror image of those of the other arm, reflected about the midline.

To facilitate this comparison, the preferred axes from Figure 5-2 have been replotted in Figure 5-3 in a circular format. Each ring corresponds to a single subject, each line marks a preferred axis and 95% confidence interval. For Z-plane movements, there is a large separation in the preferred axis for each hand. However, when the left hand values are reflected about the X-axis, the two data sets closely coincide. Similar results are seen for the Y-plane movements, although the smaller initial separation makes the comparison less striking. Finally, for movements in the sagittal plan (X), symmetry predicts the same results for either hand, as the data demonstrate. These results allow us to rule out a perceptual origin for the movement asymmetries described above.

Comparison With Stability Models

As was done for the data from Experiment 4.1, we can estimate both the manipulability and mobility matrices at the obstacle center, and compare the near point preferred axes with these estimates. From the measured joint locations, we can compute the Jacobian of the arm at the center of the workspace, and thence the manipulability matrix at that location. Furthermore, we can estimate the inertial properties of the links and calculate the mobility matrix. Since we only measured the location of the shoulder, elbow, and finger tip, we must make the assumption that the wrist and index finger were fixed during the experiment.

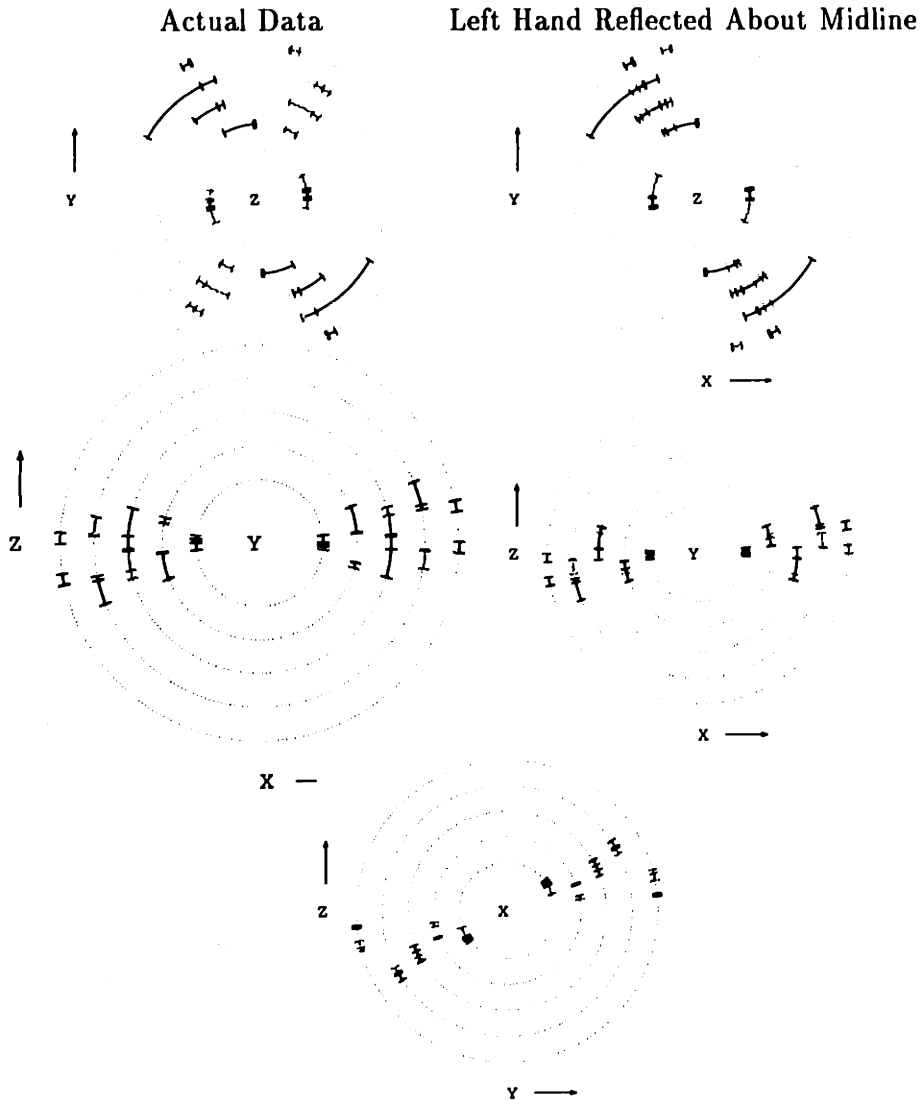

Figure 5-3: Intermanual Comparisons rule out Perceptual Explanation of Experiment 5.1. Each plot depicts the preferred axes for each a given obstacle orientation. A single circle represents one subject. The lines mark the preferred axis and 95% confidence intervals for each experiment: black line for left hand movements, the grey line for right hand movements. Left: actual data. Right: data for the left hand have been reflected about the X axis. The bottom plot shows the actual results for the X axis movements.

This turns out to be fairly well justified, as the variance of measured distance from elbow to finger was small, with a mean (s.e.) standard deviation of forearm length across subjects of 0.48cm (0.04cm), or 1.1% of the link length. This means that finger and wrist motion were minimal components of the overall movement, and the arm can be considered a 4 degree of freedom manipulator.

We use the joint coordinate system of Soechting and Terzuolo (1986). The orientation of upper arm and forearm are both indexed by an elevation, θ and β respectively, and an azimuth, η and α respectively. The elevations are angles from the -Z axis (for θ) or +Z axis (for β), and the azimuth angles are zero along the +Y axis, increasing towards the +X axis. The resulting forward kinematics of the arm are described by the equations,

$$\begin{aligned} x(\Theta) &= l_1 \, s\theta \, s\eta + l_2 \, s\beta \, s\alpha \\ y(\Theta) &= l_1 \, s\theta \, c\eta + l_2 \, s\beta \, c\alpha \\ z(\Theta) &= -l_1 \, c\theta + l_2 \, c\beta, \end{aligned} \tag{5.1}$$

where $\Theta = (\theta, \eta, \beta, \alpha)$, $c\phi$ and $s\phi$ will be used to represent the sine and cosines of an angle ϕ, and l_1 and l_2 are the upper arm and forearm link lengths. Equation 5.1 is enough to compute the Jacobian and manipulability matrix. For the mobility, we need to make some assumptions about the inertia of the arm segments. As in the planar case, we make the simplifying assumption that the mass of the arm is concentrated at a single point. One implication of this assumption is that there will be no inertia associated with the rotation of any link about its major axis. The resulting inertia matrix is,

$$
\begin{pmatrix}
a^2 l_1^2 m_1 + l_1^2 m_2 & 0 & B\,c\theta\,c\eta\,c\beta\,c\alpha - B,s\theta\,s\beta + B\,c\theta\,c\beta\,s\eta\,s\alpha & B\,c\theta\,c\alpha\,s\eta\,s\beta - B\,c\theta\,c\eta\,s\beta\,s\alpha \\
0 & .5\,a^2 l_1^2 m_1 + 0.5 l_1^2 m_2 - .5\,a^2 l_1^2 m_1 \cos(2\theta) - .5 l_1^2 m_2 \cos(2\theta) & B\,c\beta\,c\alpha\,s\theta\,s\eta + B\,c\eta\,c\beta\,s\theta\,s\alpha & B\,c\eta\,c\alpha\,s\theta\,s\beta + B\,s\theta\,s\eta\,s\beta\,s\alpha \\
B\,c\theta\,c\eta\,c\beta\,c\alpha - B\,s\theta\,s\beta + B\,c\theta\,c\beta\,s\eta\,s\alpha & -B\,c\beta\,c\alpha\,s\theta\,s\eta + B\,c\eta\,c\beta\,s\theta\,s\alpha & b^2 l_2^2 m_2 & 0 \\
B\,c\theta\,c\alpha\,s\eta\,s\beta - B\,c\theta\,c\eta\,s\beta\,s\alpha & B\,c\eta\,c\alpha\,s\theta\,s\beta + B\,s\theta\,s\eta\,s\beta\,s\alpha & 0 & .5\,b^2 l_2^2 m_2 - .5\,b^2 l_2^2 m_2 \cos(2\beta)
\end{pmatrix}
$$

where $B = b\,l_1\,l_2\,m_2$, the m_i are the link masses, and a and b are the distances from the proximal joint to the center of mass as a fraction of link length (radii of gyration). Values for all parameters except link lengths were the same as those used in Experiment 4.1 (Section 4.3.2). Again, it should be noted that a variety of other values were tried, making little difference on the quantities of interest here.

Figure 5-4 shows the how the orientation of the minor axes of the calculated manipulability and mobility matrices compares with the preferred axes from Experiment 5.1. Note that only data for the right hand movements were available. The models once again qualitatively capture the results from the obstacle rotation experiment. For the X and Z plane movements, both models are in rough agreement, although the mobility prediction is more accurate. For movements in the Y plane, the mobility matrix orientation does not coincide with the data from Experiment 5.1. However, it should be noted that the condition number of the mobility estimate was much smaller in the Y plane than in the other two planes:[1] 1.3 in the Y-plane compared to 1.7 and 4.0 in the X and Z planes, respectively. This fact means that the determination of the minor axis in the Y-plane will be sensitive to small changes in the value of the matrix. Given that our model of the arm's inertia is quite simple, we

[1]The condition number of a matrix is the ratio of the largest to smallest eigenvalue. Condition numbers near 1 mean that the associated ellipse is roughly circular, making determination of the minor axis less precise.

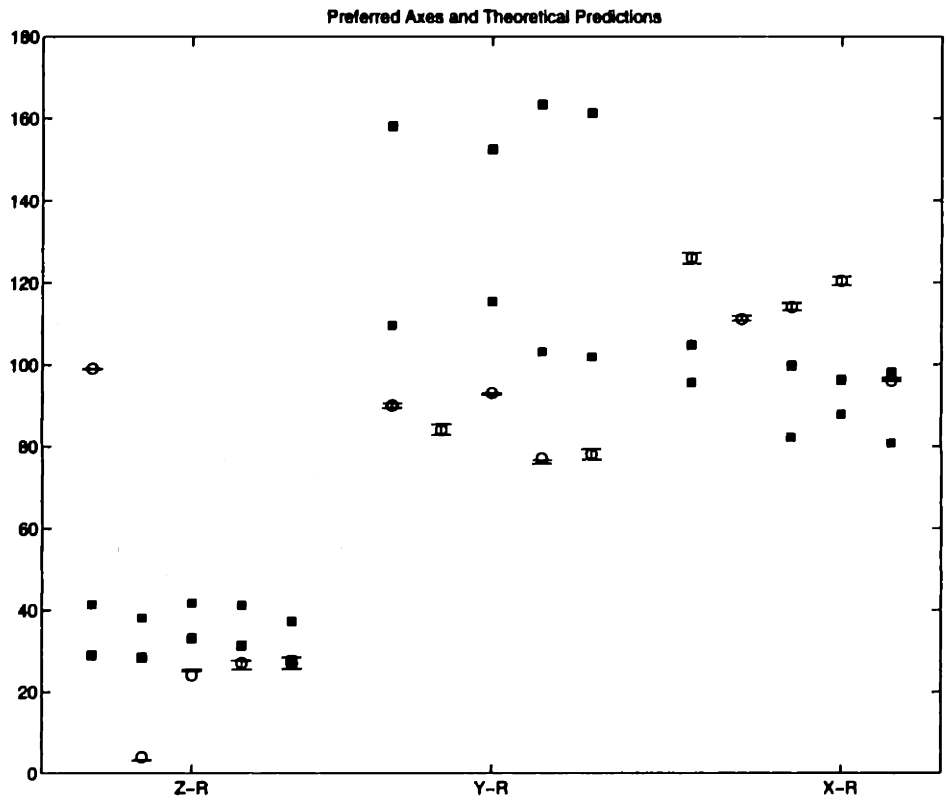

Figure 5-4: Comparison of model predictions and preferred axes from Experiment 5.1. Open circle show the preferred angles and 95% confidence intervals for the right hand movements of Experiment 5.1. Black squares are the mobility matrix minor axis orientations, and grey squares are the same for the manipulability matrix.

should thus view these particular values with suspicion.

5.3 Direct Measurement of the Mobility Matrix in 3D: Experiment 5.2

For four of the five subjects that participated in Experiment 5.1, we made direct measurements of the mobility matrices using the Phantom 3D manipulandum. The idea of the experiment is to perturb the position of the hand with known forces and measure the subsequent acceleration. By repeating this process with a sampling of force directions, the mobility matrix can be estimated.

5.3.1 Methods

Subjects CS, DW, SG, and TF from Experiment 5.1 participated in the experiment. Subjects were seated at the same experimental apparatus as in Experiment 5.1, except that they held the handle of a low inertia Phantom manipulandum which is capable of producing up to 20N of force in any direction in 3D space. The handle was designed to rotate freely about the center in all three directions so that no torques would be transferred to the hand.

A target circle appeared in the 3D visual display at the same location as the center of the obstacles in Experiment 5.1. At the beginning of each measurement, the robot assisted the subject back to this location by simulating a weak spring. When the subject was within 2cm of the center point for 200ms consecutively and the hand velocity was less than 1cm/sec, the robot began exerting a force in a given direction. The forces ramped up linearly from 0 to 4.0N in 80ms, and then held constant at 4.0N for 275ms. The position of the subject's hand was monitored with the Optotrak for a 1 second window beginning 20ms before the force onset. The position sampling occurred at 1500 Hz.

An experiment consisted of 72 randomly ordered force perturbations in equally spaced directions along the circle in either the sagittal (X), frontal (Y), or horizontal (Z) planes. For each subject, 6 experiments were conducted, one for each hand in each plane.

5.3.2 Results

The goal of this experiment was to measure the mobility matrix, $W(\theta)$, at the joint configuration corresponding to the center of the obstacle in the previous experiment. We calculated

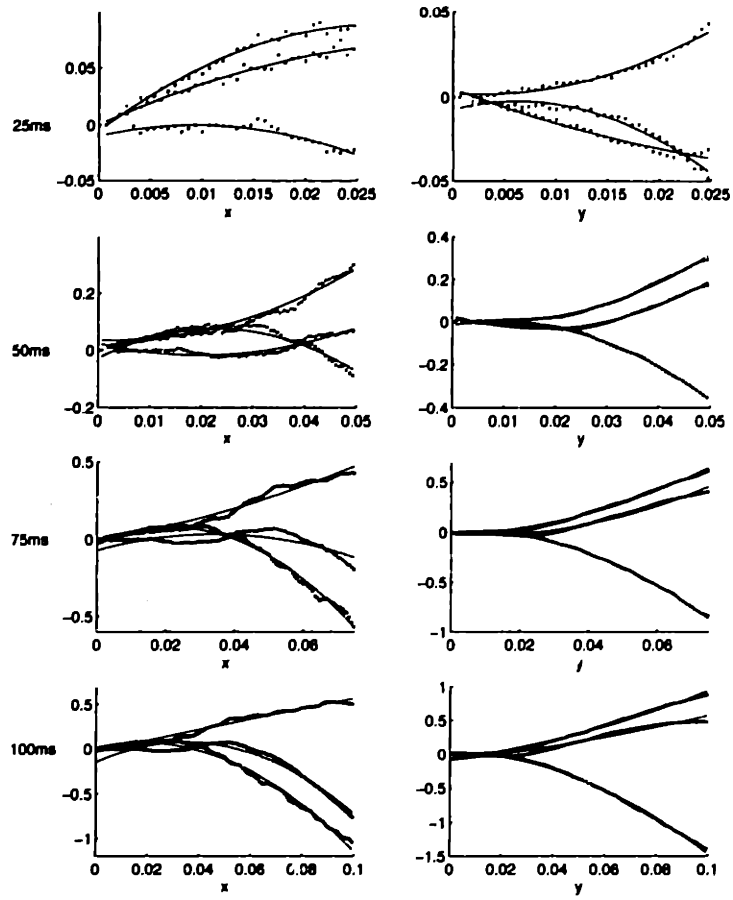

Figure 5-5: Sample position traces from the horizontal plane (Z) experiment with Subject CS, right hand. The $-110°$, $100°$ and $130°$ traces are shown: x positions in the left column, y positions in the right column, both versus time in secs. Each row corresponds to a time interval marked at the left of the figure. The plots show both the position data (dots) for that interval as well as the quadratic fits used to compute the average acceleration over the interval (solid lines).

$W(\theta)$ using the relationship,

$$\mathbf{a} = W(\theta)\mathbf{f}. \tag{5.2}$$

For each of the 72 measurement angles in an experiment, the nominal force profile at the handle was known. From the position traces we could estimate the acceleratory response. Typical position traces for the first 25, 50, 75, and 100ms after the onset of the perturbation are shown in Figure 5-5, along with the quadratic fits used to estimate acceleration. It can be seen from this figure that the 25ms traces are noisy and sometimes exhibit little curvature. On the other hand, the 75ms and 100ms traces deviate significantly from the fit, at least for the x coordinate. We will return to the issue of the appropriate time window below, but for now we will note that these informal observations are consistent with later conclusions

that a time window of about 50ms is appropriate.

Given a set of force and acceleration measurements, we used linear regression to estimate the mobility matrix,

$$W = \left[\sum_{i=0}^{72} a_i f_i'\right] \left[\sum_{i=0}^{72} f_i f_i'\right]^{-1} . \tag{5.3}$$

Examples of these fits for three subjects, each in a different plane, are shown in Figures 5-6 to 5-8. Each Figure shows four fits, one for each of the time intervals above. The dashed ellipse shows the predicted accelerations based on Equation 5.2. Note that this trace hides the fact that there may be significant curl in the matrix, i.e. there could be a rotation component to the fit. As we know that the mobility matrix should be symmetric (zero curl), we might also choose as our estimate of the mobility the symmetrized version, $W_s = (W + W')/2$. This prediction is shown in solid.

Note that although the dashed and solid lines in these figures nearly coincide, the matrices W and W_s may differ significantly. This is due to the fact mentioned above that the curl of the matrix is not shown in this plot. In fact, the W matrices did contain sizable curl components. This rotation could be due to a number of sources. First, the IRED was not positioned exactly at the point where the force acted on the hand, so there may be some genuinely rotation in the data. Secondly, at very short time intervals, the measurements are noisy, which could result in spurious non-symmetric components to the least squares estimate of W. And thirdly, while we know theoretically that the mobility matrix should be symmetric, the matrix only relates force to acceleration when the hand is at rest. Thus, as the time window increases, we expect that other terms of the dynamics will come into the measurements. Also, the arm will have moved during the longer time windows and the inertia will depend in a non-symmetric way on the new location.

Figures 5-6 to 5-8 make clear the dependence of the mobility matrix regression on the time window over which we choose to regress. Ideally, we would like to measure the acceleration as early as possible. There are several reasons for this. As mentioned above, at longer intervals, the arm will be moving which will bias the result. Also, at longer intervals, reflexes may come into play. However, at very early latencies, the noise level is too high.

In order to choose an acceptable time window, we calculated the regression of Equation 5.3 for a series of time windows, $[T_1, T_2]$ with T_1 varying between 10ms and 80ms and T_2 between T_1 + 20ms and 100ms. For each estimate, we considered the regression

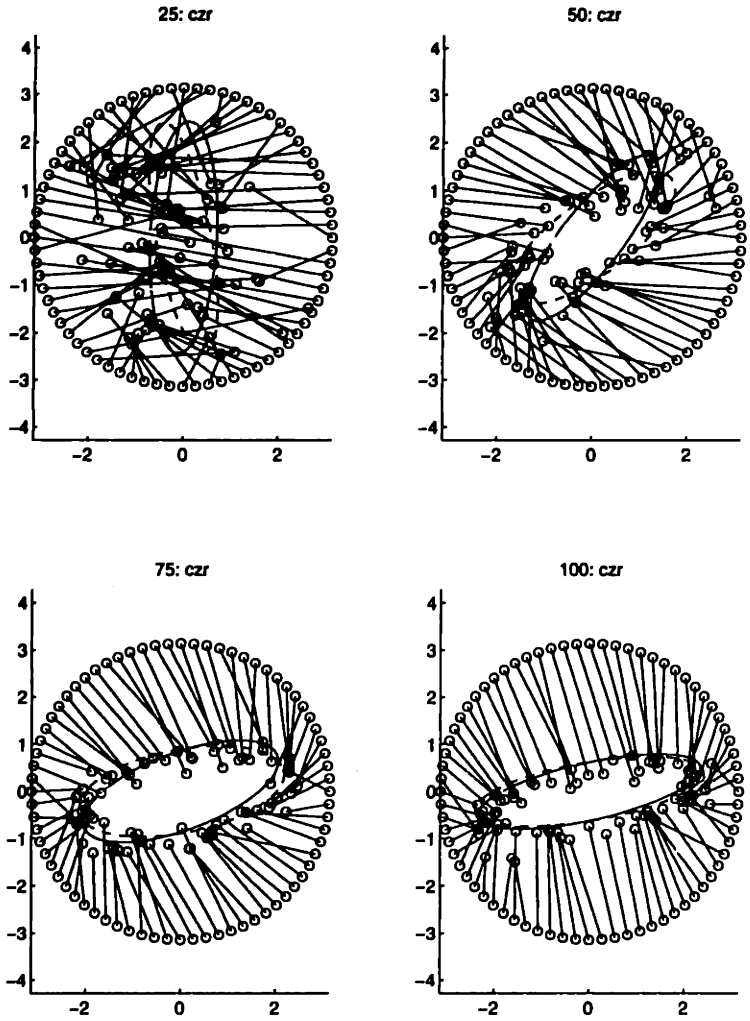

Figure 5-6: Force and acceleration data for Subject CS in the horizontal (Z) plane, right hand. Both the forces and accelerations are arbitrarily scaled, as only the relative changes in the force/acceleration relationship around the circle are of interest. The scaling was chosen so that the forces would lie on the circle of radius 2 and the accelerations would have a mean length of one. The solid lines connect force and acceleration points from the same measurement. The dashed ellipse traces through the predicted accelerations based on Equation 5.2. The solid ellipse uses the symmetrized estimate of the mobility matrix, W_s.

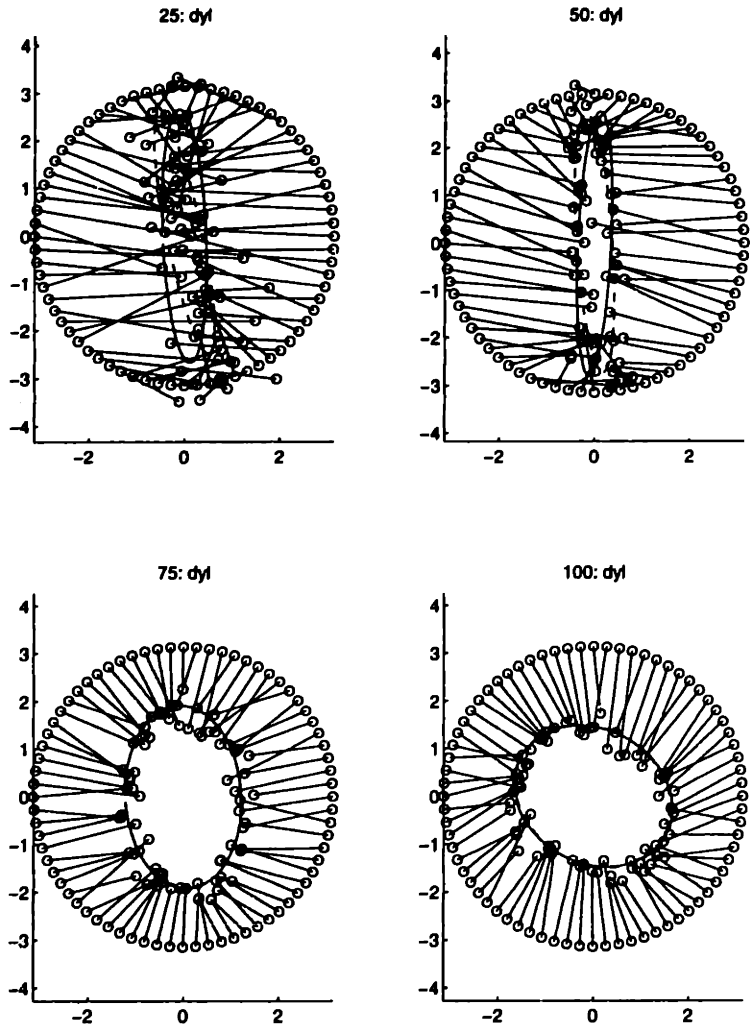

Figure 5-7: Force and acceleration data for Subject DW in the frontal (Y) plane, left hand. See for Figure 5-6 details.

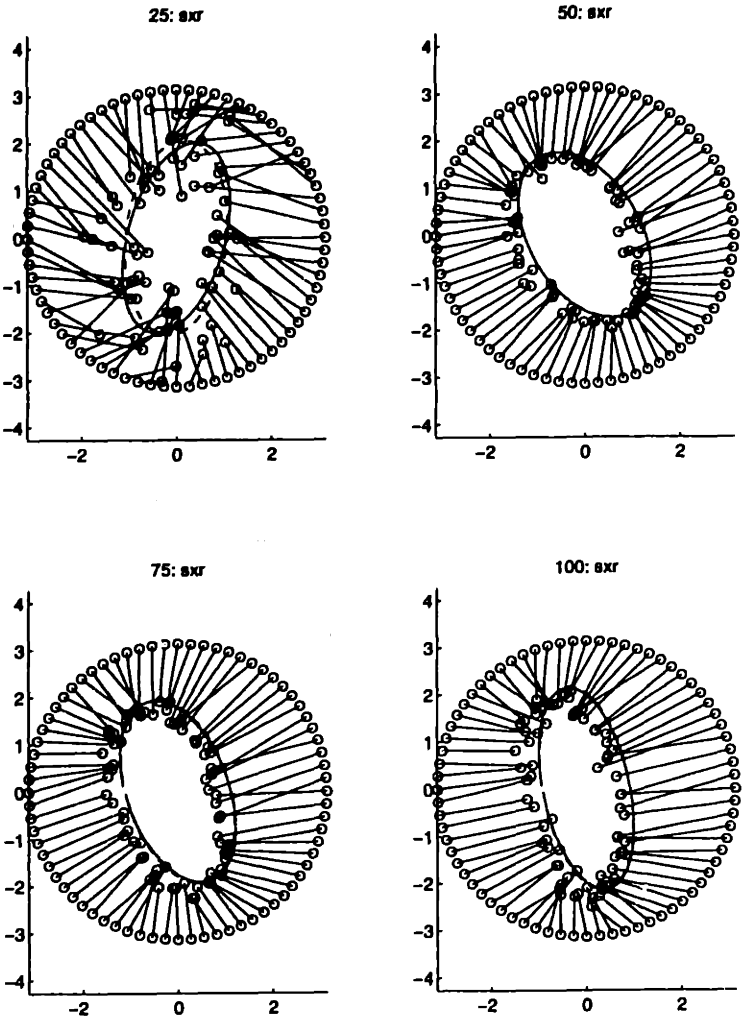

Figure 5-8: Force and acceleration data for Subject SG in the sagittal (X) plane, right hand. See for Figure 5-6 details.

error and a measure of the curl in our estimate. Note that a curl matrix is antisymmetric, while the mobility matrix should be symmetric. Thus, a measure of the amount of curl in W is $\det(W - W') / \det(W_s)$. Figure 5-9 shows the median value of the two measures across subjects as a function of T_1 and T_2. We note that the regression error is smallest for T_1 = 100ms and generally deceases with window size. We would like to use the earliest time window possible, and it can be seen that around T_2 = 60ms the error first reaches a nearly minimal value. Also, the curl component of the regression is not unduly high at that value. Thus, we will use the time window [10ms,60ms] in comparisons with the obstacle rotation data.

Figure 5-10 shows the obstacle rotation preferred axes and measured mobility matrix minor axes for all four subjects in each condition. Note that although there are some conditions in which there seems to be a systematic discrepancy, for example Z-plane movements with the left hand, the overall match is excellent. Figure 5-11 shows a bar graph of angular distance between preferred axes and mobility minor axes for each data set, in order of increasing distance. Note that all but four of the 24 distances are less than 45 deg.

5.3.3 Discussion

It must be acknowledged that there were some technical shortcomings with this experiment. Firstly, we were not able to directly measure the forces exerted by the robot on the hand. Since the Phantom is a cable driven robot and the links are designed for low inertia not rigidity, the transmission of motor torque to the end-point has appreciable dynamics. Also, the coupling of subjects' hands to the robot arm was not rigid. These effects are probably responsible for the high level of noise in the first 25ms. Finally, the estimated mobility matrices depend critically on the time window chosen for regression.

Despite these concerns, there is good agreement between the measured mobility orientations and preferred axes from Experiment 5.1. The correspondence in results between two completely different experiments is remarkable and provides fairly clear support for the spirit of the model: the trajectory plan varies in a manner explainable by the arm's dynamic properties.

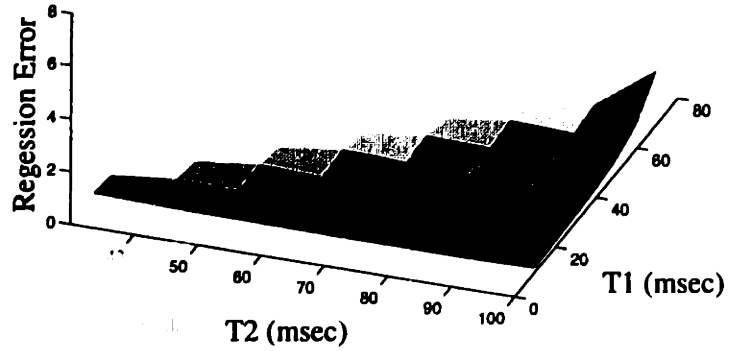

(a)

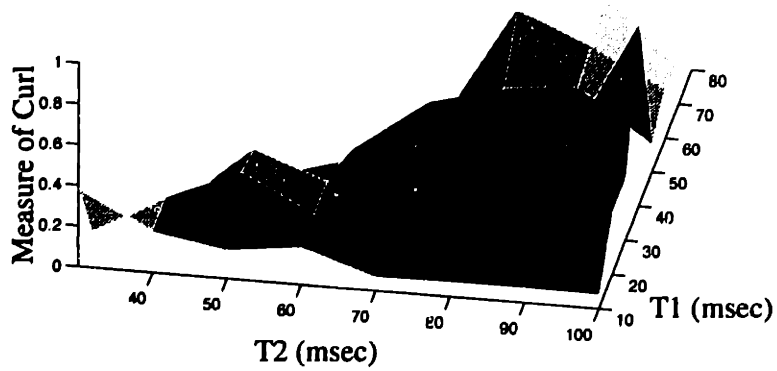

(b)

Figure 5-9: Comparison of Regression Windows for Experiment 5.2. (a) Median regression error in arbitrary units. (b) A measure of curl in the regressed matrix (see text).

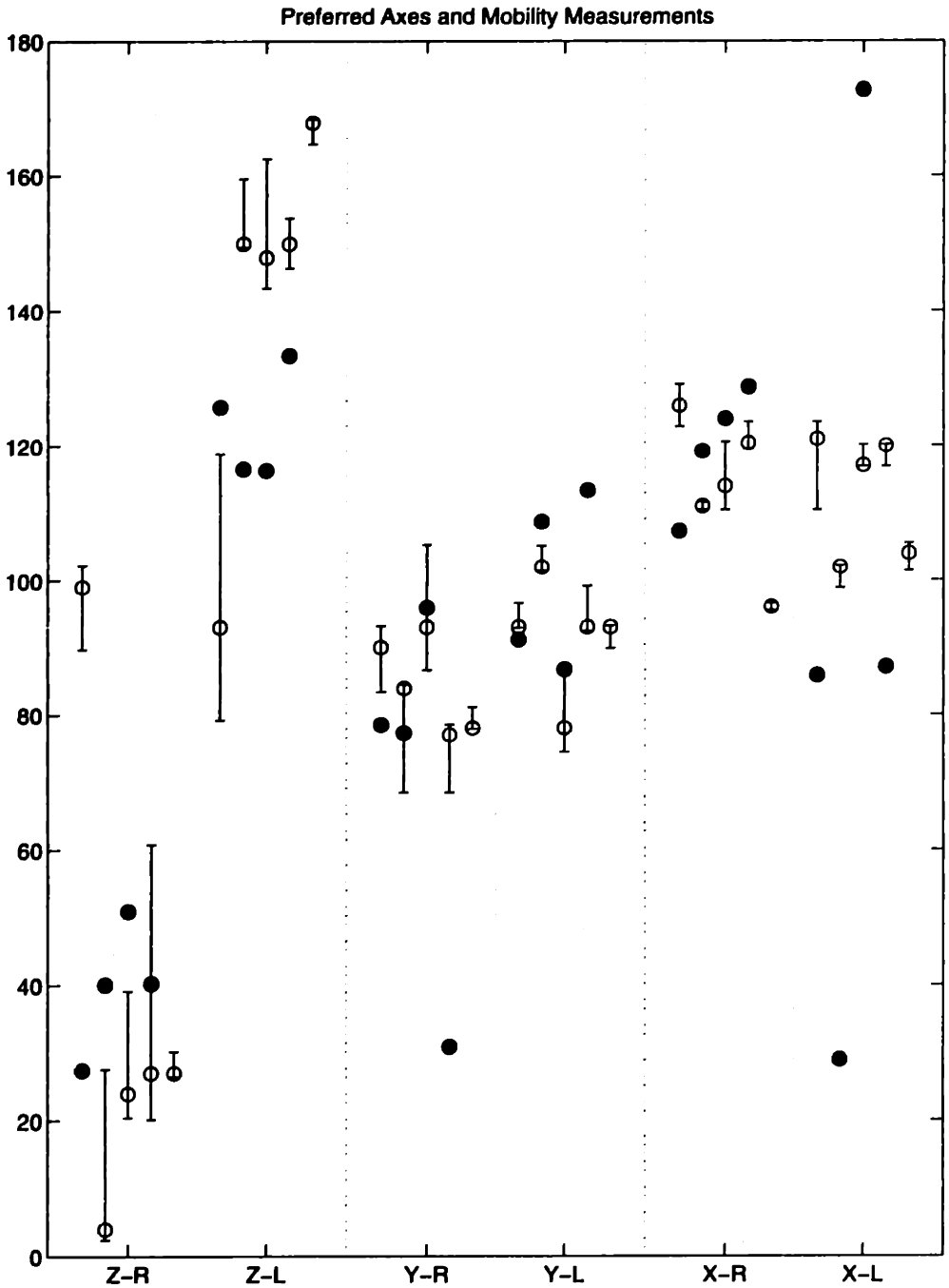

Figure 5-10: Comparison of measured mobility matrices (Experiment 5.2) and obstacle preferred axes (Experiment 5.1) in 3D. Open circles represent preferred axis. Closed circles are the measured mobility matrix minor axes.

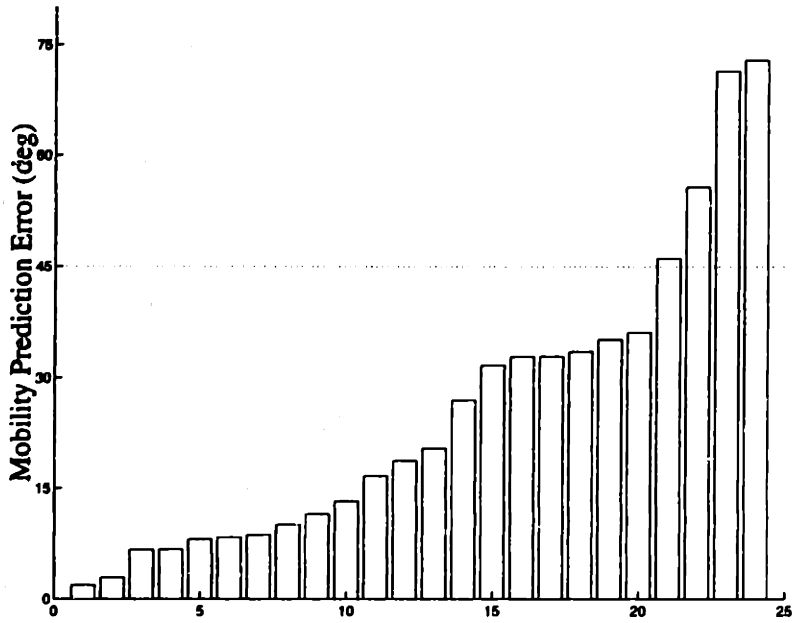

Figure 5-11: Bar plot of angular distances between preferred axes and mobility minor axes.

5.4 Conclusions

There are several main results of this chapter. First, Experiment 5.1 confirms the conclusions of the previous chapter that the obstacle rotation paradigm brings to light a robust, systematic asymmetry in movement planning which is not consistent with the visual planning model. Additionally, the intermanual comparisons of Experiment 5.1 rule out a perceptual explanation of these asymmetries. Finally, Experiment 5.2 provides additional support for a dynamic model of movement planning, in which the CNS uses information about the inertial properties of the arm to optimize movement stability.

Returning to the discussion at the end of Chapter 4, we consider again the potential origins of the movement asymmetries under investigation. Figure 5-12 provides an updated summary of the possibilities. In Section 5.2.2, it was shown that the paths taken by opposite hands display a symmetry across the midline. This would not be expected if the path variations were perceptual in origin, ruling out a predominately perceptual explanation. Thus, if the effects are planned, they must be based on the details of actuator.

We still do not have conclusive evidence to distinguish between the dynamic and kinematic models. However, the experiments in this chapter are suggestive. The agreement between the results of Experiment 5.2 and the theoretically derived mobility matrices compare

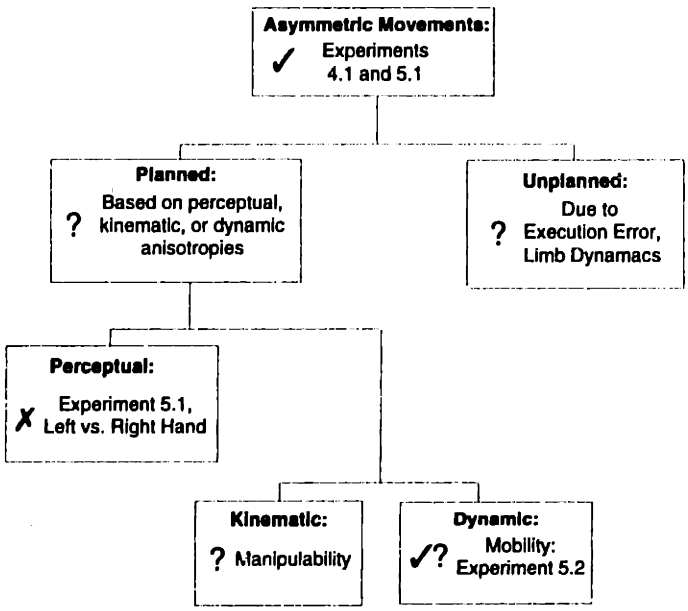

Figure 5-12: An updated version of Figure 4-16 incorporating the results of Chapter 5. The check marks refer to nodes which have been confirmed experimentally, the crosses to nodes which have been ruled out experimentally.

favorably to those of the manipulability matrix (with the exception of the fronto-parallel plane, but see the discussion at the end of section Section 5.2.2). Furthermore, the direct measurements of subjects' mobility yielded close agreement with the near point results (particularly in the fronto-parallel plane!). Taken together, the experiments of this and the previous chapter support the notion that the CNS utilizes dynamic criteria in the planning of obstacle avoidance movements. More concretely, aside from the concern of a low-level explanation of the data (which will be ruled out in the Chapter 6), these two chapter provide strong evidence that some aspect of the actuator plays a role in path planning. These results confirm our initial hypothesis that adding constraints to the task specification would bring to light additional criteria for the movement plan beyond the cartesian smoothness criteria observable in simple point-to-point movements.

Chapter 6

The Central Planning of Obstacle Avoidance Movements

6.1 Introduction

In the previous two chapters, we presented the results of the obstacle rotation experiment showing that the CNS takes the actuator into account when planning obstacle avoidance movements. Additionally, we presented a stability model which can account well for the orientational dependent variations observed in movement path. However, there was one main issue left unresolved from that work: it remains to be shown that the path anisotropies under investigation are not due to a combination of the arm's dynamics and inexact movement execution. This possibility, which we will call the execution model, is particularly pernicious because it is difficult to distinguish from the planning models under consideration. Under the execution model, observable path anisotropies would be expected to correlate with dynamic quantities such the arm's inertia. Furthermore, if the execution model were correct, it would make the results presented in this and the previous two chapters of much less theoretical interest, since they would not be telling us about the criteria that CNS wants to control, but rather exactly those features of the movement which it leaves uncontrolled. This concern is dealt with in Section 6.2, which presents a visual perturbation experiment, and Section 6.3 in which the neuromuscular dynamics of the arm are modeled, and the model is tested in a simulated obstacle rotation experiment.

6.2 Obstacle Rotation under Shifted Visual Feedback: Experiment 6.2

If there execution model holds, then the path variations observed in the obstacle rotation experiment should correlate with the dynamics of the arm rather than the visually presented scene. Consider the case where the visual feedback is "prism shifted" uniformly to the left or right such that movements appear to be located at location A in the workspace, but are actually occurring at some other location, B. We know from the wealth of literature on prism adaptation that subjects can adapt to such shifts in a small number of movements when both the target and hand are visible (see Welch, 1986, for a comprehensive review). The execution model predicts that any variations seen in the paths of these movements should be due to the dynamics of the arm and it's neuromuscular controller. Thus, movements made at location B should look largely the same independent of the location of the visual feedback. Likewise, the movements made at location B should look different from those made at position A, even if the visual feedback appears at A.

We first conducted the obstacle rotation experiment in two locations in the workspace. We then repeated the experiment with the visual feedback shifted in the manner described above, and finally removed the perturbation and tested again at both locations. The experimental question under investigation whether the systematic path variations during prism exposure correspond to those seen normally at the visual or the kinematic location.

6.2.1 Methods

Six right handed subjects, 3M, 3F, ages 19-33yrs, participated in Experiment 6.2. All six had normal or corrected to normal vision, and were naive as to the purpose of the experiment. Subjects were seated at the virtual visual feedback system described in Appendix A so that their right shoulder abutted a padded shoulder rest and their chin rested on a support. Subjects were asked to keep their shoulder against the rest for the duration of the experiment, insuring that their posture and position relative to the externally defined workspace remained constant during the experiment. An IRED marker was mounted on the tip of subjects' right index finger and monitored with a Northern Digital Optotrak infrared position monitoring system at 144 HZ.

Subjects' view of the table in front of them was blocked by a mirror which reflected

A_vA_k	•		•		•		•									•		•	
B_vB_k		•		•		•		•									•		•
B_vA_k										•	•	•	•	•					
$A_v(A/B)_k$									•						•				

Table 6.1: The order of blocks for Experiment 6.2. The left column contains block types (see text for description), and each remaining column represents a trial block.

a projection screen in the plane of the table. This allowed us to provided virtual visual feedback in the form of a 1cm diameter filled circle located either at the position of the index finger or shifted laterally some fixed distance. Obstacles and start and target locations were also displayed using the visual feedback system.

The details of the experimental procedure for a single trial are identical to those for Experiment 4.1 (see Section 4.2.1). Trials were organized into blocks of 30 movement pairs, with randomly ordered presentation angles located at 12° intervals around the circle. All of the trials within a block were centered about the same location in visual space, either at position A, $(-7, 30)$, or position B, $(23, 30)$, where the units are cm, the positive x-axis corresponds to the subjects right, and the origin is the approximate location of the subjects eyes, projected into the plane of the table.

There were four kinds of blocks: A_vA_k and B_vB_k blocks,[1] where the visual feedback was not shifted and the obstacles were centered about A and B respectively; B_vA_k, where the obstacle appeared to be centered at location B, but a 30cm rightward shift (approximately 45°) in the subjects visual feedback forced them to move as if the obstacles were centered at position A; and $B_v(A/B)_k$ where the prism was phased in or out at a constant increment each of 0.5cm each trial. The experiment consisted of 19 blocks, or 1140 movements in all. The order of the blocks is shown in Table 6.1.

6.2.2 Results

Trial blocks can be grouped into five sets of interest: the sets of A_vA_k and B_vB_k blocks for both the PRE and POST prism shift phases of the experiment, and the prism SHIFT set B_vA_k. Preferred axes were calculated by grouping all the trials in one of the five sets for each subject and performing the Maximum Likelihood estimation described in Section 4.2.2.

[1]The subscript v refers to the visual location, k to the kinematic location.

Figure 6-1 shows the preferred axis and 95% confidence intervals for each subject. It is clear from the figure that the preferred axes during the prism shift (B_vA_k) are different from those found at the same hand location before or after the shift (B_vB_k). In fact, the SHIFT phase data seem to lie in between the preferred axes for the A and B locations. This observation is confirmed in the bottom row of Table 6.2, which shows the mean preferred axes across subjects for each trial set.

Analyses of Variation

We now provide a more comprehensive analysis of the preferred axis results. We do not necessarily expect that subjects will have the same preferred axes at the two workspace locations, as the joint angles needed to achieve that position vary from subject to subject, as do the dynamic properties of the arm. However, this variation is expected to be small compared to the variation across the workspace. Therefore it is reasonable to combine the data across subjects and perform oneway anovas between trial blocks. These results are shown in Table 6.2.

The tests between A_vA_k and B_vB_k were preplanned comparisons needed as a precondition for the experiment: if there is no significant difference between the preferred axes for the two positions then the comparison between them and the B_vA_k trials will not yield interesting results. These comparisons correspond to cells b-1, d-2, e-1, and e-4. Each of these pairwise comparisons is significant – the preferred axes at positions A and B are not the same.

The tests between the B_vA_k block and the four A_vA_k and B_vB_k blocks were the preplanned comparisons designed to evaluate whether the behavior during prism shift corresponded to the visually relevant location (B), or the actual location of the arm (A). Cells c-2 and e-3 compare the preferred axes of the B_vB_k and prism shifted B_vA_k trials. Neither difference is significant, suggesting that the prism shifted behavior is similar to that seen in the *visual* location in normal circumstances.

Cells c-1 and d-3 compare the preferred axes for the prism shifted B_vA_k block to the PRE and POST A_vA_k blocks. The former difference is marginally significant, p= 0.065, the latter is highly significant. Note that this is the main comparison of interest in the experiment. Contrasting these results to those in the preceding paragraph, we see that the preferred axes during the prism shift are closer to those seen in the *visually* relevant location

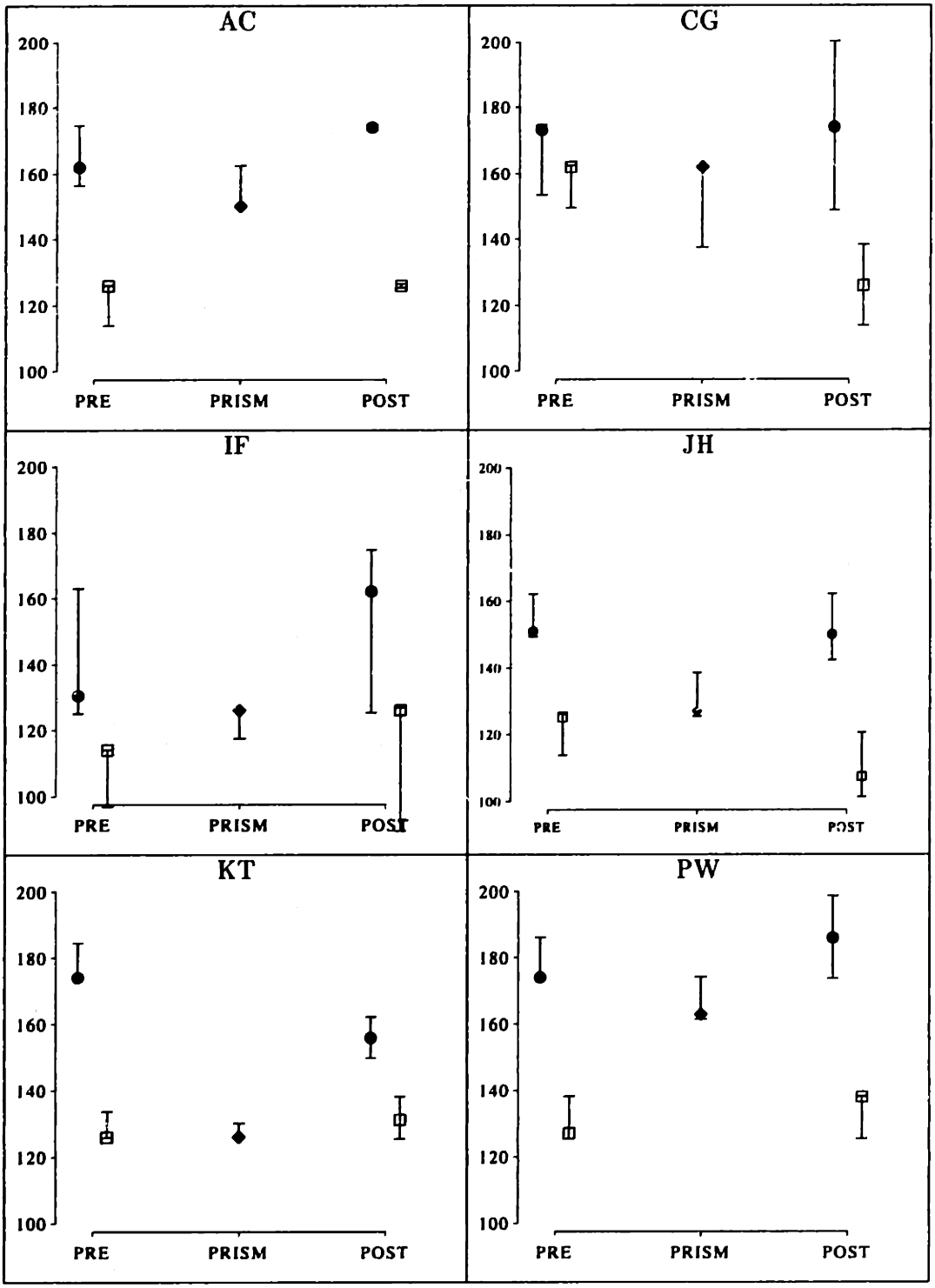

Figure 6-1: Preferred axes for each subject in Experiment 6.2. Each point shows the preferred axis and 95% confidence interval over a set of blocks. Solid circles: A_vA_k; Open squares: B_vB_k; Grey diamonds: B_vA_k blocks. The S's initials are above each plot.

		A_vA_k PRE	B_vB_k PRE	B_vA_k SHIFT	A_vA_k POST	B_vB_k POST
		1	2	3	4	5
A_vA_k PRE	a	—				
B_vB_k PRE	b	12.9 0.004*	—			
B_vA_k SHIFT	c	4.12 0.065	1.52 0.245	—		
A_vA_k POST	d	0.479 0.505	17.8 0.001*	7.21 0.023*	—	
B_vB_k POST	e	18.1 0.002*	0.288 0.603	3.82 0.079	37.2 <.001*	—
MEAN (SE)		161° (7°)	130° (6°)	142° (7°)	167° (5°)	126° (4°)

Table 6.2: Analysis of the results of Experiment 6.2. Mean (s.e) preferred axes across subjects for each set of blocks are shown at the bottom of the table. The rest of the table presents the results of oneway anovas of preferred axis between trial blocks: upper numbers are F(1,12) values, lower numbers are the corresponding p-values. Significant differences are marked with (*).

(B) than the kinematically relevant location (A). The difference in mean preferred axes is 12° and 16° for location (B) and 18° and 25° for location (A).

Finally, we note that the remaining comparisons, cells d-1 and e-2, show that differences across time for the same location are not significant. This point is made more clearly in Figure 6-1. Here we see that 10 of the 12 pairs of PRE and POST blocks at the same location have preferred axes which lie within each others 95% confidence intervals. The movements represented by these statistics comprise the first 480 and last 240 movements of a total of 1200 movements. This provides additional evidence that the path asymmetries seen in the obstacle rotation experiment are a robust phenomenon.

In summary, the one-way anovas presented here support our initial conclusion that the preferred axis during the SHIFT phase does not correspond to the PRE and POST phase preferred axes at the kinematic location, B.

Before drawing any conclusions from these results, we must address the issue of the effects due to the prism shift itself. Welch (1971) showed that post-exposure negative aftereffects to a 20 diopter prism (approximately 11°) assymptoted by about 35 trials of target pointing with visual feedback. Although the shift employed in this experiment was

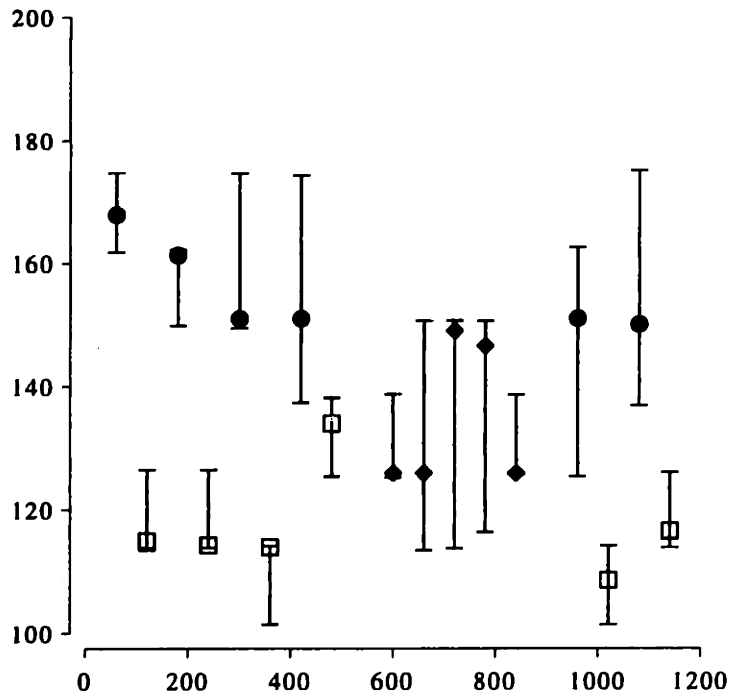

Figure 6-2: Time course of behavior for one subject in Experiment 6.2. Preferred axis for each trial block. The preferred axis (degrees) and 95% confidence interval for each 60 trial block in a single experiment (subject JH). Solid circles, $A_v A_k$; Open squares, $B_v B_k$; Grey diamonds, $B_v A_k$. The abscissa corresponds to the trial number.

considerably larger, the $B_v(B/A)_k$ block at the onset of prism adaptation consisted of 60 movements. Furthermore, if we look at the time course of behavior, there is no noticeable change in the near point locations over the course of the of the prism shift phase. Figure 6-2 is an example, showing the preferred axis for each 60 movement block in the experiment (except the 2 $A_v(A/B)_k$ blocks). This suggests that subjects were able to adapt to the shift in a within the span of the $A_v(A/B)_k$ block.

6.2.3 Discussion

We have shown that the near point placement of obstacle avoidance movements under prism shifted feedback does depend only on the configuration of the arm. These data imply that the anisotropies in near point distribution in the obstacle rotation experiment are not merely an emergent property of the plant.

In fact, the behavior during the SHIFT phase of the experiment lies between that seen in either the visually or kinematically relevant positions. This result is understandable in light of the additivity hypothesis from the prism adaptation literature (Welch, 1986). It has

been shown that exposure to a prism shift results in both a partial adaptation of the visual system, quantified for example by asking subjects to press a button when a moving cursor passes directly in front of them, and a partial adaptation of the proprioceptive system, tested by asking subjects to point straight ahead without visual feedback. Furthermore, the sum of the magnitudes of these two partial adaptations equals the total visuomotor adaptation, as evidenced by the error in pointing to visual targets (Wallace and Redding, 1979; Redding and Wallace, 1988). This suggests that the if the CNS were to estimate the location of the arm while under the effects of the prism shift, it would determine a location somewhere between the actual location and the location of the visual feedback. If the CNS then uses this information to determine the optimal path for circumventing the obstacle, we would expect a pattern of behavior which is somewhere between that seen in the two locations in normal conditions, as was found above.

On the other hand, if the execution model were correct, the planner would choose the same path independent of location in the workspace, and so any variation would depend on the low level control structure and the dynamics of the arm. These processes have no direct access to the visual input, and so the details of the executed paths should vary with location of the arm, not location of the visual feedback. Thus, the results of this experiment provide strong evidence against the execution model.

6.3 A Computational Investigation of Execution Effects: Experiment 6.3

As described in Chapter 4, the variations in the paths taken in the obstacle rotation experiment are explainable by a model based on the inertia of the arm. This fact raises the possibility that the effect might simply be due to low level inertial effects and have nothing to do with the centrally formulated plan. It is worth assuring oneself the results described in the previous chapter do not fall out of the physics due to the non-isotropic inertial properties of the arm. In this section, we will present a simple model of the neuromuscular dynamics of the arm, and investigate its behavior in a simulated obstacle rotation experiment. The model is not intended to be a complete (or completely accurate) description of the dynamics of the arm or its controller. Rather, it is meant to set aside the worry that our results are "obvious and uninteresting if you just look at the physics".

For our model, we will adopt the Equilibrium Trajectory Hypothesis as described in (Flash, 1987). Specifically, we assume that a virtual trajectory is specified in joint space and serves as a time varying set point for the arm's neuromuscular controller.

6.3.1 Methods

Two virtual trajectories were chosen which would satisfy the constraints of the obstacle rotation experiment of Section 4.2 with a presentation angle of 0°. These canonical virtual trajectories were both specified by picking a via point along the line of the obstacle and solving for the minimum jerk trajectory which passes thought that point (Flash and Hogan, 1985). The via points were located 2.8cm and 4cm from the obstacle tip. The points also represented the near points of the trajectories, and both trajectories were symmetric in time and space about the via point.

A two joint, planar model of the arm was used, which means that the joint trajectories were uniquely specified by the end-point trajectories described above. Using the same notation as Section 4.3.2, the dynamics of the arm can be written,

$$\tau = I(\theta)\ddot{\theta} + C(\dot{\theta},\theta)\dot{\theta}, \tag{6.1}$$

where τ is a vector of torques at the two joints, $I(\theta)$ is the inertia (c.f. Equation 4.3), and

$$C(\theta) = b\, l_1\, l_2\, m_2\, \mathrm{s}\theta_2 \begin{bmatrix} -2\,\dot{\theta}_2 & -\dot{\theta}_2 \\ \dot{\theta}_1 & 0 \end{bmatrix}.$$

This last term describes the centripetal and Coriolis interaction forces (see for example Craig, 1986).

The Equilibrium Trajectory Hypothesis then states that the torques at each joint at time t will be,

$$\tau(t) = R(t)\,(\theta^*(t) - \theta(t)) + B(t)\,\dot{\theta}(t),$$

where $\theta^*(t)$ is the prespecified virtual joint trajectory (Flash, 1987). The matrix $R(t)$ represents the stiffness of the neuromuscular control loop and $B(t)$ its viscosity. It is known that during single joint movements, the joint stiffness varies over the course of the movement (Bennet, 1990). However, for simplicity, the stiffness matrix was chosen to remain constant

in time. R was parameterized following Flash:

$$R = \begin{bmatrix} G_s R_s + G_t R_t & G_t R_t \\ G_t R_t & G_e R_e + G_t R_t \end{bmatrix}.$$

where the $R_.$ represent the static stiffness matrix and the $G_.$ represent the scaling factors for dynamic stiffness. We chose to maintain the same static stiffness for every simulation and to vary only the scaling factors. The values used were $R_s = 29.5, R_e = 39.3,$ and $R_t = 14.3$ N-m/rad (Flash, 1987). Finally, we chose 4 different sets of scaling factors to use in our simulations. The goal was simply to cover the range of reasonable values. Thus, we set $G_s = G_e = G_t = G$ for all four cases, with G taking on the values 0.5, 1, 1.5, 2, and 3. These choices bracketed the range of estimated dynamic stiffnesses in Flash (1987).

Given the initial conditions of the arm and the virtual joint trajectory, Equation 6.1 can be integrated numerically to find the trajectory of the arm. Furthermore, if an obstacle center location, a presentation angle and a movement direction (clockwise/counterclockwise), are chosen, a canonical virtual trajectory can be translated, rotated, and, if necessary, reversed in time to satisfy the path constraints of the obstacle rotation experiment.[2] An experiment consisted of 144 simulated movements, centered around the same location in the workspace, one in each direction for 72 equally spaces presentation angles.

6.3.2 Results

We simulated the obstacle rotation experiment at two locations in the workspace, $\theta = (30°, 110°)$ and $\theta = (75°, 75°)$, corresponding to Positions 1 and 2 from Experiment 4.1. For each location, we repeated the experiment ten times, once with each of the five dynamic stiffnesses and with both virtual trajectories.

For higher stiffness values, the simulated trajectories follow the virtual trajectory closely, and the near point does not stray far from the virtual trajectory via point. This can be seen in Figure 6-3(a), for which G=3.0. The near points are nearly evenly distributed around the circle, and the near point angle never exceeds 10°. When the stiffness is lowered to G=2.0, the near points begin to cluster slightly at certain locations, as in Figure 6-3(b). However, the effect is small, with near point angles around $10-15°$. Finally, when the stiffness during

[2]The solution to the minimum jerk optimization problem is reversible in time, remaining an optimal solution.

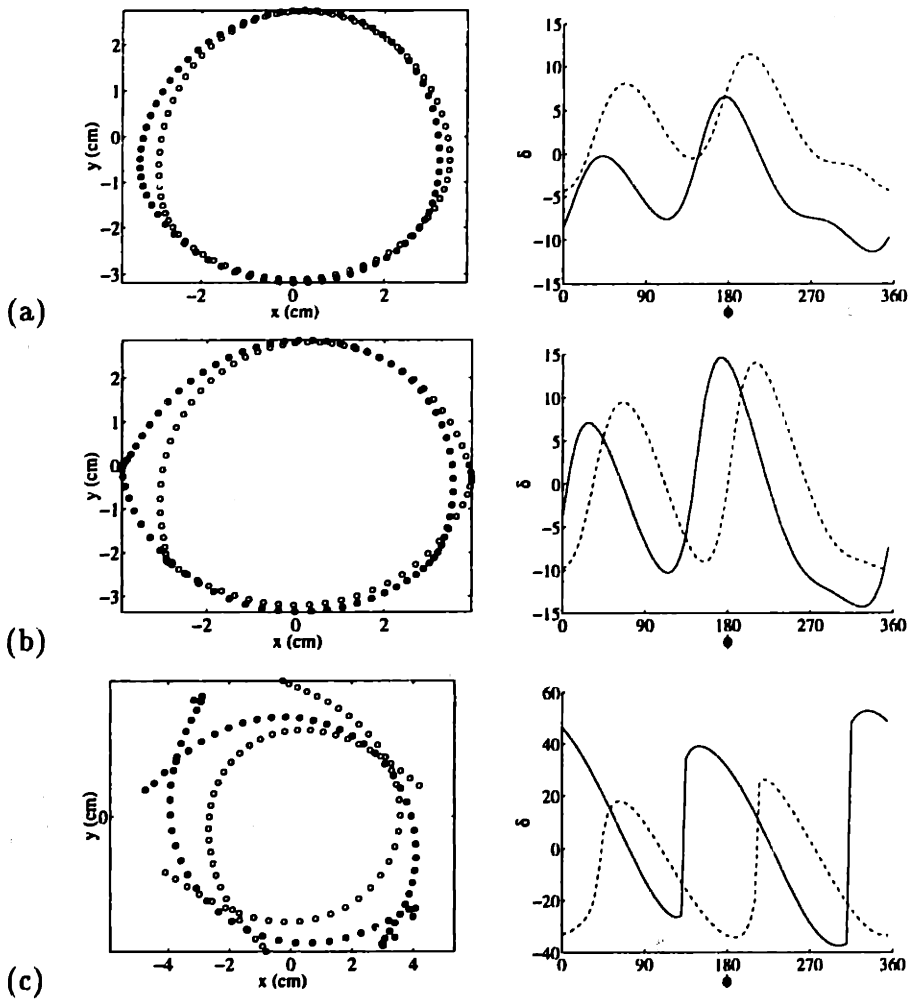

Figure 6-3: Sample results from the simulated obstacle rotation experiment. Left: near point locations. Solid, clockwise movements; Open, counterclockwise. Right: near point angle vs. presentation angle (degrees). Solid, clockwise movements; Dashed, counterclockwise. (a) G= 0.5, (b) G=1.5, (c) G=3.0. All plots are for the 4.0cm clearance virtual trajectory, in Position 1.

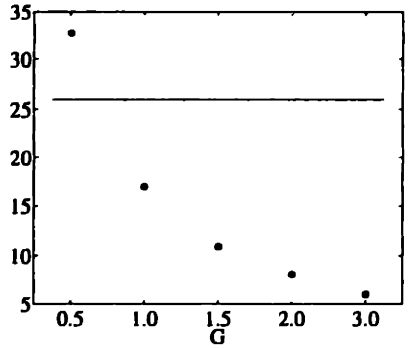

Figure 6-4: Median absolute near point angles for the simulated obstacle rotation experiment. Each point is an average over the four experiments with that dynamics stiffness. For comparison, the solid line is average value over all subjects in Experiment 4.1.

movement is reduced to half of the static stiffness, the near points cluster at opposite poles, and the near point angles become as high as 28°. The most striking similarity between this data and those from Experiments 4.1 and 4.2 is the nearly piecewise linear dependency of δ on ϕ at the lower stiffnesses. This relationship is particularly clear for the clockwise movements in Figure 6-3(c).

There are two important differences between the simulated and experimental data. First, the simulated near point angles do not exceed 30°, whereas the experimental data showed near point angles as high as 50° in every subject. This difference can be seen in Figure 6-4, which compared the median absolute near point angles in these simulations to those from Experiment 4.1. Only in the case of the lowest stiffnesses do the near point angle magnitudes match those seen in experimental data.

More importantly, in the simulations, the near point behavior is highly dependent on the direction of movement. This fact is evident in both the raw near point plots and the δ versus ϕ plots in Figure 6-3. The effect can be clearly seen in Figure 6-5, which presents the preferred axis regressions for each simulation as well as all of the experimental data sets in Experiment 6.1. The regressions were carried out separately for each of the two movement directions. In all but three of the simulated data sets, the difference in preferred axis between the two directions of movement is nearly 90°, i.e. maximally separated. In contrast, the preferred axes for the experimental data shows little dependence on the direction of movement – the mean (s.d.) absolute difference in preferred axes for the two directions is 22°(11°). We note that three of the data sets do show overlapping preferred axis for the two directions of movement. One of those (the one at Position 1) is the data set shown in

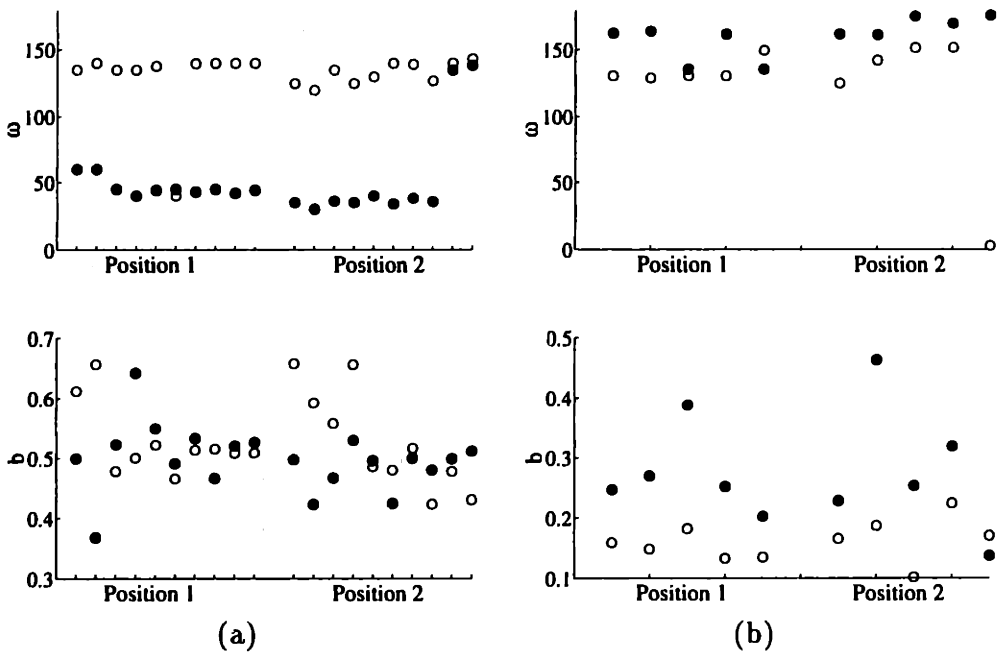

Figure 6-5: Preferred axis regressions for (a) simulated obstacle rotation experiment, (b) Experiment 4.1. Top: preferred axis, Bottom: regression slope. For all plots: Solid, clockwise movements; Open, counterclockwise. (a) Each pair of data points is for one set of computational parameters. For each position in the workspace, the data are organized in order of increasing stiffness. (b) Each pair of data points is for a single subject in one location of the workspace.

Figure 6-3(b), with G=1.5. The other two (at Position 2) have G=3.0.

6.3.3 Discussion

The simulations presented in this section show marked qualitative differences from the behavior of human subjects in similar experimental conditions. In particular, dynamics of the arm predict that with most values of the dynamic stiffness matrix, the near point placement depends critically on the direction of movement. In contrast, the experimental data shows close agreement in near point locations for the two directions of movement. These results reinforce the conclusions of the previous experiment that the anisotropies observed in the obstacle rotation experiment are not due to controller error or imprecision in the execution of movement.

While it is true that for a few of the simulations the preferred axis of the two directions of movement do coincide, there is no rule as to the stiffnesses required to elicit this behavior. Additionally, all three of these simulations exhibit near point angle magnitudes about three times smaller than the experimental data. In any case, if it is necessary to carefully re-tune the arm's stiffness to reproduce the experimental data at each location in the workspace, then we would argue that our point has been made. There is every reason to believe that the CNS makes use of the adjustable visco-elastic properties of the arm in controlling movement. Such explicit manipulations by the central controller would not fall under the execution model.

6.4 Conclusions

The two experiments in this chapter make a low level explanation of the obstacle rotation results unlikely. Experiment 6.1 shows that the movement anisotropies depend both on the physical configuration of the arm and on the location in the visual workspace. This result is consistent with a dynamic or kinematic planning model in which the relevant quantities are based on an estimate of the arm's location arrived at through a fusion of visual and proprioceptive information The simulated obstacle rotation experiments in Section 6.3 provide assurance the results of the previous two chapter are not an obvious consequence of the non-isotropic inertial properties of the arm.

We now consider one last time the possible explanations for the movement asymmetries

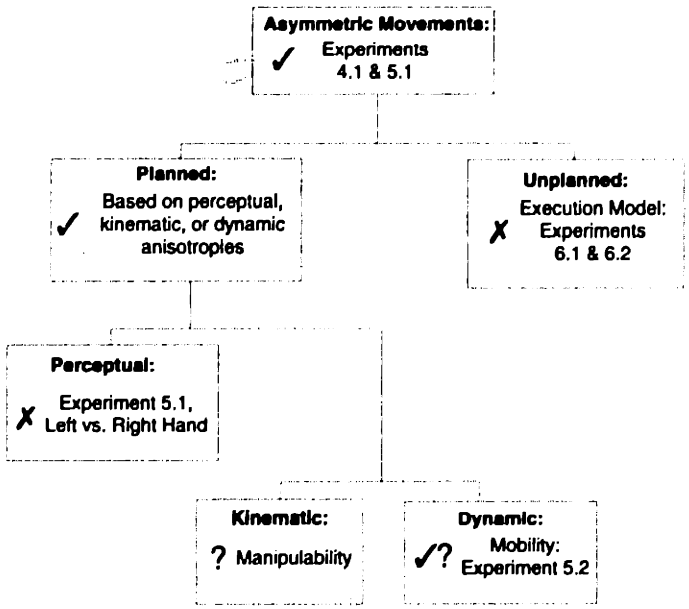

Figure 6-6: An updated version of Figure 4-16 incorporating the results of Chapter 6. The check marks refer to nodes which have been confirmed experimentally, the crosses to nodes which have been ruled out experimentally.

observed in the obstacle rotation experiment. This chapter has rules out the execution model, leaving only dynamic or kinematic based models. Although the results of Chapters 4 and 5 favor a dynamic model, this distinction is not crucial. The important result is that the CNS does not treat the arm as a simple point in Cartesian space. Rather, the intrinsic properties of the arm are taken into account in order to optimize the movement path.

Chapter 7

Summary and Conclusions

In the first part of this thesis, we presented two sets of perturbation experiments which support the model of Cartesian planning of movement trajectories. These results are consistent with the bulk of the recent perturbation studies in the literature (Flash and Gurevich, 1991; Shadmehr and Mussa-Ivaldi, 1994; Lackner and DiZio, 1994; Wolpert et al., 1995; Flanagan and Rao, 1995) and extend those studies in two ways. Experiment 2.1 shows that a reorganization of the static visuomotor map is sufficient to affect changes in movement path. These results provide evidence for explicit path planning in visual space, as opposed to just visual based planning (see Section 1.5 for a discussion of this issue). Experiment 3.2 shows that for discrete, goal directed movements, the CNS will adapt movement velocity as well as movement path, suggesting that movement velocity is also preplanned.

The second part of the thesis focused on the planning of obstacle avoidance movements. Chapters 4 and 5 introduced the obstacle rotation paradigm and presented a series of experiments showing that such movements are not consistent with an actuator independent planner which relies solely on the details of the cartesian end-point trajectory. We presented two models which account for the observed movement anisotropies, a kinematic and a dynamic model. We also discussed some preliminary results which support the dynamic model. Chapter 6 presented two studies which ruled out a purely low-level (execution error) explanation of the effects.

At this point the reader might be wondering about the juxtaposition of the two preceding paragraphs, the first claiming that movement is visually planned, the second arguing for the influence of the actuator. In fact, these two claims are not mutually exclusive. The first

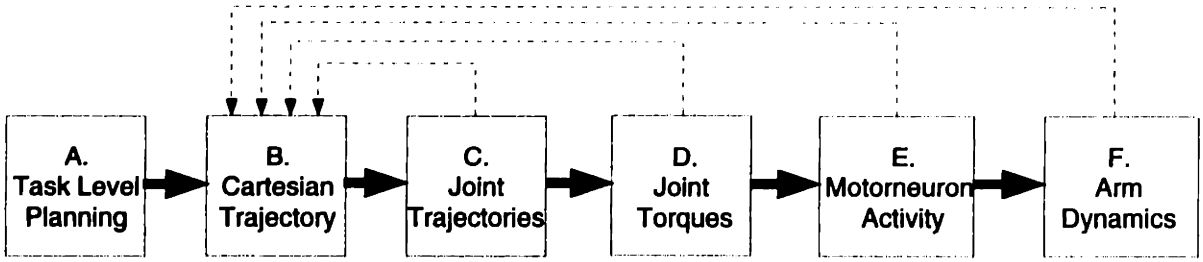

Figure 7-1: A modified hierarchy for motor control.

half of the thesis argues for planning *in cartesian space*, that is for the prespecification of the movement trajectory in extrinsic space. This leaves open the question of how that trajectory is specified. We posit that for most of the movements which have been investigated in the literature, the specification is also primarily visual. Because simple point-to-point movements do not present any additional constraints, smoothness considerations dominate. However, with the introduction of obstacles, other features of the movement become relevant. In particular, we claim that the stability of the arm with respect to the obstacle is of crucial concern to the planner. In order to take this consideration into account, the CNS must utilize information about the dynamics or kinematics of the arm. Hence, although the planner is still a cartesian planner, it's planning criteria are not wholly extrinsic.

These considerations lead us to a modified hierarchical model of movement control, Figure 7-1, which includes a limited bi-directional flow of information (Kawato, 1994). The Cartesian planner now has access to low level information which it can use when it is relevant to a particular task. The results of Part II of the thesis, for example, suggest that the planner is able to make use of information about the structure of the arm. This would be represented by the line from either the kinematic planner (module C) or the arm dynamics (module F) to the Cartesian planner, depending on whether the kinematic or dynamic model of Chapter 4 proves to be correct. The other lines are speculative, but we suggest that given the right task demands, evidence for these too could be experimentally elicited. The exact nature of this upward information flow is not determined by our results. The CNS could access such information during the planning process for use in on-line computations. Or the information could be used during the formation and adaptation of the central controller, which then only implicitly utilizes the information during planning. In either case, the point we stress here is that Cartesian planner does not treat the arm as merely a point in extrinsic space.

Finally, then, we return to the two questions posed at the beginning of Chapter 1. We conclude that the Cartesian trajectory is planned, but based on criteria which take into account a variety of information, including the intrinsic properties of the arm.

Appendix A

Virtual Visual Feedback System

Most of the experiments in this thesis were conducted using the virtual visual feedback system, first developed by Wolpert and Ghahramani (cf. Wolpert et al., 1995).

Subjects were seated at a table with their right arms resting on the surface of the table. The location of the subject's finger tip and the configuration of the subject's arm could be monitored using a Northern Digital Optotrak infrared position monitoring system. Subjects always wore one IRED (Infrared Emitting Diode) marker on their finger tip. In some experiments, additional markers were places at other locations on the arm to measure joint angles. The three dimensional positions of the IREDs were sent at rates of 144Hz-200Hz to a Pentium PC which controlled the experiment.

Subjects view of their arm and the table it rested on was blocked by a mirror. Through the mirror, subjects saw a projection screen illuminated by a Sayett MediaShow 72 HZ 640x480 VGA projector, also controlled by the PC. The screen and mirror were adjusted so that the image of the screen appeared to lie in the plane of the table. Thus, while subjects were not able to see their hand or arm, we could provided them with virtual visual feedback which was located at the same position as their hand. For most experiments, this feedback was in the form of a while filled circle 1cm in diameter. Any other arbitrary visual objects could be places in the scene, such as start and target locations, obstacles, and paths for tracing. The feedback apparatus is shown in Figure A-1.

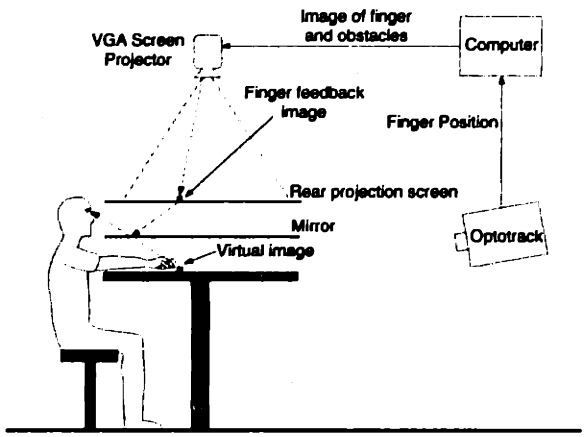

Figure A-1: Experimental apparatus for measuring arm trajectories in the horizontal plane with virtual visual feedback. Adapted from (Wolpert et al., 1995).

Appendix B

Visual Perturbations along Parametric Curves

In order the investigate the planning of velocity in human movement, we wanted to be able to perturb the visual feedback by keeping the path constant but making specific changes to the shape of the tangential velocity profile, such as flattening the profile, accentuating peaks and valleys, or inducing a skew. It is necessary to be able to calculate the required shift in feedback location on-line. One approach is to assume that subjects will follow a some theoretically predicted velocity profile such as the 2/3's power law (Lacquaniti et al., 1983) or minimum jerk (Flash and Hogan, 1985) profiles. One can then calculate a priori a positional perturbation which will yield the desired effect on the velocity profile, as long as the actual movements don't stray too far from the theoretical predictions. Such an approach was taken in (Sabes, 1996), but the resulting feedback did not always turn out as desired due to the fact that subjects behavior deviated from the theoretical predictions. To improve upon those methods, we turned to a new approach in which the data from a pre-perturbation phase of the experiment were processed on-line to calculate the desired feedback perturbation.

The goal is to compute a positional perturbation which will not change the movement path but will have some desired effect on the velocity profile, assuming that subjects' behavior does not change from the pre-perturbation baseline. Furthermore, we need to find simple methods for doing this, such that the compute time and memory costs for collecting the movement statistics and calculating the perturbation do not interfere with the normal

course of the experiment. In fact, there is a simple methods for doing this, as long as it is not too difficult to parameterize the path along which the movement will process and to be able to reliably project back onto this path when the actual movement strays from it. In the first section we present a general method for computing index perturbations. We then present details of the two perturbation used in Chapter 3. Finally, we show how to implement the index perturbations during an experiment.

B.1 Index Perturbation from Velocity Perturbations

We will develop the method for the case of an ellipse, since that is what is used in Chapter 3. However, at the end of this section, we will explain how to generalize to arbitrary paths. Assume that the path of the finger traces out an ellipse,

$$\begin{aligned} x(t) &= a\cos\theta(t), \\ y(t) &= b\sin\theta(t), \end{aligned}$$

where $\theta(t)$ is a parameter for indexing the path. The velocity at a given point in time is given by

$$\begin{aligned} v(t) &= \sqrt{a^2\sin^2\theta(t) + b^2\cos^2\theta(t)}\,\dot{\theta}(t) \\ &= \ell(\theta)\,\dot{\theta}(t), \end{aligned} \tag{B.1}$$

where $\ell(\theta)$ is the derivative of the mapping from the index θ to the path length. In the sequel, we will assume that the velocity of movement is determined by location on the path. Thus we will use the notation $v(\theta) \equiv v(\theta(t))$.

Imagine that whenever the finger is located at position $(x(\theta), y(\theta))$, we perturb the index of the feedback by $\delta_\theta(\theta)$. The finger will now appear to be located at $(x(\theta_f), y(\theta_f))$, where $\theta_f = \theta + \delta_\theta(\theta)$ is the feedback index. We have,

$$\dot{\theta_f} = \dot{\theta} + \delta'_\theta(\theta)\dot{\theta}. \tag{B.2}$$

Combining Equations B.1 and B.2, we can calculate the feedback velocity:

$$\begin{aligned} v_f(\theta) &= \ell(\theta)\,\dot{\theta} + \ell(\theta)\,\delta'_\theta(\theta)\dot{\theta} \\ &= v(\theta) + \delta_v(\theta) \end{aligned} \tag{B.3}$$

Finally, equating the right hand sides of Equation B.3, we get a differential equation for the index perturbation required to achieve a desired velocity perturbation,

$$\delta'_\theta(\theta) = \frac{\delta_v(\theta)}{\ell(\theta)\,\dot{\theta}}. \tag{B.4}$$

In practice, the path is represented by discrete set of index values, and the differential equation B.4 becomes a difference equation:

$$\Delta\delta_\theta(\theta) = \delta_v(\theta)\ell^{-1}(\theta)\Delta t. \tag{B.5}$$

In our experiments, we divided the path into N bins, and calculated the angle perturbation for each bin: $\delta_{\theta i} = \delta_\theta(\theta_i), i \in [0, N-1]$. To solve the difference equation we need an initial condition. We are free to pick an arbitrary perturbation $\delta_{\theta 0}$ for the first bin, though in practice this was always chosen to be zero. Summing Equation B.5,

$$\delta_{\theta i} = \sum_{j=0}^{i-1} \delta_{vj}\ell_j^{-1}\Delta t_i + \delta_{\theta 0}. \tag{B.6}$$

Note that the form of Equation B.6 would be the same for an arbitrary path, only $\ell(\theta)$ would have to be redefined appropriately for that curve. In general, if $s(\theta)$ is the distance along the path, then $\ell(\theta) \equiv ds/d\theta$.

In order to calculate the perturbation, we need values for δ_{vi}, l_i, and Δt_i for each bin $i \in [0, N-1]$. The first of these terms is the desired velocity perturbation. We will discuss the forms these took in the next two sections. The second term, $l_i = \sqrt{a^2 \sin^2\theta_i + b^2\cos^2\theta_i}$, can be calculated in advance given the parameters a and b of the ellipse and the number of bins. Finally, Δt_i is the time spent on average in bin i. The value of Δt_i is be recorded during the pre-perturbation trials, along with other statistics needed for the particular δ_{vi} be used.

Note that early in the development above we made the assumption that the velocities

were a function of θ. This is necessary if the perturbation is to implemented as a fixed perturbation on the θ itself, but it is not sufficient. For circular paths, a consistent solution also requires that our initial condition is matched at the end of the path, i.e. $\delta_{\theta 0} = \delta_{\theta N}$. For open paths, we would like both the start and end of the movement to be unperturbed, which also requires $\delta_{\theta 0} = \delta_{\theta N}$. It can easily be seen that this requirement is equivalent to the condition that the sum in Equation B.6 equals zero when taken over the entire length of the path,

$$\sum_{j=0}^{N} \delta_{vj} \ell_j^{-1} \Delta t_i = 0. \tag{B.7}$$

This "zero sum" constraint is quite reasonable, for it means that the position of the feedback cannot drift endlessly from the actual location of the finger. In the following sections we present two useful perturbations that respect this constraint.

B.2 Eliminating and Accentuating Velocity Extrema

The 2/3 power law states human arm movements are centrally constrained such the tangential velocity varies according to the curvature of the path. This hypothesis can be tested by varying the strength of this relationship in the visual feedback. In particular, we would like to be able to adjust the magnitude of variations in the velocity profile around an elliptical path. The approach we take it to find the average velocity around the loop, and then multiply the deviations from that average by an arbitrary factor.

First, we take a weighed average of the velocity around the ellipse, with the weight of bin i chosen to be $\ell_i^{-1} \Delta t_i$,

$$\bar{v} = \frac{\sum_{i=1}^{N} v_i \ell_i^{-1} \Delta t_i}{\sum_{i=1}^{N} \ell_i^{-1} \Delta t_i}, \tag{B.8}$$

Now, the desired perturbation is the difference between that average velocity and the actual velocity profile, multiplied by a scaling factor of our choice,

$$\delta_{vi} = \alpha(\bar{v} - v_i). \tag{B.9}$$

The fact that this perturbation respects the zero sum constraint follows directly from the definition of $\bar{v}$.

To use this perturbation in an experiment, we have to collect statistics for v_i and Δt_i

during the pre-perturbation trials. Between the pre-perturbation and perturbation phases, we can compute the positional perturbation,

$$\begin{aligned} \delta_{\theta i} &= \sum_{i=1}^{j-1} \delta_{vi} \ell_i^{-1} \Delta t_i \\ \delta_{\theta i} &= \alpha \sum_{i=1}^{j-1} [\bar{v} - v_i] \ell_i^{-1} \Delta t_i \end{aligned} \tag{B.10}$$

In practice, the time required to perform this calculation on a Pentium PC does not add a noticeable delay before the first perturbation trial.

This perturbation was used in Experiment 3.1. Figure 3-2 displays the resulting feedback velocity profile for $\alpha = +1$. In this case the target feedback velocity would be perfectly flat, which is not the case in this example. However, the fluctuations in feedback velocity are much smaller than those of the actual movement. Furthermore, it is shown in Section 3.2.2 that such statistics as the best fit power law exponent and ratio of velocity maxima to minima are significantly altered in the desired direction. Figure 3-2 shows results for $\alpha = -1$. Here, the desired effect is to double the magnitude of fluctuation about the mean velocity. Again, although the resulting feedback is a good approximation to the desired perturbed feedback.

The differences between the target feedback velocity profile and what are actually attained in experimental conditions can be due both to the normal variability of movement as well as any drift in behavior over the course of the experiment. The latter could be dealt with by continually updating the perturbation according to the current behavior. However, it has been shown that in the case of prism adaptation, a stable perturbation is required for adaptation (see Welch, 1986 for a review), and so we chose not maintain a fixed $\delta_{\theta i}$ for the duration of the perturbation phase.

B.3 Skewing the Feedback Velocity

Given a velocity profile, $v(\theta)$, the skew transformation is defined as,

$$v_S(\theta) = v(\sigma) \text{ such that } \theta = \sigma + \beta v(\sigma), \tag{B.11}$$

where β is the skew parameter. Positive values of β result in rightward shifts of the velocity peaks, lengthening the left tails. As in the previous section, we collected statistics for v_i and Δt_i during the pre-perturbation trials. We then performed the skew transformation, and set the desired velocity perturbation to the difference between the two:

$$\delta_{vi} = v_{Si} - v_i. \tag{B.12}$$

All that remains to be shown is that this perturbation obeys the zero sum constraint, Equation B.7. Although the skew transformation preserves area under the curve, the zero sum constraint is not necessarily preserved. This is due both to discretization noise and the fact that Equation B.7 uses a weighted sum. In practice however, we found that deviations from the zero were very small. To adjust for these discrepancies, we multiplicitively scaled $v_S(\theta)$.

The effects of the skew perturbation on discrete obstacle avoidance movements can be seen in Figure 3-21 for positive skew and Figure 3-22 for negative skew. The perturbed feedback is nicely skewed in the desired direction. For continuous movements, the fluctuations in velocity were small compared to the overall magnitude, and so the effect of the perturbation was primarily to rotate the velocity profile around the center of the movement. This can be seen in for both positive and negative skews in Figure 3-16.

B.4 Implementing Index Perturbations

In experimental conditions, a subject's movements will not always lie directly on the desired path. Thus, in order to implement the perturbations described above, it is necessary to first decompose an arbitrary position in the workspace into a position along the path and an error from the path, and then to transform both component of the position. Transforming the position along the path is the topic of the preceding sections of this appendix. Here, we concentrate on how to project to the path from an arbitrary location, and how to transform the error from the path.

The most obvious way to proceed is to project to the nearest point on the path. This always yields an error vector perpendicular to the path, and so once the new location on the path has been determined, the error can be added back with the same magnitude and sign, but in a direction orthogonal to the path in the new location. This method would work

well for paths of low curvature, however two problems crop up with high curvature paths. First, the projection itself can have singularities which lie near the path. As an example, consider an ellipse of high eccentricity. If the finger is just inside the path and on the major axis, the segments of the path on either side of the major axis are equally close. The second problem has to do with the error transformation. Take the same example, but consider the case where the finger lies outside the ellipse near the high curvature end. As the finger rounds the corner, small changes in the path index can lead to very large changed in the normal to the path. The situation could occur, for example, where the finger is appear to lie on the opposite side of the ellipse to where is actually is.

For elliptical paths, there is a simpler and more reliable method. Every point in space lies on a unique ellipse which shares the same center, orientation and eccentricity as the desired path. We can treat the situation as if that were the target path, and perturb the position along that ellipse. This is implemented by finding the index θ and radius r:

$$\begin{aligned} \theta &= \arctan 2(y/b, x/a), \\ r &= \sqrt{\frac{x^2}{a^2} + \frac{y^2}{b^2}}. \end{aligned}$$

After calculating the new index θ', the feedback position is easily calculated as,

$$\begin{aligned} x' &= r\,a\,\cos\theta', \\ y' &= r\,b\,\sin\theta'. \end{aligned}$$

This transformation is illustrated in Figure B-1. This method was used for Experiment 3.1.

In Experiment 3.2, there was no elliptical figure to act as a guide for subjects movements. Rather, an obstacle was presented around which subjects were asked to move. As a target path for the calculations, we chose an ellipse which fit the behavior seen in pilot studies. The method described in the previous paragraph for projecting to the nominal target path worked well. However, there were significant deviations from that path, and so a more robust method of transforming the errors was needed. We chose to simply add the original error, untransformed, back to the new location on the target path.

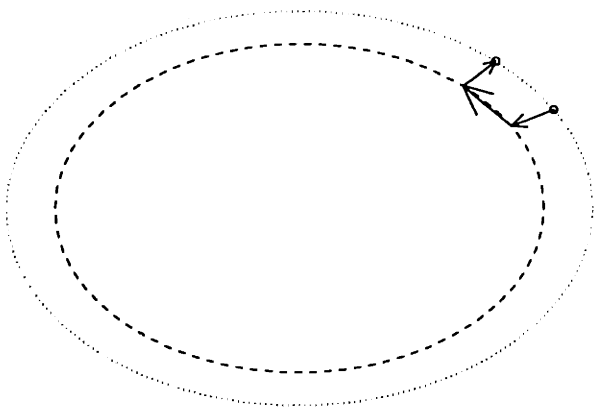

Figure B-1: Perturbing an arbitrary point in space when the target path is an ellipse. The inner, dashed ellipse is the target path, and the outer curve is the unique ellipse which shares the same center, orientation and eccentricity and also passes through the current finger location.

Bibliography

Abend, W., Bizzi, E., and Morasso, P. (1982). Human arm trajectory formation. *Brain*, 105:331–348.

Atkeson, C. and Hollerbach, J. (1985). Kinematic features of unrestrained vertical arm movements. *Journal of Neuroscience*, 5:2318–2330.

Bedford, F. (1989). Constraints on learning new mappings between perceptual dimensions. *Journal Experimental Psychology: Human Perception and Performance*, 15:232–248.

Bennet, D. J. (1990). *The Control of Human Arm Movements: Models and Mechanical Constraints.* PhD thesis, Massachusetts Institute of Technology.

Bernstein, N. (1967). *The Co-ordination and Regulation of Movements.* Pergamon Press, Oxford.

Bizzi, E., Accornero, N., Chapple, B., and Hogan, N. (1984). Posture control and trajectory formation during arm movement. *Journal of Neuroscience*, 4:2738–2744.

Bizzi, E., Hogan, N., Mussa-Ivaldi, F., and Giszter, S. (1992). Does the nervous system use equilibrium-point control to guide single and multiple joint movements. *Behavioral and Brain Sciences*, 15:603–613.

Bizzi, E., Polit, A., and Morasso, P. (1976). Mechanism underlying achievement of final head position. *Journal of Neurophysiology*, 39:435–444. Original end-pt only EqPtHyp.

Brüwer, M. and Cruse, H. (1990). A network model for the control of the movement of a redundant manipulator. *Biological Cybernetics*, 62:549–555.

Craig, J. J. (1986). *Introduction to Robotics : Mechanics & Control.* Addison-Wesley, Reading, MA.

Crossman, E. and Goodeve, P. (1983). Original work presented at the meeting of the of the experimental psychology society, oxford england, july, 1963. *Quarterly Journal Experimental Psychology*, 35A:251–278.

Cruse, H. (1986). Constraints for joint angle control of the human arm. *Biological Cybernetics*, 54:125–132.

Dean, J. and Brüwer, M. (1994). Control of human arm movements in two dimensions: paths and joint control in avoiding simple linear obstacles. *Experimental Brain Research*, 97:497–514.

Desmurget, M., Prablanc, C., Rossetti, Y., Arzi, M., Y., P., and C., U. (1995). Postural and synergic control for three-dimensional movements of reaching and grasping. *Journal of Neurophysiology*, 74:905–910.

DiZio, P. and Lackner, J. R. (1995). Motor adaptation to coriolis force perturbations of reaching movements: Endpoint but not trajectory adaptation transfers to the nonexposed arm. *Journal of Neurophysiology*, 74:1787–1792.

Feldman, A. G. (1986). Once more on the equilibrium point hypothesis (lambda model) for motor control. *Journal of Motor Behavior*, 18:17–54.

Flanagan, J. and Ostry, D. (1991). Trajectories of human multi-joint arm movements: Evidence of joint level planning. In *Experimental robotics*, Lecture notes in control and information sciences., London. Springer-Verlag.

Flanagan, J. and Rao, A. K. (1995). Trajectory adaptation to a nonlinear visuomotor transformation: Evidence of motion planning in visually perceived space. *Journal of Neurophysiology*, 74:2174–2178.

Flanders, M. and Soechting, J. F. (1990). Parcellation sensorimotor transformations for arm movements. *Journal of Neuroscience*, 10:2420–2427.

Flash, T. (1987). The control of hand equilibrium trajectories in multi-joint arm movements. *Biological Cybernetics*, 57:257–274.

Flash, T. and Gurevich, I. (1991). Human motor adaptation to external loads. *Annual International Conference of the IEEE Engineering in Medicine and Biology Society.*, 13:885–886.

Flash, T. and Gurevich, I. (1996). Models of motor adaptation and impedance control in human arm movements. In Morasso, P. and Sanguineti, V., editors, *Self-organization, computational maps and motor control.* Elsevier, Amsterdam. In Press.

Flash, T. and Hogan, N. (1985). The co-ordination of arm movements: An experimentally confirmed mathematical model. *Journal of Neuroscience*, 5:1688–1703.

Georgopoulos, A., Caminiti, R., Kalaska, J., and Massey, J. (1983). Spatial coding of movement: A hypothesis concerning the coding of movement direction by motor cortical populations. *Experimental Brain Research*, 327(Suppl. 7):327–336.

Georgopoulos, A., Schwartz, A., and Kettner, R. E. (1986). Neuronal population coding of movement direction. *Science*, 233:1416–1419.

Ghahramani, Z. (1995). *Computation and psychophysics of sensorimotor integration.* PhD thesis, Massachusetts Institute of Technology, Cambridge, MA.

Ghahramani, Z., Wolpert, D., and Jordan, M. (1996). Generalization to local remappings of the visuomotor coordinate transformation. *Journal of Neuroscience*, In Press.

Gordon, J., Ghilardi, M., Cooper, S., and Ghez, C. (1994a). Accuracy of planar reaching movements: II. systematic extent errors resulting from inertial anisotropy. *Experimental Brain Research*, 99:112–130.

Gordon, J., Ghilardi, M., and Ghez, C. (1994b). Accuracy of planar reaching movements: I. independence of direction and extent variability. *Experimental Brain Research*, 99:97–111.

Gribble, P. and Ostry, D. (1996). Origins of the power law relation between movement velocity and curvature: Modeling the effects of muscle mechanics and limb dynamics. *Journal of Neurophysiology.* In Press.

Haggard, P., Hutchinson, K., and Stein, J. (1996). Patterns of coordinated multi-joint movement. *Experimental Brain Research*, In press.

Hasan, Z. (1986). Optimized movement trajectories and joint stiffness in unperturbed, inertially loaded movements. *Biological Cybernetics*, 53:373–382.

Held, R. and Hein, A. (1958). Adaptation of disarranged hand-eye coordination contingent upon re-afferent stimulation. *Perceptual and Motor Skills*, 8.

Hogan, N. (1984). An organizing principle for a class of voluntary movements. *Journal of Neuroscience*, 4:2745–2754.

Hogan, N. (1985). The mechanics of multi-joint posture and movement control. *Biological Cybernetics*, 52:315–331.

Hogan, N. and Winters, J. M. (1990). Principles underlying movement organization: Upper limb. In Winters, J. and Woo, S.-Y., editors, *Multiple Muscle Systems: Biomechanics and Movement Organization*, pages 182–194. Springer-Verlag, New York.

Hollerbach, J. (1982). Computers, brains, and the control of movement. *TINS*, 5:189–192.

Hollerbach, J. and Atkeson, C. (1986). Characterization of joint-interpolated arm movements. *Experimental Brain Research*, 15:41–54.

Jordan, M., Flash, T., and Arnon, Y. (1994). A model of the learning of arm trajectories from spatial deviations. *Journal Cognitive Neuroscience*, 6:359–376.

Jordan, M. I. and Rumelhart, D. (1992). Forward models: Supervised learning with a distal teacher. *Cognitice Science*, 16:307–354.

Kaminsky, T. and Gentile, A. (1986). Joint control strategies and hand trajectories in multijoint pointing movements. *Journal of Motor Behavior*, 18:a261–278.

Kawato, M. (1994). Uni-directional versus bi-directional theory for trajectory planning and control. Technical Report TR-H-068, ATR Technical Reports, Kyoto, Japan.

Kirk, D. E. (1970). *Optima Control Theory: an introduction.* Printice-Hall, Englewood Cliffs, NJ.

Lackner, J. R. and DiZio, P. (1994). Rapid adaptation to coriolis force perturbations of arm trajectory. *Journal of Neurophysiology*, 72:??

Lacquaniti, F., Terzuolo, C. A., and Viviani, P. (1983). The law relating kinematic and figural aspects of drawing movements. *Acta Psychologica*, 54:115–130.

LeVeau, B. (1992). *Williams & Lissner's Biomechanics of Human Motion.* W.B. Saunders Company, Philadelphia.

McCullagh, P. and Nelder, J. (1989). *Generalized Linear Models.* Chapman and Hall, London.

Meyer, D., Smith, J., and Wright, C. (1982). Models for the speed and accuracy of aimed movements. *Psychological Review*, 89:449–482.

Milner, T. (1992). A model for the generation of movements requiring endpoint precision. *Neuroscience*, 49:487–496.

Morasso, P. (1981). Spatial control of arm movements. *Experimental Brain Research*, 42:223–227.

Morasso, P. (1983). Three dimensional arm trajectories. *Biological Cybernetics*, 48:187–194.

Morasso, P., Mussa-Ivaldi, F., and Ruggiero, C. (1983). How a discontinuous mechanism can produce continuous patterns in trajectory formation and handwriting. *Acta Psychologica*, 54:83–98.

Mussa-Ivaldi, F., Hogan, N., and Bizzi, E. (1985). Neural, mechanical, and geometric factors subserving arm posture. *Journal of Neuroscience*, 5:2732–2743.

Nelson, W. L. (11983). Physical principles for economies of skilled movements. *Biological Cybernetics*, 46:135–147.

Poggio, T. and Girosi, F. (1990). Regularization algorithms for learning that are equivalent to multilayer networks. *Science*, 247:978–9.

Redding, G. and Wallace, B. (1988). Adaptive mechanisms in perceptual-motor coordination: Components of prism adaptation. *Journal of Motor Behavior*, 20:242–254.

Rosenthal, R. and Rosnow, R. (1985). *Contrast Analysis.* Cambridge University Press, Cambridge, England.

Sabes, P. (1996). The role of velocity feedback in the planning of human arm movements. Technical Report 9601, Computational Cognitive Science Technical Report, M.I.T., Cambridge, MA.

Saltzman, E. (1979). Levels of sensorimotor representation. *Journal of Mathematical Psychology*, 20:91–163.

Schwartz, A. (1994). Direct cortical representation of drawing. *Science*, 265:540–542.

Scott, S. and Kalaska, J. (1995). Changes in motor cortex activity during reaching movements with similar hand paths but different arm postures. *Journal of Neurophysiology*, 73:2563–2567.

Shadmehr, R. and Mussa-Ivaldi, F. (1994). Adaptive representation of dynamics during learning of a motor task. *Journal of Neuroscience*, 14(5):3208–3224.

Soechting, J. and Lacquaniti, F. (1981). Invariant characteristics of a pointing movement in man. *Journal of Neuroscience*, 1:710–720.

Soechting, J. F. and Flanders, M. (1989a). Errors in pointing are due to approximations in sensorimotor transformations. *Journal of Neurophysiology*, 62:595–608.

Soechting, J. F. and Flanders, M. (1989b). Sensoimotor representations for pointing to targets in three-dimensional space. *Journal of Neurophysiology*, 62:582–594.

Soechting, J. F. and Terzuolo, C. A. (1986). An algorithm for the generation of curvilinear wrist motion in an arbitrary plane in three-dimensional space. *Neuroscience*, 19:1393–1405.

Uno, Y , Kawato, M., and Suzuki, R. (1989). Formation and control of optimal trajectories in human multijoint arm movements: Minimum torque-change model. *Biological Cybernetics*, 61:89–101.

Viviani, P. and Cenzato, M. (1985). Segmentation and coupling in complex movements. *Journal Experimental Psychology: Human Perception and Performance*, 11:828–845.

Viviani, P. and Flash, T. (1995). Minimum jerk model, two-thirds power law, and isocrony: Converging approaches to the study of movement and planning. *Journal Experimental Psychology: Human Perception and Performance*, 21:32–53.

Viviani, P. and Stucchi, N. (1992). Biological movements look uniform: evidence of motor-perceptual interactions. *Journal Experimental Psychology: Human Perception and Performance*, 18:603–623.

Viviani, P. and Terzuolo, C. A. (1982). Trajectory determines movement dynamics. *Neuroscience*, 7:431–437.

Wallace, B. and Redding, G. (1979). Additivity in prism adaptation as manifested in intermanual and interocular transfer. *Perception and Psychophysics*, 25:133–136.

Wann, J., Nimmo-Smith, I., and Wing, A. M. (1988). Relation between velocity and curvature in movement: equivalence and divergence between a power law and a minimum jerk model. *Journal Experimental Psychology: Human Perception and Performance*, 14:622–637.

Welch, R. (1971). Prism adaptation: The "target pointing effect" as a function of exposure trials. *Perception and Psychophysics*, 10:90–92.

Welch, R. (1986). Adaptation of space perception. In Boff, K., Kaufman, L., and Thomas, J., editors, *Handbook of Human Perception and Performance.* Wiley, New York, NY.

Wolpert, D., Ghahramani, Z., and Jordan, M. I. (1994). Perceptual distortion contributes to the curvature of human reaching movements. *Experimental Brain Research*, 98:153–156.

Wolpert, D., Ghahramani, Z., and Jordan, M. I. (1995). Are arm trajectories planned in kinematic or dynamic coordinates? an adaptation study. *Experimental Brain Research*, 103:460–470.

Yamaguchi, G., Sawa, A., Moran, D., Fessler, M., and Winters, J. (1990). A survey of human musculotendon actuator parameters systems. In Winters, J. and Woo, S.-Y., editors, *Multiple Muscle Systems: Biomechanics and Movement Organization*, pages 159–164. Springer-Verlag, New York.

Yoshikawa, T. (1990). *Foundations of Robotics: Analysis and Control.* MIT Press, Cambridge, MA.